COMPARISON OF THRESHOLDING TECHNIQUES FOR EXTRACTION OF ELECTRICAL HOTSPOTS FROM INFRARED IMAGES

By
Asaduzzaman Abir
19121147
Md. Rifat Islam Joy
16321066
Mobtasim Fuad
15121011
Nafiul Ahmed Emon
15221006

A Thesis submitted to the Department of Electrical and Electronic Engineering Of BRAC University, in partial fulfillment of the requirements for the degree of Bachelor of Science in Electrical and Electronic Engineering

Department of Electrical and Electronic Engineering
Brac University
October, 2020

© [2020]. Brac University
All rights reserved

Declaration

It is hereby declared that

1. The thesis submitted is my/our own original work while completing degree at Brac University.
2. The thesis does not contain material previously published or written by a third party, except where this is appropriately cited through full and accurate referencing.
3. The thesis does not contain material which has been accepted, or submitted, for any other degree or diploma at a university or other institution.
4. I/We have acknowledged all main sources of help.

Student's Full Name & Signature:

Asaduzzaman Abir
19121147

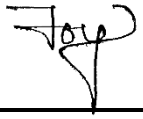

Md. Rifat Islam Joy
16321066

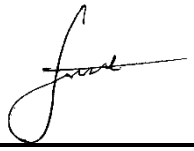

Mobtasim Fuad
15121011

Nafiul Ahmed Emon
15221006

Approval

The thesis/project titled "Comparison of Thresholding Techniques for Extraction of Electrical Hotspots from Infrared Images" submitted by

1. Asaduzzaman Abir (19121147)
2. Md. Rifat Islam Joy (16321066)
3. Mobtasim Fuad (15121011)
4. Nafiul Ahmed Emon (15221006)

of Summer, 2020 has been accepted as satisfactory in partial fulfillment of the requirement for the degree of Bachelors of Engineering in Electrical and Electronic Engineering on 5th October, 2020.

Examining Committee:

Supervisor:
(Member)

22/11/2020

Dr. A. S. Nazmul Huda
Assistant Professor, Department of
Electrical and Electronic Engineering
BRAC University

Thesis Coordinator:
(Member)

Dr. Abu S.M. Mohsin
Assistant Professor, Department of
Electrical and Electronic Engineering
BRAC University

Departmental Head:
(Chair)

Shahidul Islam Khan, PhD
Professor and Chairperson, Department of
Electrical and Electronic Engineering
BRAC University

Abstract

The objective of this study is to evaluate the performance of different thresholding techniques to extract the hotspots of electrical equipment through infrared thermal imaging. The abnormal thermal pattern can be found from faulty electrical equipment compared to the components in the normal condition. Detecting hotspots is very important to protect the equipment from complete failure or fire hazards. In the production line, sudden fault and shutdown cause huge losses. That's why using thermal imaging can warn us before a sudden failure by giving the heat signature of the equipment. For getting the correct hotspot area from the thermal image, different thresholding methods are used. However, it is important to know which of the particular thresholding technique can perform best for implementing an automatic inspection of electrical equipment. In this study, seven different thresholding techniques were applied to 24 different sample images of electrical equipment to measure the overall performance of the thresholding techniques. Among those techniques, the Moment thresholding technique has appeared as the most reliable segmentation method based on different test index results.

The result from this study can help in future to implement automatic thresholding-based condition monitoring of electrical equipment to detect any fault criteria without interrupting the service of equipment or disassembling them.

Keywords: Infrared thermography; Thresholding; Condition monitoring; Electrical equipment; Hotspot detection; Thermal imaging

Dedication

We would like to dedicate our thesis to our parents for their continuous support and encouragement to achieve excellence and showering love and support during every phase of our lives without which it would not be possible for us to come this far.

Acknowledgement

Thanks to the Almighty Allah for giving us the opportunity, determination and strength to complete this thesis successfully. We want to express our heartfelt gratitude and sincere thanks to honorable thesis supervisor Dr. A. S. Nazmul Huda, Assistant Professor, Department of Electrical and Electronics Engineering (EEE), Brac University; for his support, important guidance and valuable opinions throughout the thesis period which led us to successfully completing this thesis. We would also like to show our gratitude towards the Opex Garments Ltd. for providing us access to all of their factories to collect necessary data and help us with the Fluke TiS10 Infrared Camera. We are also grateful to Brac University for providing us with all the support for managing the permission to visit the factories for collecting data and analysis it in thesis lab.

Table of Contents

Declaration ii

Approval iii

Abstract iv

Dedication v

Acknowledgement vi

Table of Contents vii

List of Tables xii

List of Acronyms xx

Chapter 1 Introduction 1

1.1 Background 2

1.2 Motivation 3

1.3 Literature Review 4

1.4 Flowchart of thesis overview 5

Chapter 2 Reports of Collected Thermal Images 6

2.1 Method of Measurement and Analysis 7

2.2 NETA Standard Table 8

2.3 Reports of Collected Thermal Images 8

2.3.1 Report of Thermal Image-01 9

2.3.2 Report of Thermal Image-02 11

2.3.3 Report of Thermal Image-03 13

2.3.4 Report of Thermal Image-04 15

2.3.5 Report of Thermal Image-05 17

2.3.6 Report of Thermal Image-06 19

2.3.7 Report of Thermal Image-07 21

2.3.8 Report of Thermal Image-08 23

2.3.9 Report of Thermal Image-09 25

2.3.10 Report of Thermal Image-10 27

2.3.11 Report of Thermal Image-11 29

2.3.12 Report of Thermal Image-12 31

2.3.13 Report of Thermal Image-13 33

2.3.14 Report of Thermal Image-14 35

2.3.15 Report of Thermal Image-15 37

2.3.16 Report of Thermal Image-16 39

2.3.17 Report of Thermal Image-17 41

2.3.18 Report of Thermal Image-18 43

2.3.19 Report of Thermal Image-19 45

2.3.20 Report of Thermal Image-20 47

2.3.21 Report of Thermal Image-21 49

2.3.22 Report of Thermal Image-22 51

2.3.23 Report of Thermal Image-23 53

2.3.24 Report of Thermal Image-24 55

Chapter 3 Thresholding Techniques 57

3.1 Basic Principles of Thresholding 58

3.2 IsoData Thresholding Technique 59

3.4 MaxEntropy/Kapur Thresholding Technique 62

3.5 MET Thresholding Technique 64

3.6 Otsu Thresholding Technique 65

3.7 Moments Thresholding Technique 68

3.8 RenyiEntropy Thresholding Technique 71

3.9 Yen Thresholding Technique 73

Chapter 4 Performance Evaluation 75

4.1 Terms used for Performance Evaluation 76

4.2 Image Dataset of Segmentation 78

4.2.1 Image-01 Dataset 79

4.2.2 Image-02 Dataset 80

4.2.3 Image-03 Dataset 81

4.2.4 Image-04 Dataset 82

4.2.5 Image-05 Dataset 83

4.2.6 Image-06 Dataset 84

4.2.7 Image-07 Dataset 85

4.2.8 Image-08 Dataset 86

4.2.9 Image-09 Dataset 87

4.2.10 Image-10 Dataset 88

4.2.11 Image-11 Dataset 89

4.2.12 Image-12 Dataset 90

4.2.13 Image-13 Dataset 91

4.2.14 Image-14 Dataset 92

4.2.15 Image-15 Dataset 93

4.2.16 Image-16Dataset 94

4.2.17 Image-17 Dataset 95

4.2.18 Image-18 Dataset 96

4.2.19 Image-19 Dataset 97

4.2.20 Image-20 Dataset 98

4.2.21 Image-21 Dataset 99

4.2.22 Image-22 Dataset 100

4.2.23 Image-23 Dataset 101

4.2.24 Image-24 Dataset 102

4.3 Software and MATLAB Coding for Performance Evaluation 103

4.3.1 Software Usage 103

4.3.2 MATLAB Coding 105

4.3.3 Images of execution procedure through Software & Coding 107

4.3.4 Performance data tables of different thresholding techniques 109

Chapter 5 Results & Discussion 116

5.1 Combined Performance Evaluation Results 117

5.2 Final Results 117

Chapter 6 Conclusion 119

6.1 Summary 120

6.2 Future Recommendation 120

Reference 122

List of Tables

Table 2.1: Maintenance testing Specifications for Electrical Equipment 8

Table 2.2: Defect classification of Image-01 according to the “NETA” Standards 9

Table 2.3: Defect classification of Image-02 according to the “NETA” Standards 11

Table 2.4: Defect classification of Image-03 according to the “NETA” Standards 13

Table 2.5: Defect classification of Image-04 according to the “NETA” Standards 15

Table 2.6: Defect classification of Image-05 according to the “NETA” Standards 17

Table 2.7: Defect classification of Image-06 according to the “NETA” Standards 19

Table 2.8: Defect classification of Image-07 according to the “NETA” Standards 21

Table 2.9: Defect classification of Image-08 according to the “NETA” Standards 23

Table 2.10: Defect classification of Image-09 according to the “NETA” Standards 25

Table 2.11: Defect classification of Image-10 according to the “NETA” Standards 27

Table 2.12: Defect classification of Image-11 according to the “NETA” Standards 29

Table 2.13: Defect classification of Image-12 according to the “NETA” Standards 31

Table 2.14: Defect classification of Image-13 according to the “NETA” Standards 33

Table 2.15: Defect classification of Image-14 according to the “NETA” Standards 35

Table 2.16: Defect classification of Image-15 according to the “NETA” Standards 37

Table 2.17: Defect classification of Image-16 according to the “NETA” Standards 39

Table 2.18: Defect classification of Image-17 according to the “NETA” Standards 41

Table 2.19: Defect classification of Image-18 according to the “NETA” Standards 43

Table 2.20: Defect classification of Image-19 according to the “NETA” Standards 45

Table 2.21: Defect classification of Image-20 according to the “NETA” Standards 47

Table 2.22: Defect classification of Image-21 according to the “NETA” Standards 49

Table 2.23: Defect classification of Image-22 according to the “NETA” Standards 51

Table 2.24: Defect classification of Image-23 according to the “NETA” Standards 53

Table 2.25: Defect classification of Image-24 according to the “NETA” Standards 55

Table 4.1: IsoData Thresholding Test Result 109

Table 4.2: MaxEntropy/Kapur Thresholding Result 110

Table 4.3: Moments Thresholding Test Result 111

Table 4.4: Otsu Thresholding Test Result 112

Table 4.5: RenyiEntropy Thresholding Test Result 113

Table 4.6: Yen Thresholding Test Result 114

Table 4.7: MET Thresholding Test Result 115

Table 5.1: Average Test Result of Each Thresholding Techniques 117

List of Figures

Figure 1.1: Flowchart of thesis overview 5

Figure 2.1: (a) Visible and (b) Thermal representation of sample Image-01 9

Figure 2.2: (a) Line diagram, (b) Histogram and (c) 3D IR Graph of sample Image-01 10

Figure 2.3: (a) Visible and (b) Thermal representation of sample Image-02 11

Figure 2.4: (a) Line diagram, (b) Histogram and (c) 3D IR Graph of sample Image-02 12

Figure 2.5: (a) Visible and (b) Thermal representation of sample Image-03 13

Figure 2.6: (a) Line diagram, (b) Histogram and (c) 3D IR Graph of sample Image-03 14

Figure 2.7: (a) Visible and (b) Thermal representation of sample Image-04 15

Figure 2.8: (a) Line diagram, (b) Histogram and (c) 3D IR Graph of sample Image-04 16

Figure 2.9: (a) Visible and (b) Thermal representation of sample Image-05 17

Figure 2.10: (a) Line diagram, (b) Histogram and (c) 3D IR Graph of sample Image-05 18

Figure 2.11: (a) Visible and (b) Thermal representation of sample Image-06 19

Figure 2.12: (a) Line diagram, (b) Histogram and (c) 3D IR Graph of sample Image-06 20

Figure 2.13: (a) Visible and (b) Thermal representation of sample Image-07 21

Figure 2.14: (a) Line diagram, (b) Histogram and (c) 3D IR Graph of sample Image-07 22

Figure 2.15: (a) Visible and (b) Thermal representation of sample Image-08 23

Figure 2.16: (a) Line diagram, (b) Histogram and (c) 3D IR Graph of sample Image-08 24

Figure 2.17: (a) Visible and (b) Thermal representation of sample Image-09 25

Figure 2.18: (a) Line diagram, (b) Histogram and (c) 3D IR Graph of sample Image-09 26

Figure 2.19: (a) Visible and (b) Thermal representation of sample Image-10 27

Figure 2.20: (a) Line diagram, (b) Histogram and (c) 3D IR Graph of sample Image-10 28

Figure 2.21: (a) Visible and (b) Thermal representation of sample Image-11 29

Figure 2.22: (a) Line diagram, (b) Histogram and (c) 3D IR Graph of sample Image-11 30

Figure 2.23: (a) Visible and (b) Thermal representation of sample Image-12 31

Figure 2.24: (a) Line diagram, (b) Histogram and (c) 3D IR Graph of sample Image-12 32

Figure 2.25: (a) Visible and (b) Thermal representation of sample Image-13 33

Figure 2.26: (a) Line diagram, (b) Histogram and (c) 3D IR Graph of sample Image-13 34

Figure 2.27: (a) Visible and (b) Thermal representation of sample Image-14 35

Figure 2.28: (a) Line diagram, (b) Histogram and (c) 3D IR Graph of sample Image-14 36

Figure 2.29: (a) Visible and (b) Thermal representation of sample Image-15 37

Figure 2.30: (a) Line diagram, (b) Histogram and (c) 3D IR Graph of sample Image-15 38

Figure 2.31: (a) Visible and (b) Thermal representation of sample Image-16 39

Figure 2.32: (a) Line diagram, (b) Histogram and (c) 3D IR Graph of sample Image-16 40

Figure 2.33: (a) Visible and (b) Thermal representation of sample Image-17 41

Figure 2.34: (a) Line diagram, (b) Histogram and (c) 3D IR Graph of sample Image-17 42

Figure 2.35: (a) Visible and (b) Thermal representation of sample Image-18 43

Figure 2.36: (a) Line diagram, (b) Histogram and (c) 3D IR Graph of sample Image-18 44

Figure 2.37: (a) Visible and (b) Thermal representation of sample Image-19 45

Figure 2.38: (a) Line diagram, (b) Histogram and (c) 3D IR Graph of sample Image-19 46

Figure 2.39: (a) Visible and (b) Thermal representation of sample Image-20 47

Figure 2.40: (a) Line diagram, (b) Histogram and (c) 3D IR Graph of sample Image-20 48

Figure 2.41: (a) Visible and (b) Thermal representation of sample Image-21 49

Figure 2.42: (a) Line diagram, (b) Histogram and (c) 3D IR Graph of sample Image-21 50

Figure 2.43: (a) Visible and (b) Thermal representation of sample Image-22 51

Figure 2.44: (a) Line diagram, (b) Histogram and (c) 3D IR Graph of sample Image-22 52

Figure 2.45: (a) Visible and (b) Thermal representation of sample Image-23 53

Figure 2.46: (a) Line diagram, (b) Histogram and (c) 3D IR Graph of sample Image-23. 54

Figure 2.47: (a) Visible and (b) Thermal representation of sample Image-24 55

Figure 2.48: (a) Line diagram, (b) Histogram and (c) 3D IR Graph of sample Image-24 56

Figure 3.1: 2-D Histogram 72

Figure 4.1: Overlapping of ground truth and segmented image 77

Figure 4.2: Target hotspots extraction from Image-01 using Thresholding techniques (a) Enhanced Thermal Image (b) Histogram (c) Ground truth image (d) IsoData (e) MaxEntropy/Kapur (f) Moments 79

Figure 4.3: Target hotspots extraction from Image-02 using Thresholding techniques (a) Enhanced Thermal Image (b) Histogram (c) Ground truth image (d) IsoData (e) MaxEntropy/Kapur (f) Moments 80

Figure 4.4: Target hotspots extraction from Image-03 using Thresholding techniques (a) Enhanced Thermal Image (b) Histogram (c) Ground truth image (d) IsoData (e) MaxEntropy/Kapur (f) Moments 81

Figure 4.5: Target hotspots extraction from Image-04 using Thresholding techniques (a) Enhanced Thermal Image (b) Histogram (c) Ground truth image (d) IsoData (e) MaxEntropy/Kapur (f) Moments 82

Figure 4.6: Target hotspots extraction from Image-05 using Thresholding techniques (a) Enhanced Thermal Image (b) Histogram (c) Ground truth image (d) IsoData (e) MaxEntropy/Kapur (f) Moments 83

Figure 4.7: Target hotspots extraction from Image-06 using Thresholding techniques (a) Enhanced Thermal Image (b) Histogram (c) Ground truth image (d) IsoData (e) MaxEntropy/Kapur (f) Moments 84

Figure 4.8: Target hotspots extraction from Image-07 using Thresholding techniques (a) Enhanced Thermal Image (b) Histogram (c) Ground truth image (d) IsoData (e) MaxEntropy/Kapur (f) Moments 85

Figure 4.9: Target hotspots extraction from Image-08 using Thresholding techniques (a) Enhanced Thermal Image (b) Histogram (c) Ground truth image (d) IsoData (e) MaxEntropy/Kapur (f) Moments 86

Figure 4.10: Target hotspots extraction from Image-09 using Thresholding techniques (a) Enhanced Thermal Image (b) Histogram (c) Ground truth image (d) IsoData (e) MaxEntropy/Kapur (f) Moments 87

Figure 4.11: Target hotspots extraction from Image-10 using Thresholding techniques (a) Enhanced Thermal Image (b) Histogram (c) Ground truth image (d) IsoData (e) MaxEntropy/Kapur (f) Moments 88

Figure 4.12: Target hotspots extraction from Image-11 using Thresholding techniques (a) Enhanced Thermal Image (b) Histogram (c) Ground truth image (d) IsoData (e) MaxEntropy/Kapur (f) Moments 89

Figure 4.13: Target hotspots extraction from Image-12 using Thresholding techniques (a) Enhanced Thermal Image (b) Histogram (c) Ground truth image (d) IsoData (e) MaxEntropy/Kapur (f) Moments 90

Figure 4.14: Target hotspots extraction from Image-13 using Thresholding techniques (a) Enhanced Thermal Image (b) Histogram (c) Ground truth image (d) IsoData (e) MaxEntropy/Kapur (f) Moments 91

Figure 4.15: Target hotspots extraction from Image-14 using Thresholding techniques (a) Enhanced Thermal Image (b) Histogram (c) Ground truth image (d) IsoData (e) MaxEntropy/Kapur (f) Moments 92

Figure 4.16: Target hotspots extraction from Image-15 using Thresholding techniques (a) Enhanced Thermal Image (b) Histogram (c) Ground truth image (d) IsoData (e) MaxEntropy/Kapur (f) Moments 93

Figure 4.17: Target hotspots extraction from Image-16 using Thresholding techniques (a) Enhanced Thermal Image (b) Histogram (c) Ground truth image (d) IsoData (e) MaxEntropy/Kapur (f) Moments 94

Figure 4.18: Target hotspots extraction from Image-17 using Thresholding techniques (a) Enhanced Thermal Image (b) Histogram (c) Ground truth image (d) IsoData (e) MaxEntropy/Kapur (f) Moments 95

Figure 4.19: Target hotspots extraction from Image-18 using Thresholding techniques (a) Enhanced Thermal Image (b) Histogram (c) Ground truth image (d) IsoData (e) MaxEntropy/Kapur (f) Moments 96

Figure 4.20: Target hotspots extraction from Image-19 using Thresholding techniques (a) Enhanced Thermal Image (b) Histogram (c) Ground truth image (d) IsoData (e) MaxEntropy/Kapur (f) Moments 97

Figure 4.21: Target hotspots extraction from Image-20 using Thresholding techniques (a) Enhanced Thermal Image (b) Histogram (c) Ground truth image (d) IsoData (e) MaxEntropy/Kapur (f) Moments 98

Figure 4.22: Target hotspots extraction from Image-21 using Thresholding techniques (a) Enhanced Thermal Image (b) Histogram (c) Ground truth image (d) IsoData (e) MaxEntropy/Kapur (f) Moments 99

Figure 4.23: Target hotspots extraction from Image-22 using Thresholding techniques (a) Enhanced Thermal Image (b) Histogram (c) Ground truth image (d) IsoData (e) MaxEntropy/Kapur (f) Moments 100

Figure 4.24: Target hotspots extraction from Image-23 using Thresholding techniques (a) Enhanced Thermal Image (b) Histogram (c) Ground truth image (d) IsoData (e) MaxEntropy/Kapur (f) Moments 101

Figure 4.25: Target hotspots extraction from Image-24 using Thresholding techniques (a) Enhanced Thermal Image (b) Histogram (c) Ground truth image (d) IsoData (e) MaxEntropy/Kapur (f) Moments 102

Figure 4.26: Flowchart for performance evaluation of different thresholding techniques using software and coding. 104

Figure 4.27: Viewing Thermal Image via Fluke Smart View Software 107

Figure 4.28: Converting Thermal Image via Fluke Smart View Software 107

Figure 4.29: Performing thresholding via ImageJ Software 108

Figure 4.30: Running code at MATLAB for measuring different terms result for evaluation 108

List of Acronyms

IRT	Infrared Thermography
PM	Preventive Maintenance
PdM	Predictive Maintenance
TPR	True Positive Rate
FPR	False Positive Rate
GT	Ground Truth Image
ST	Segmented Image
MCC	Matthews Correlation Coefficient

Chapter 1

Introduction

1.1 Background

In electrical equipment, faults can be occurred when its temperature reaches the level of abnormality. Electrical equipment such as transformer, fuse, capacitor, bushing, etc. can cause electrical fault due to diverse reasons like contact problems, distribution of unbalance current, cracks in the insulator, faulty relays, or block in terminals etc. When a fault occurs, there is a resistance to the current that causes an increase in temperature, produces a hot spot and subsequently failure of components, potentially resulting in unplanned outages and possible injuries. Besides the efficiency of an electrical grid also decreases. If left unchecked, heat can rise to a level at which connections will melt and break the circuit and as a result fires may occur [1]. Therefore, an inspection of electrical equipment is necessary to avoid problems that are caused by abnormal heat in the equipment. With the advantages of non-contact, easy interpretation, large inspection coverage and free from harmful radiation, infrared thermography (IRT) is one of the most popular techniques. For this reason, IRT has gained recognition as a suitable technique for Preventive Maintenance (PM) and Predictive Maintenance (PdM) to monitor Electrical Equipment for detecting any abnormal High Temperature [2-3]. Due to the nature of temperature difference between a normal and defective component of equipment or high temperature of equipment concerning surroundings, any existence of the thermal defect at the surface of equipment can be revealed directly by a thermal camera without any external heat source or a pulse generator. Therefore, for visualization purpose the temperature values are converted into pixel values then the defected component illustrates as a cluster of bright pixels.

At the end, it is very important to analyze the proper heat signature value or cluster of heat signature from the thermal images by processing it via different software and algorithms. However, manual

process via software can take a lot of time. That's why Thresholding techniques are used by researchers in this case for simplicity and easy analysis. But there are many thresholding techniques to choose from. That's why, we tried different thresholding techniques to compare & find out which thresholding techniques is more suitable and accurate for segmenting thermal images to get much more accurate result compared to the Ground Truth Image Thresholding and segmentation. We have evaluated the performances of different thresholding techniques in terms of FPR, TPR, Accuracy, Precision, MCC, Dice, Jaccard Index, Error (%).

1.2 Motivation

Electrical equipment plays a vital role in this modern world. Electricity is the key to all advancement and comfort in this modern era. However, for providing an uninterrupted electricity supply it is essential to keep the electrical equipment in good condition and running always. That's why it is necessary to monitor important electrical equipment before any fault occurs. However, manual diagnosing by inspecting the components is time-consuming and doing so hamper the continuous supply of electricity. As a result, it is high time to find effective and efficient techniques to monitor the condition of electrical equipment. And for this case IRT plays a vital role. It is more feasible and efficient to use IR thermal Camera for finding abnormal heat signatures from equipment and process it to find the results about the condition. But manual thermal Image processing can take a lot of time that's why thresholding techniques are used by many researchers to evaluate the condition of the equipment. But there are many thresholding techniques to choose from. So, we found it interesting to find the best available Thresholding techniques that can give a more accurate result like manual processing. In this thesis, we briefly evaluated seven different thresholding techniques to compare and find out the best suitable thresholding techniques. So, it

will be helpful to choose the best thresholding techniques in Automatic condition monitoring of electrical equipment for a more accurate result.

1.3 Literature Review

Electrical equipment has become an important part of our life and they are used everywhere for easing our different task at home, offices factory etc. However, fault in electrical equipment is very common and mostly it happens due to running at higher load and temperature. Moreover, it is impossible to detect condition of the equipment with human eyes. So, most of the time early symptoms of failure of electrical equipment gets unnoticed. And fault causes great loss of money and there is also fire hazard. However, recently many progresses have done for condition monitoring of the electrical equipment and in this sector IRT plays a vital role. As we know that, IRT imaging can capture images with temperature value and heat signature so it can be used to monitor the condition of the electrical equipment without any physical touch.
In the paper [4], the authors discuss how the IRT based inspection technique can further be improved. They mentioned that nowadays most of the IRT camera comes with analysis software but the evaluation process with this software is time consuming and focused on automated system for this. However, for developing automated system it is necessary to finding out the heat signature area from the ROI area correctly. In this case thresholding technique is handful and used by many scientists. However, all of the thresholding techniques does not work equally and segmentation results vary. So, for developing the automatic or intelligent diagnostic system it is essential to find out the best suitable thresholding techniques that performs best with the electrical equipment. So, different research in this field direct us to this evaluation test of different thresholding techniques to find out the best possible thresholding technique which will perform best with many real-life

samples of electrical equipment. Nevertheless, by gathering all the evaluation test results data from different thresholding techniques will help to decide which of the thresholding techniques perform similar or better than rest of the techniques. Based upon this data, most preferable thresholding algorithm can be applied for automatic and intelligent diagnostic of the electrical equipment to prevent sudden fault and danger.

1.4 Flowchart of Thesis Overview

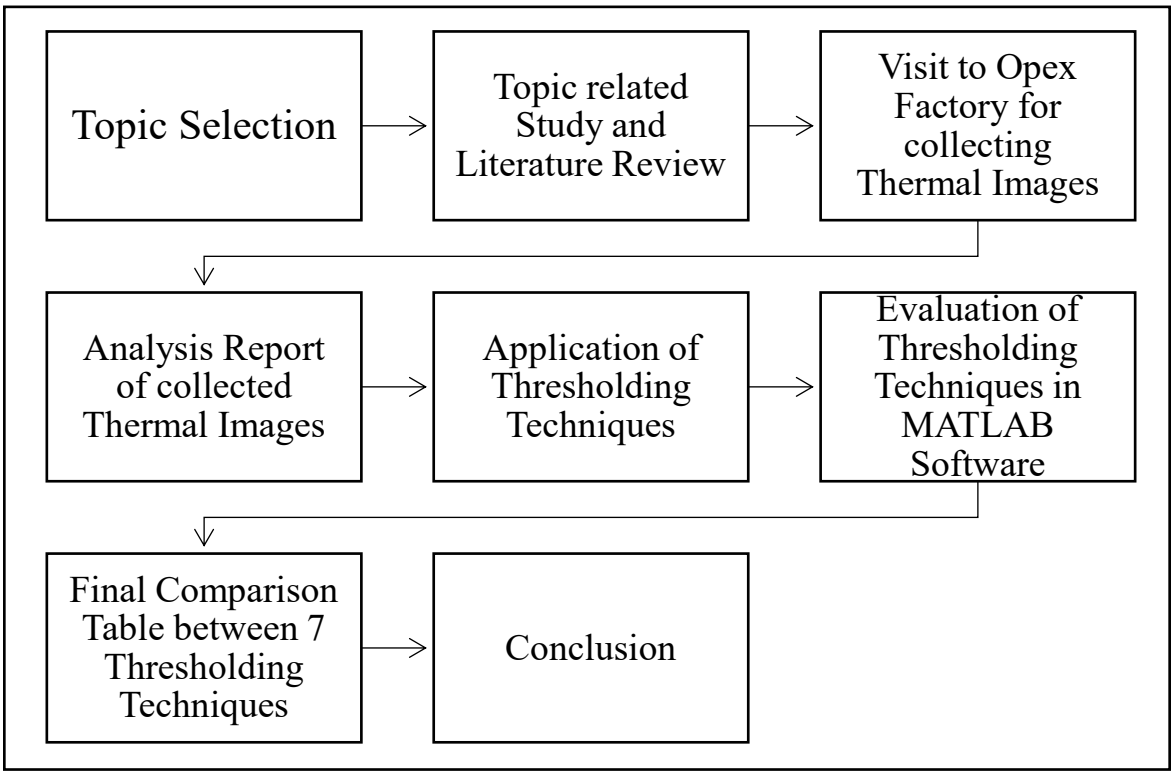

***Figure 1.1**: Flowchart of thesis overview*

Chapter 2

Reports of Collected Thermal Images

2.1 Method of Measurement and Analysis

For the purpose of thesis, we needed thermal images of different electrical equipment. For, collecting images, we visited OPEX Factory in Mirpur. There are two different ways for measuring the thermal condition of the electrical equipment. They are known as quantitative and qualitative techniques. Quantitative technique means to consider only the exact temperature reading of electrical equipment. However, in qualitative techniques it includes the relative high temperature reading of the equipment along with relative low temperature reading of the same equipment under exact same conditions. After collecting images in this way, temperature difference between the equipment is calculated and it is known as ΔT Criteria [4]. Qualitative technique is more preferred because in quantitative technique ΔT Criteria involves taking the ambient temperature reading also. However, it is not possible to take the precise ambient temperature value as temperature value can be affected by many factors. For example, ambient temperature can be increased because of heat dissipation of our equipment. So, quantitative technique is widely used for inspection in this type of scenery. In this techniques, highest value of temperature reading from electrical equipment is compared with the lowest temperature reading of the same equipment under exact same condition to find out the ΔT Criteria.

where

ΔT= (Temperature from relative high heat signature area of components (Celsius) - Temperature from relative low heat signature area of components (Celsius)) °C.

There are many standards to follow such as International Electrical Testing Association (NETA), American Society for Testing & Materials (ASTM) – E 1934 and National Fire Protection Association (NFPA) – NFPA 70-B provides a guideline for IRT inspection. However, for

measuring the level of severity to take recommended action NETA standard Table is widely used considering the ΔT criteria [4].

2.2 NETA Standard Table

Table 2.1: *Maintenance testing specifications for electrical equipment*

Priority	ΔT between similar components under similar load (°C)	ΔT over ambient temperature (°C)	Recommended action
4	1-3	1-10	Possible deficiency, warrants investigation
3	4-15	11-20	Indicates probable deficiency; repair as time permits
2	-	21-40	Monitor until corrective measures can be accomplished
1	>15	>40	Major discrepancy; repair immediately

2.3 Reports of Collected Thermal Images

In this segment collected thermal images were analyzed via Fluke Smart view Software to export visible & thermal image and to prepare the defect classification chart, line diagram, histogram and 3D IR graph.

2.3.1 Report of Thermal Image-01

Name of the equipment: Circuit Breaker

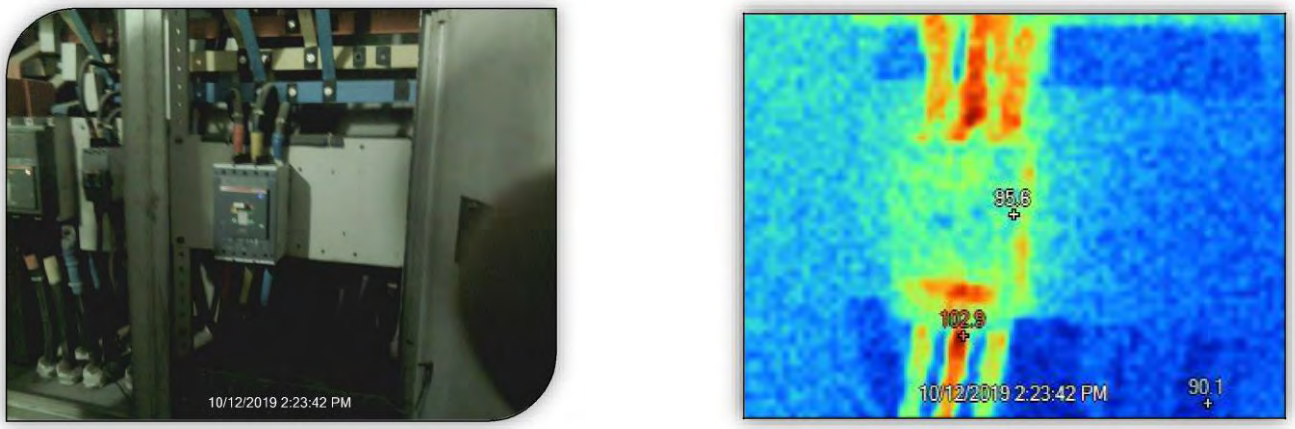

(a) **(b)**

Figure 2.1*: (a) Visible and (b) Thermal representation of sample Image-01*

Here visible image shows the electrical component and thermal image shows the heat signatures on the component.

(i) Location

This circuit breaker is located at the Main Distribution Board (MDB) of the Factory-3.

(ii) Defect

Load difference between the phases R, Y & B. Phase Y is the higher load phase and eventually because of this it was showing more heat signature.

(ii) Defect Classification

Table 2.2: *Defect classification of Image-01 according to the "NETA" Standards*

Serial	Temperature from normal heat signature area of components (Celsius)	Temperature from highest heat signature area of components (Celsius)	ΔT between similar components under similar load (Celsius)	Recommended Action/Classification
1	37.2	39.4	2.2	Possible deficiency & investigation warrants.

(iv) Graph

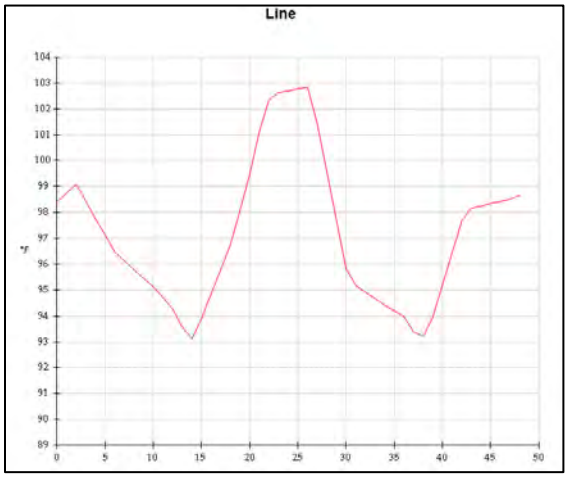

(c)

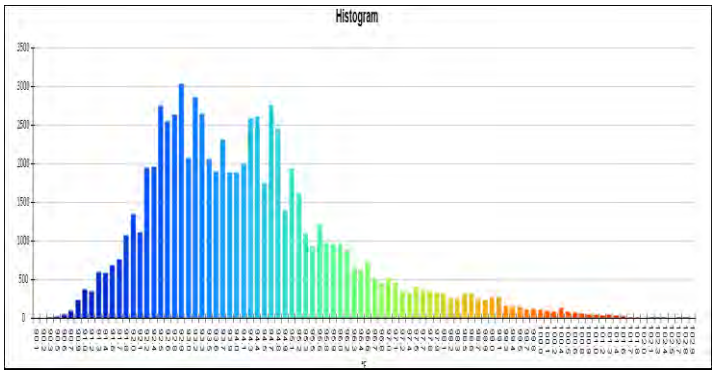

(d)

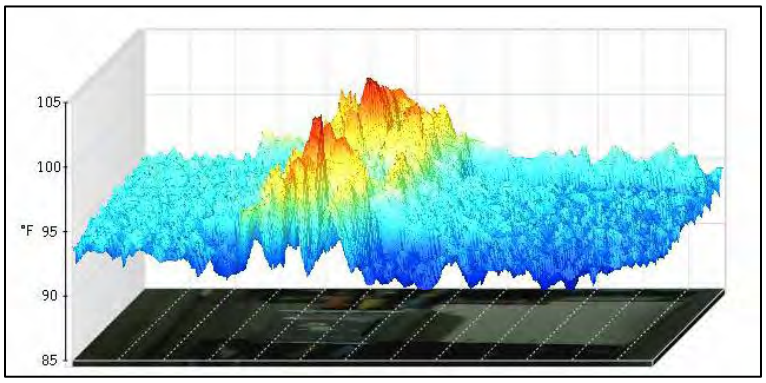

(e)

Figure 2.2*: (a) Line diagram, (b) Histogram and (c) 3D IR Graph of sample Image-01*

Therefore; line diagram, histogram and IR graph show the temperature difference between three different phases of the component.

2.3.2 Report of Thermal Image-02

Name of the equipment: Circuit Breaker

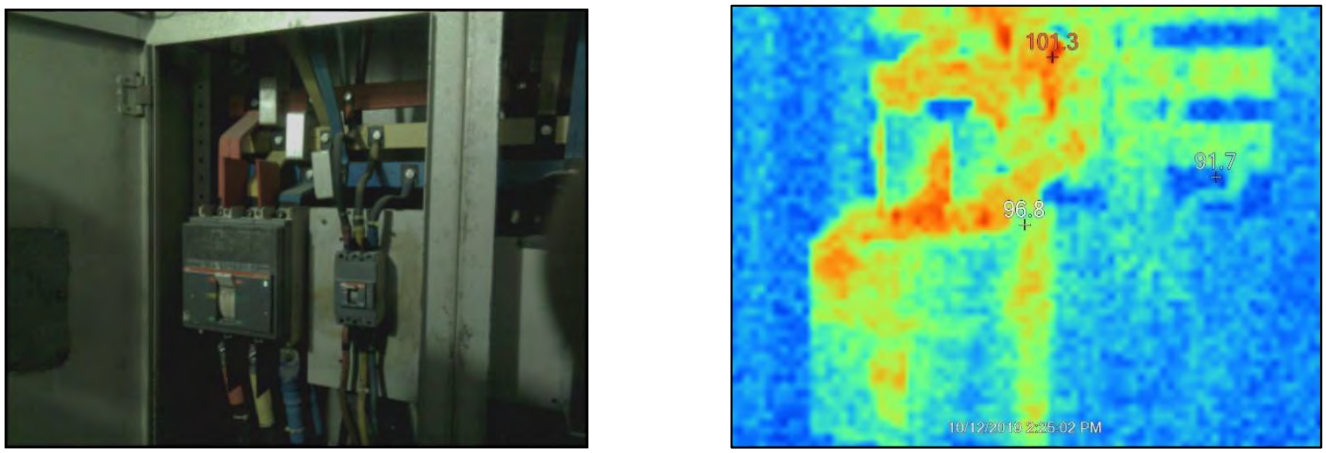

(a) **(b)**

Figure 2.3*: (a) Visible and (b) Thermal representation of sample Image-02*

Here, visible image shows the electrical component and thermal image shows the heat signatures on the component.

(i) Location

This circuit breaker is located at the Distribution Board of the factory-3.

(ii) Defect

There is no defect

(iii) Defect Classification

Table 2.3: *Defect classification of Image-02 according to the "NETA" Standards*

Serial	Temperature from normal heat signature area of components (Celsius)	Temperature from highest heat signature area of components (Celsius)	ΔT between similar components under similar load (Celsius)	Recommended Action/Classification
1	37.5	38.2	0.7	No action needed

(iv) Graph

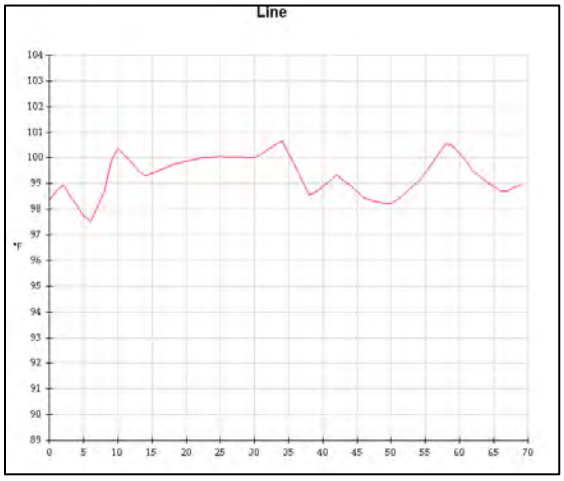

(c)

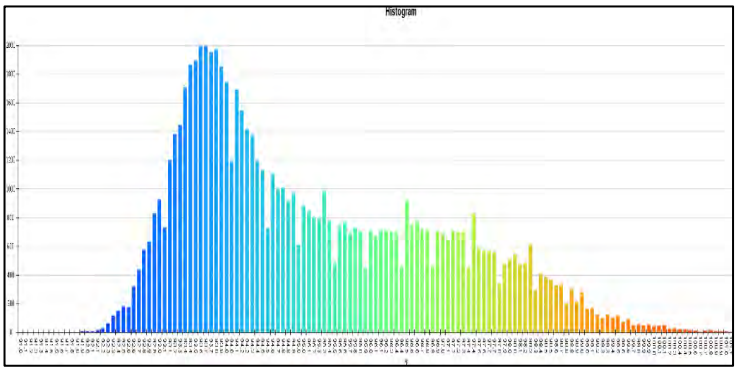

(d)

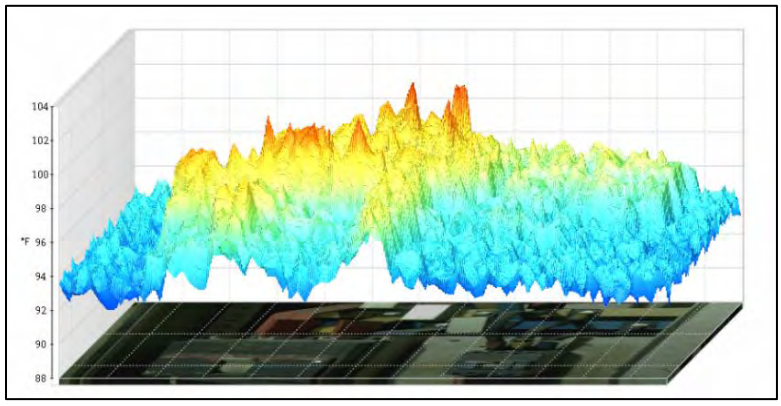

(e)

Figure 2.4*: (a) Line diagram, (b) Histogram and (c) 3D IR Graph of sample Image-02*

Therefore; line diagram, histogram and IR graph show the temperature difference between three different phases of the component.

2.3.3 Report of Thermal Image-03

Name of the equipment: Circuit Breaker

(a)

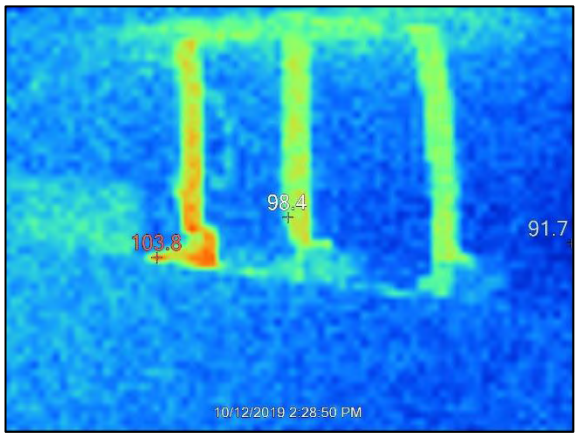

(b)

Figure 2.5*: (a) Visible and (b) Thermal representation of sample Image-03*

Here, visible image shows the electrical component and thermal image shows the heat signatures on the component.

(i) Location:

This circuit breaker is located at the Distribution Board of the Factory-3.

(ii) Defect:

Load imbalance/Overload.

(iii) Defect Classification:

Table 2.4: *Measuring the defect classification of Image-03 according to the "NETA" Standards*

Serial	Temperature from normal heat signature area of components (Celsius)	Temperature from highest heat signature area of components (Celsius)	ΔT between similar components under similar load (Celsius)	Recommended Action/Classification
1	37.2	39.9	2.7	Possible deficiency & investigation warrants.

(iv) Graph:

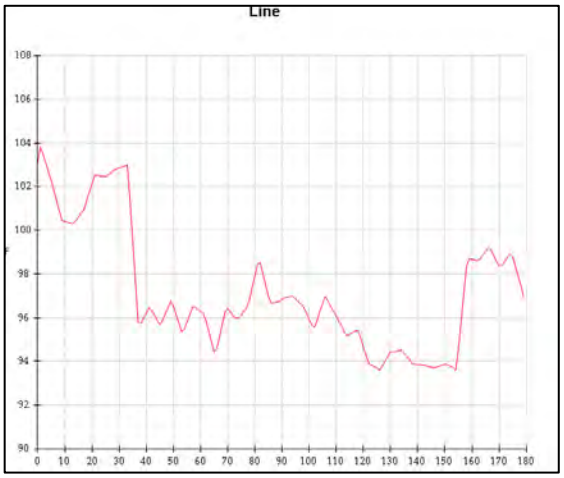

(c)

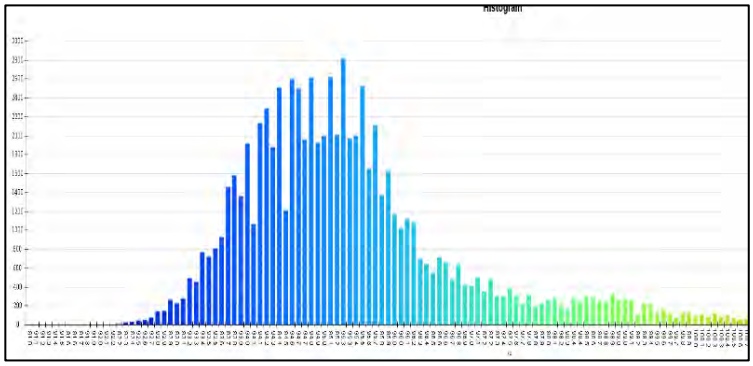

(d)

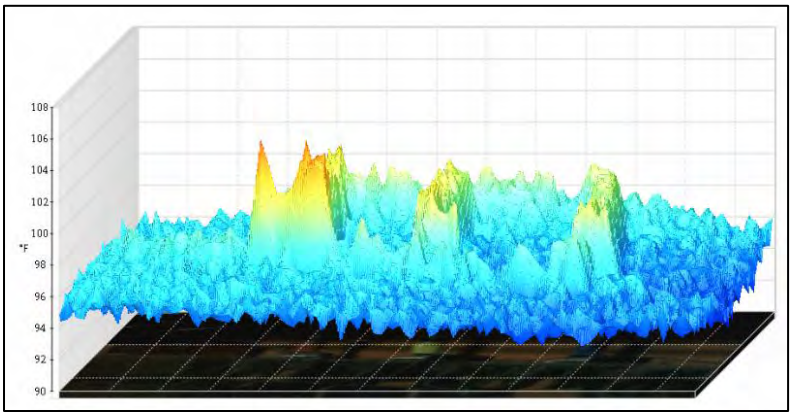

(e)

Figure 2.6*: (a) Line diagram, (b) Histogram and (c) 3D IR Graph of sample Image-03*

Therefore; line diagram, histogram and IR graph show the temperature difference between three different phases of the component.

2.3.4 Report of Thermal Image-04

Name of the equipment: Circuit Breaker

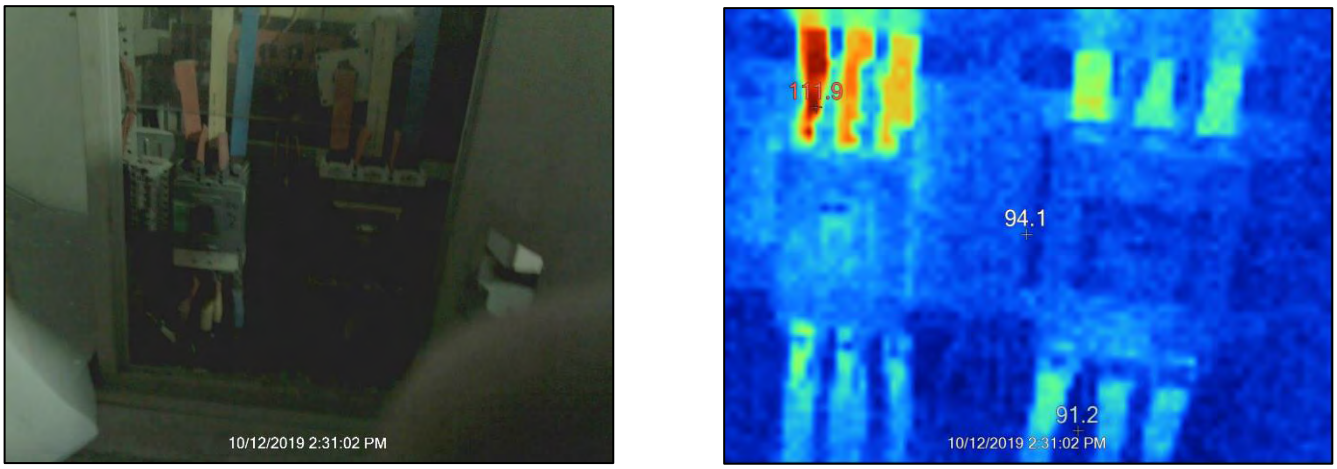

(a) **(b)**

Figure 2.7*: (a) Visible and (b) Thermal representation of sample Image-04*

Here, visible image shows the electrical component and thermal image shows the heat signatures on the component.

(i) Location

This circuit breaker is located at the Distribution Board of the factory-3.

(ii) Defect

Overload in R phase.

(iii) Defect Classification

Table 2.5: *Defect classification of Image-04 according to the "NETA" Standards*

Serial	Temperature from normal heat signature area of components (Celsius)	Temperature from highest heat signature area of components (Celsius)	ΔT between similar components under similar load (Celsius)	Recommended Action/Classification
1	40.3	44.4	4.1	Indicates probable deficiency; repair as time permits

(iv) Graph

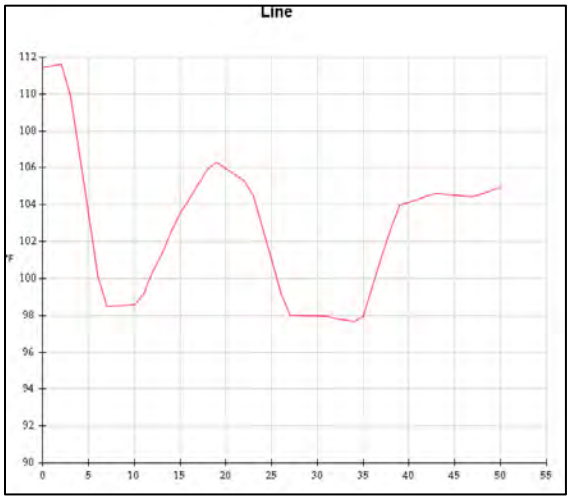

(c)

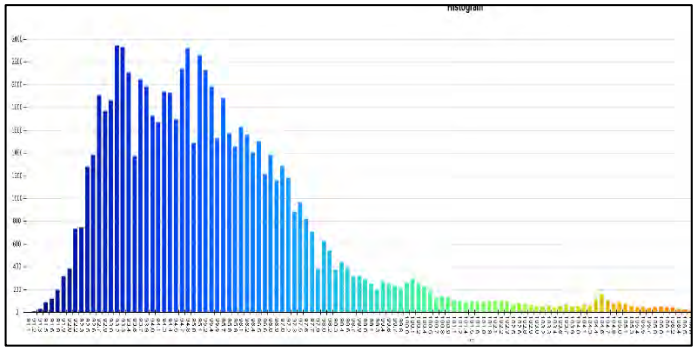

(d)

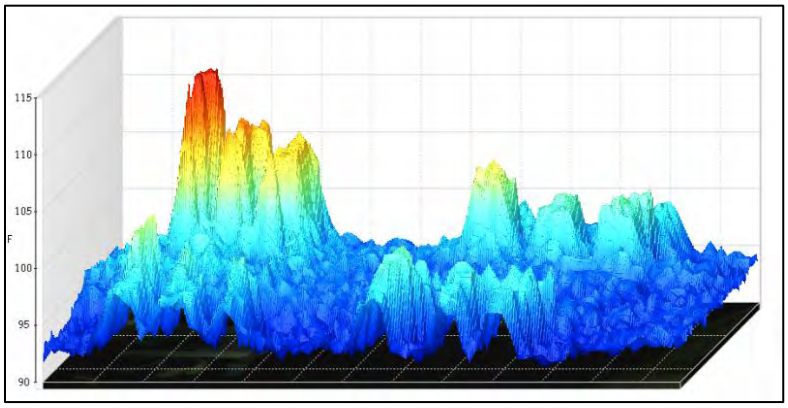

(e)

Figure 2.8*: (a) Line diagram, (b) Histogram and (c) 3D IR Graph of sample Image-04*

Therefore; line diagram, histogram and IR graph show the temperature difference between three different phases of the component.

2.3.5 Report of Thermal Image-05

Name of the equipment: Circuit Breaker

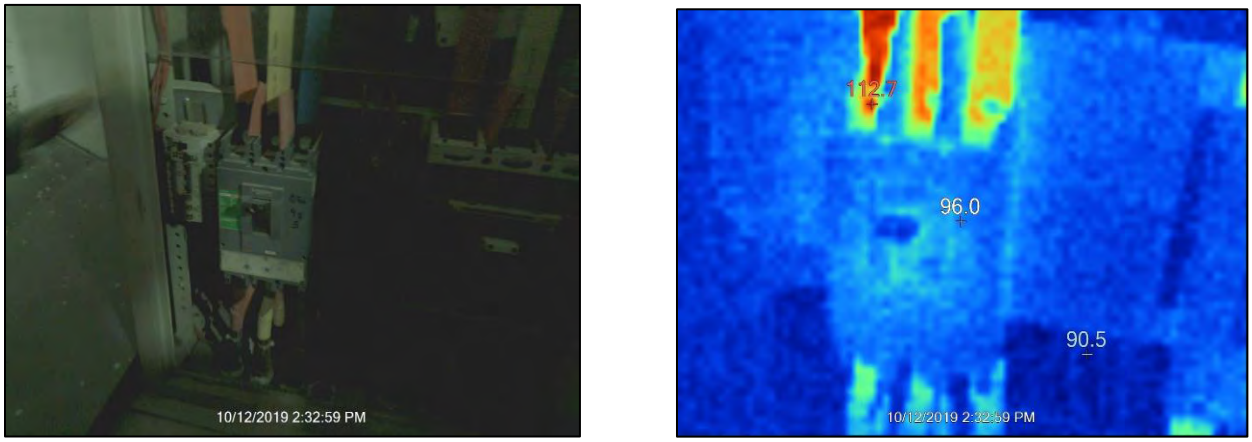

(a) **(b)**

***Figure 2.9**: (a) Visible and (b) Thermal representation of sample Image-05*

Here, visible image shows the electrical component and thermal image shows the heat signatures on the component.

(i) Location

This circuit breaker is located at the Distribution Board of the factory-3.

(ii) Defect

Overload in R phase.

(iii) Defect Classification

***Table 2.6:** Defect classification of Image-05 according to the "NETA" Standards*

Serial	Temperature from normal heat signature area of components (Celsius)	Temperature from highest heat signature area of components (Celsius)	ΔT between similar components under similar load (Celsius)	Recommended Action/Classification
1	40.8	44.8	4	Indicates probable deficiency; repair as time permits

(iv) Graph

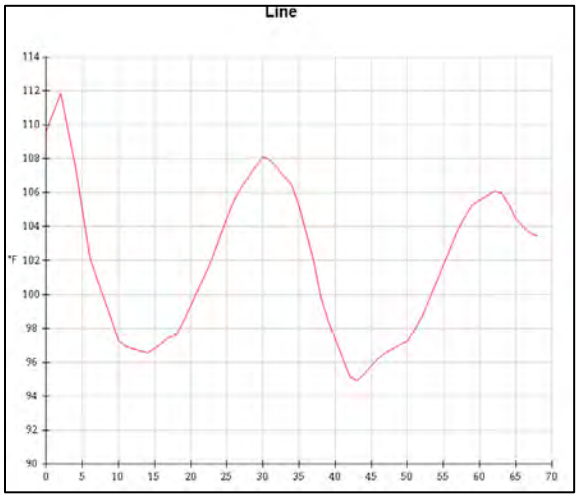

(c)

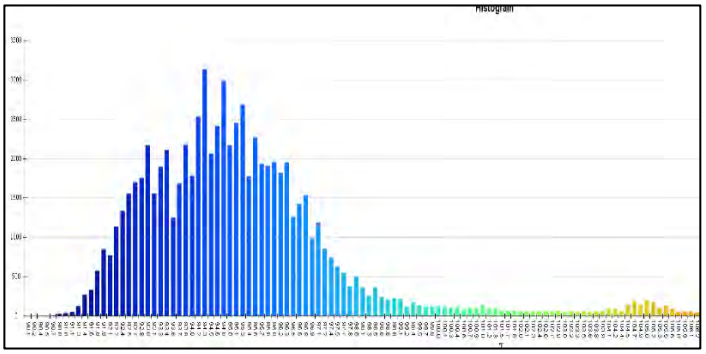

(d)

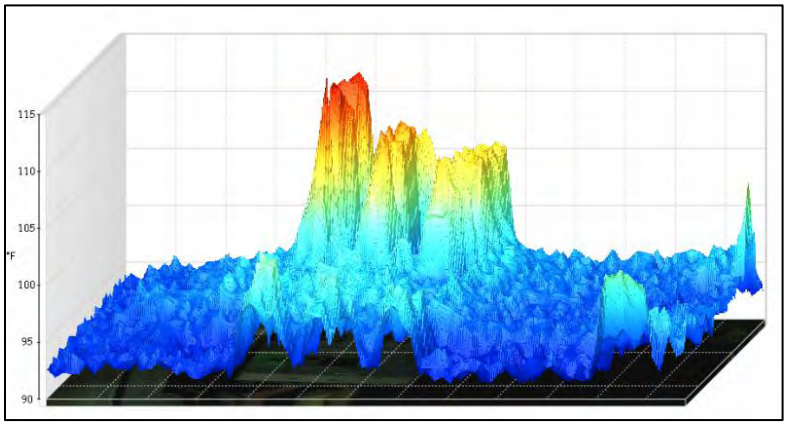

(e)

Figure 3*: (a) Line diagram, (b) Histogram and (c) 3D IR Graph of sample Image-05*

Therefore; line diagram, histogram and IR graph show the temperature difference between three different phases of the component.

2.3.6 Report of Thermal Image-06

Name of the equipment: Transformer

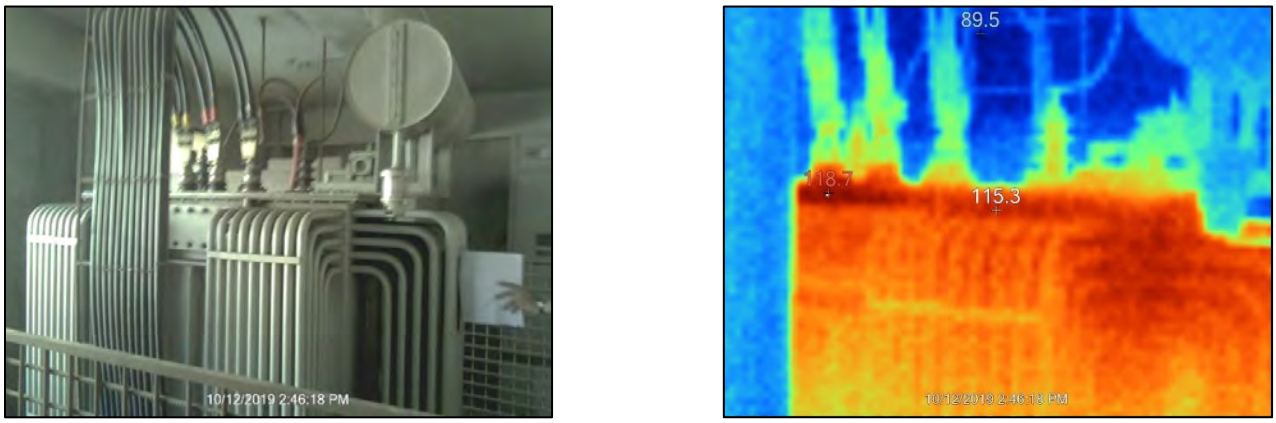

(a) **(b)**

Figure 4*: (a) Visible and (b) Thermal representation of sample Image-06*

Here, visible image shows the electrical component and thermal image shows the heat signatures on the component.

(i) Location

Transformer is on the 1st Floor of the Factory-3 and connected through High voltage transmission line from Substation.

(ii) Defect

Overload in Y phase.

(iii) Defect Classification

Table 2.7: *Defect classification of Image-06 according to the "NETA" Standards*

Serial	Temperature from normal heat signature area of components (Celsius)	Temperature from highest heat signature area of components (Celsius)	ΔT between similar components under similar load (Celsius)	Recommended Action/Classification
1	44.4	48.2	3.8	Indicates probable deficiency; repair as time permits

(iv) Graph

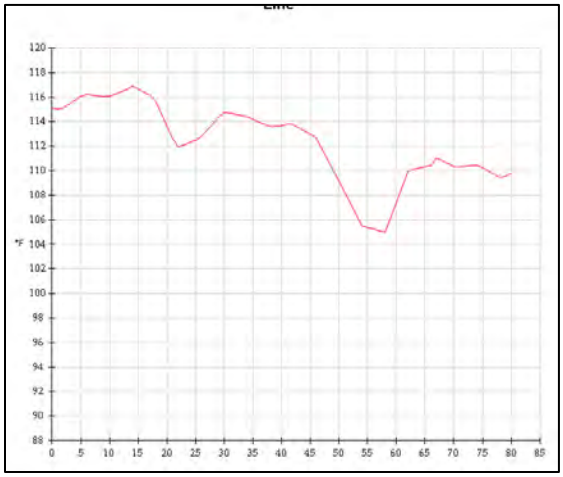

(c)

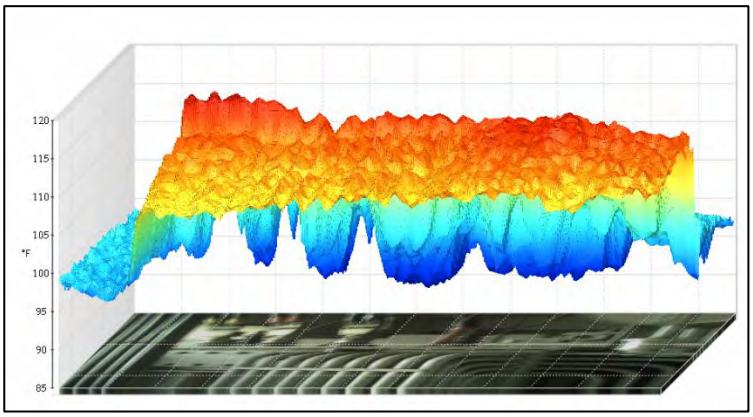

(e)

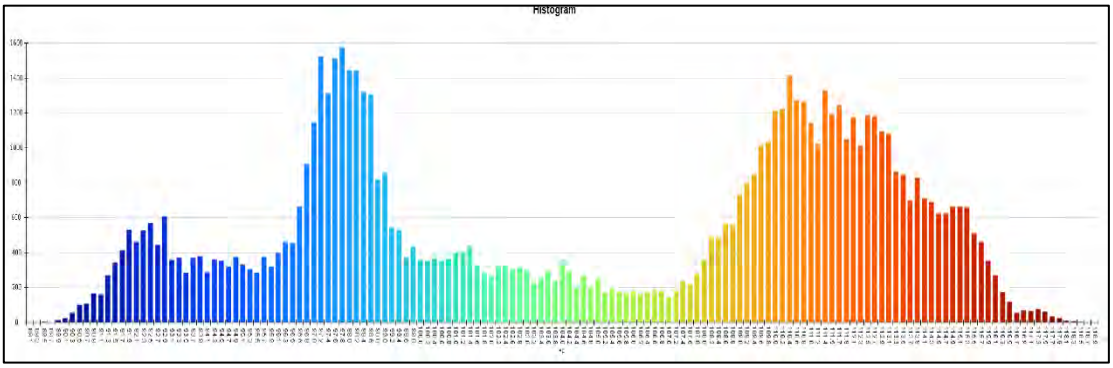

(d)

Figure 5*: (a) Line diagram, (b) Histogram and (c) 3D IR Graph of sample Image-06*

Therefore; line diagram, histogram and IR graph show the temperature difference between three different phases of the component.

2.3.7 Report of Thermal Image-07

Name of the equipment: Transformer

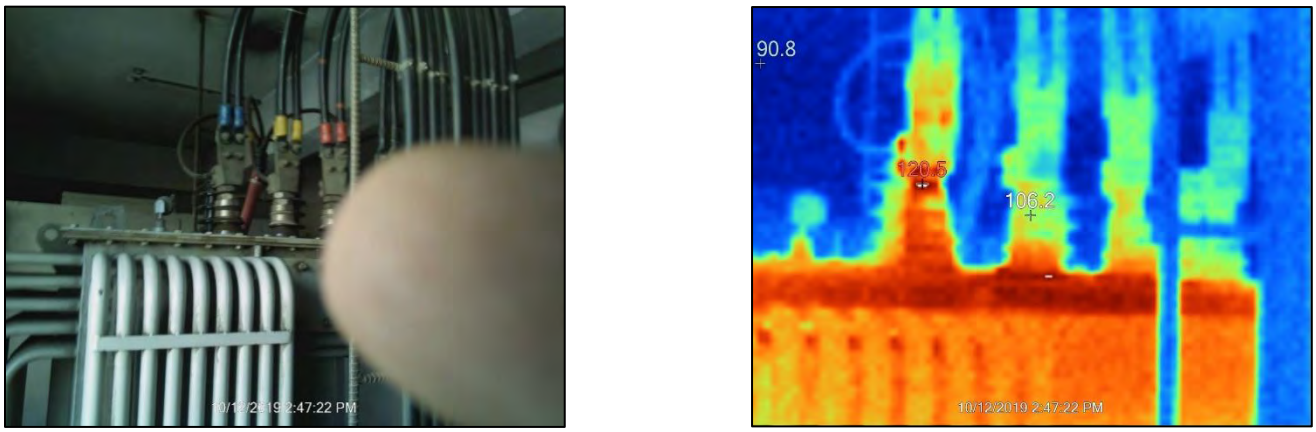

(a) **(b)**

***Figure 2.13**: (a) Visible and (b) Thermal representation of sample Image-07*

Here, visible image shows the electrical component and thermal image shows the heat signatures on the component.

(i) Location

Transformer is on the 1st Floor of the factory-3 and connected through High voltage line from Substation.

(ii) Defect

Overload in B phase.

(iii) Defect Classification

***Table 2.3:** Defect classification of Image-07 according to the "NETA" Standards*

Serial	Temperature from normal heat signature area of components (Celsius)	Temperature from highest heat signature area of components (Celsius)	ΔT between similar components under similar load (Celsius)	Recommended Action/Classification
1	42.8	49.2	6.4	Indicates probable deficiency; repair as time permits

(iv) Graph

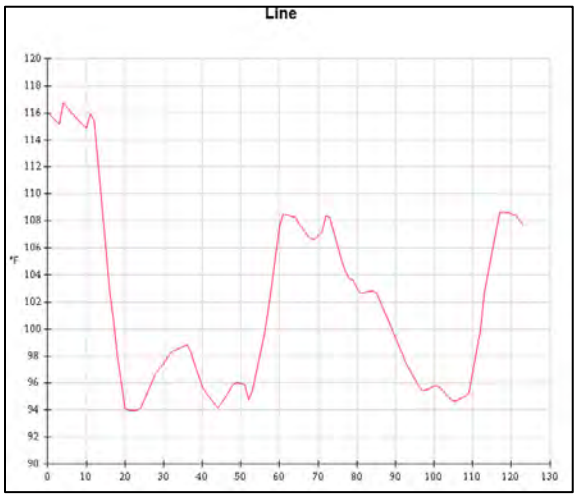

(c)

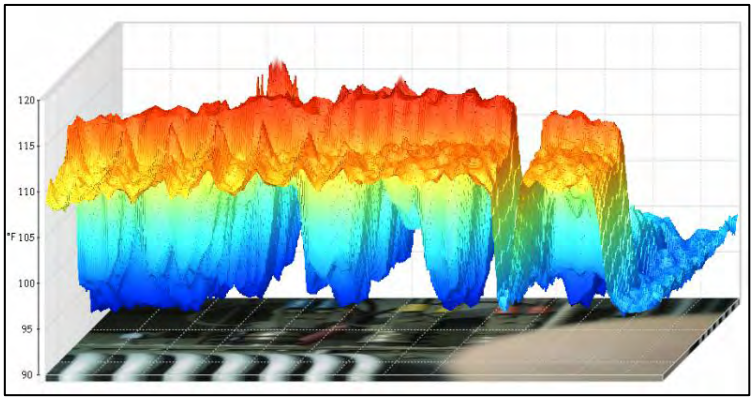

(e)

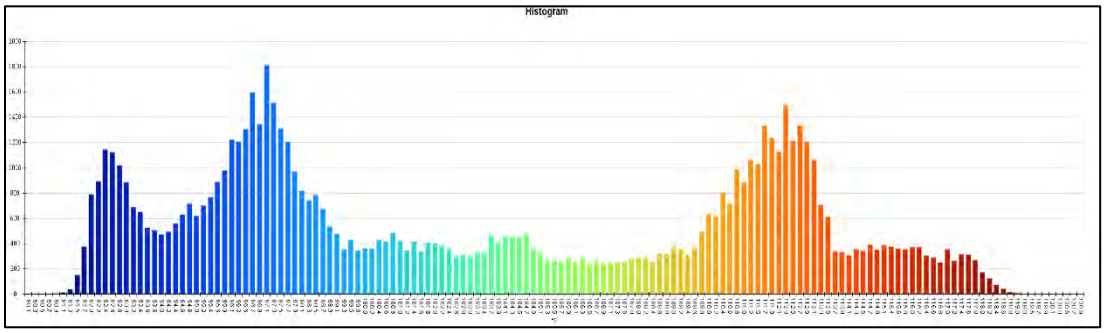

(d)

Figure 2.14*: (a) Line diagram, (b) Histogram and (c) 3D IR Graph of sample Image-07*

Therefore; line diagram, histogram and IR graph show the temperature difference between three different phases of the component.

2.3.8 Report of Thermal Image-08

Name of the equipment: Transformer

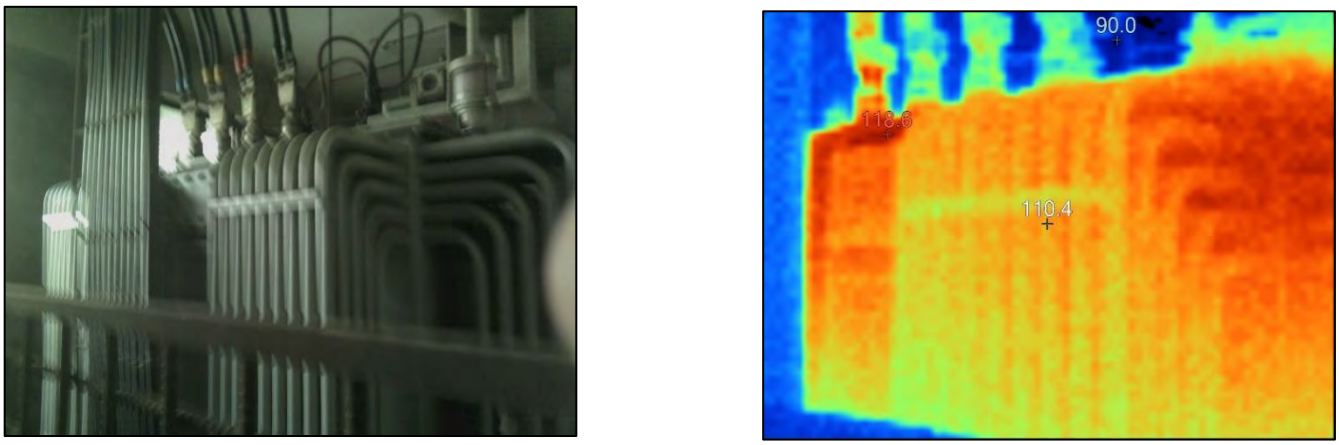

(a) **(b)**

Figure 6*: (a) Visible and (b) Thermal representation of sample Image-08*

Here, visible image shows the electrical component and thermal image shows the heat signatures on the component.

(i) Location

This Transformer is located at the first floor of the factory-3.

(ii) Defect

Load difference between the phases R, Y & B.
Phase B is the higher load phase and that is why it was showing more heat signature.

(iii) Defect Classification

Table 2.4: *Defect classification of Image-08 according to the "NETA" Standards*

Sl. No.	Temperature from normal heat signature area of components (Celsius)	Temperature from highest heat signature area of components (Celsius)	ΔT between similar components under similar load (Celsius)	Recommended Action/Classification
1	43.9	48.11	4.21	Indicates probable deficiency repair as time permits

(iv) Graph

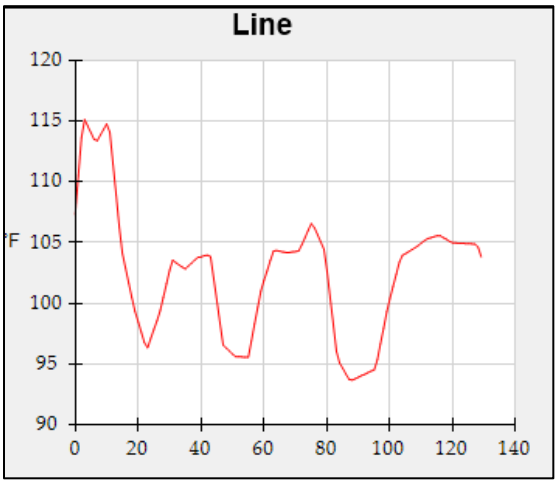

(c)

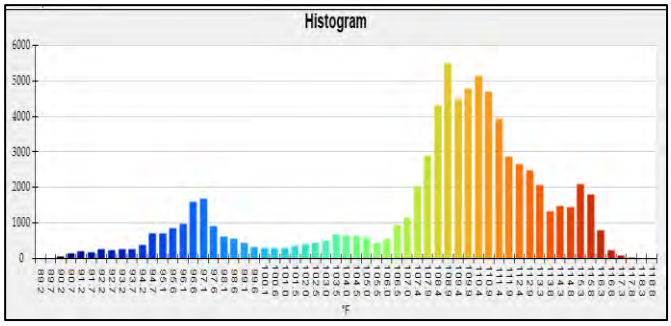

(d)

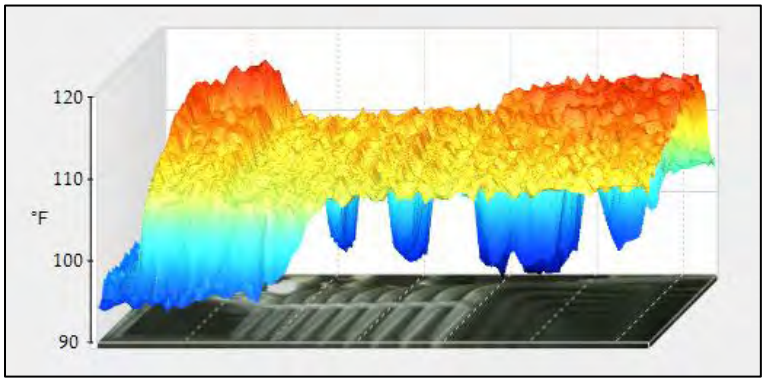

(e)

Figure 7.16*: (a) Line diagram, (b) Histogram and (c) 3D IR Graph of sample Image-08*

Therefore; line diagram, histogram and IR graph show the temperature difference between three different phases of the component.

2.3.9 Report of Thermal Image-09

Name of the equipment: Transformer

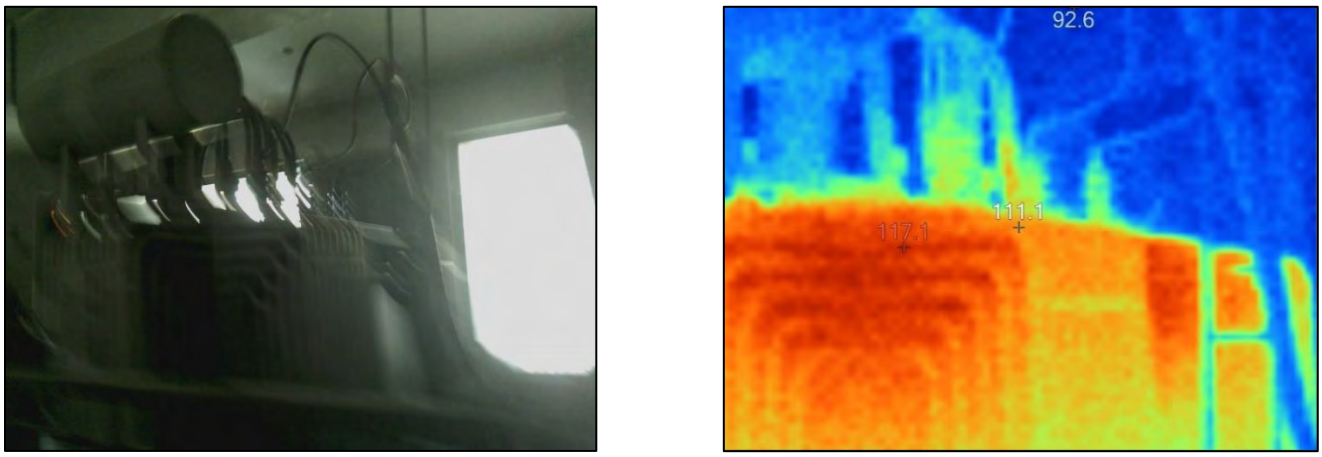

(a) **(b)**

Figure 2.17*: (a) Visible and (b) Thermal representation of sample Image-09*

Here, visible image shows the electrical component and thermal image shows the heat signatures on the component.

(i) Location

This Transformer is located at the first floor of the Factory-3.

(ii) Defect

Not detected in the Image

(iii) Defect Classification

Table 2.5: *Defect classification of Image-09 according to the "NETA" Standards*

Sl. No.	Temperature from normal heat signature area of components (Celsius)	Temperature from highest heat signature area of components (Celsius)	ΔT between similar components under similar load (Celsius)	Recommended Action/Classification
1	43.9	47.28	3.38	Indicates probable deficiency repair as time permits

(iv) Graph

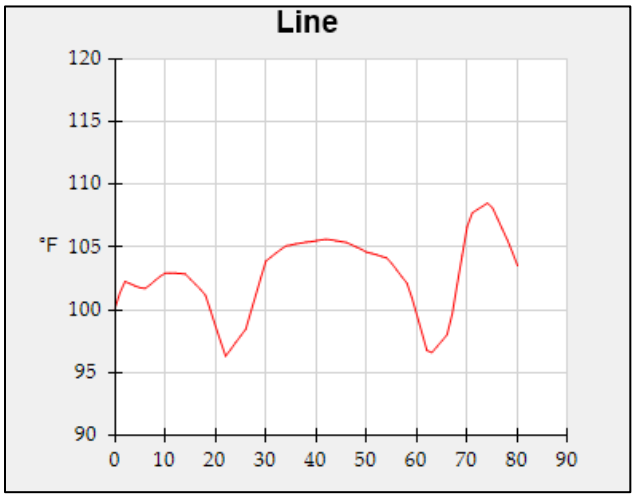

(c)

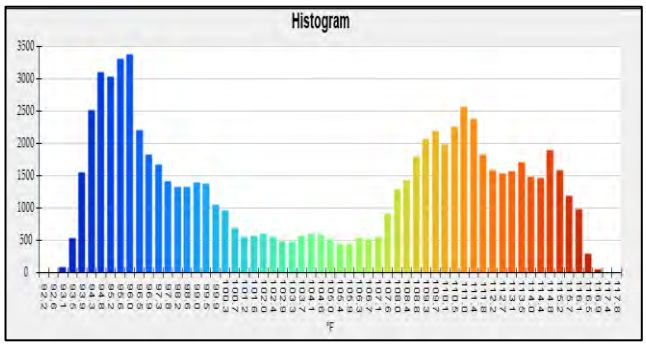

(d)

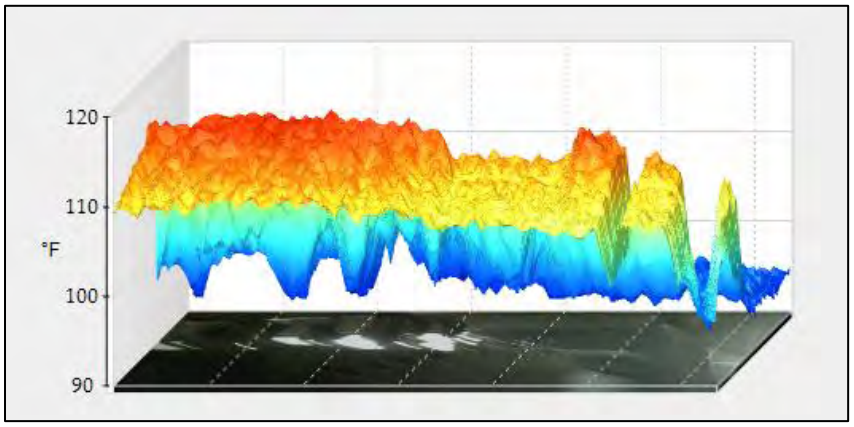

(e)

Figure 2.18*: (a) Line diagram, (b) Histogram and (c) 3D IR Graph of sample Image-09*

Therefore; line diagram, histogram and IR graph show the temperature difference between three different phases of the component.

2.3.10 Report of Thermal Image-10

Name of the equipment: Circuit Breaker

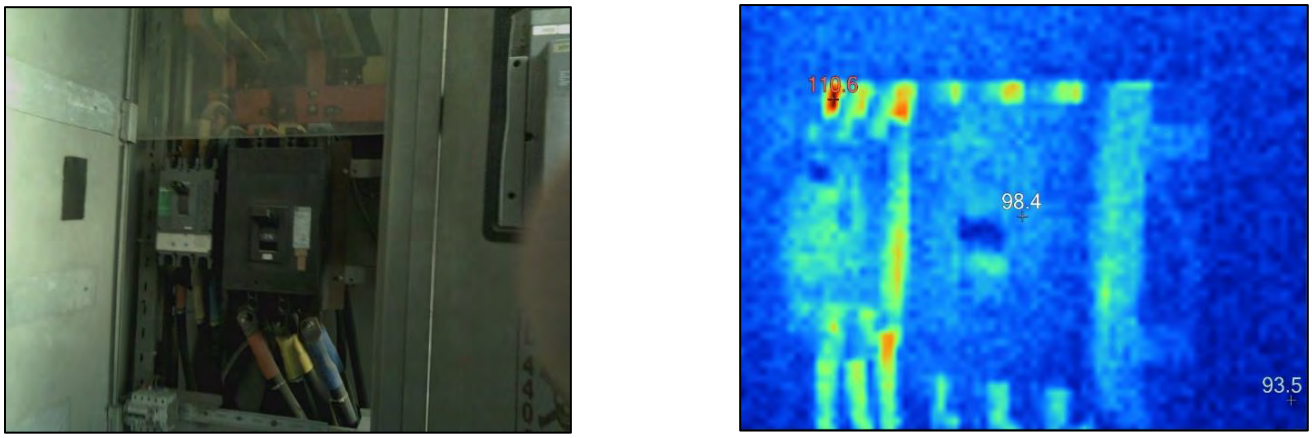

(a) **(b)**

Figure 8*: (a) Visible and (b) Thermal representation of sample Image-10*

Here, visible image shows the electrical component and thermal image shows the heat signatures on the component.

(i) Location

This Transformer is located at the Main Distribution Board (MDB) of the Factory-3.

(ii) Defect

Load difference between the phases R, Y & B.
Phase R is the higher load phase and that is why it was showing more heat signature.

(iii) Defect Classification

Table 2.6: *Defect classification of Image-10 according to the "NETA" Standards*

Sl. No.	Temperature from normal heat signature area of components (Celsius)	Temperature from highest heat signature area of components (Celsius)	ΔT between similar components under similar load (Celsius)	Recommended Action/Classification
1	40.22	43.7	3.48	Indicates probable deficiency repair as time permits

(iv) Graph

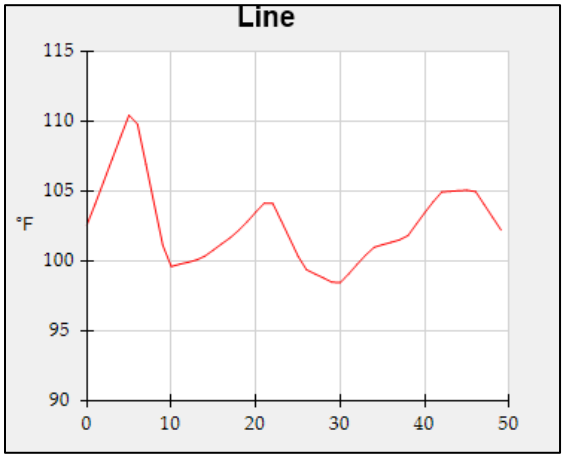

(c)

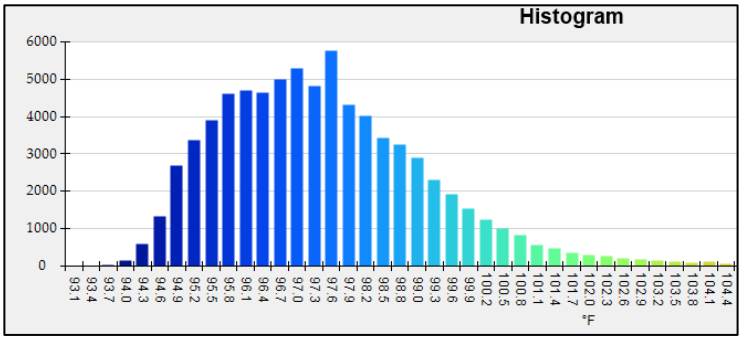

(d)

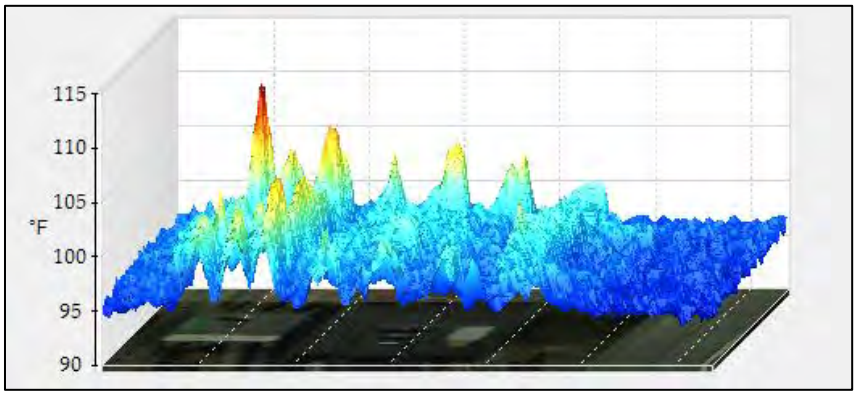

(e)

***Figure 9**: (a) Line diagram, (b) Histogram and (c) 3D IR Graph of sample Image-10*

Therefore; line diagram, histogram and IR graph show the temperature difference between three different phases of the component.

2.3.11 Report of Thermal Image-11

Name of the equipment: Circuit Breaker

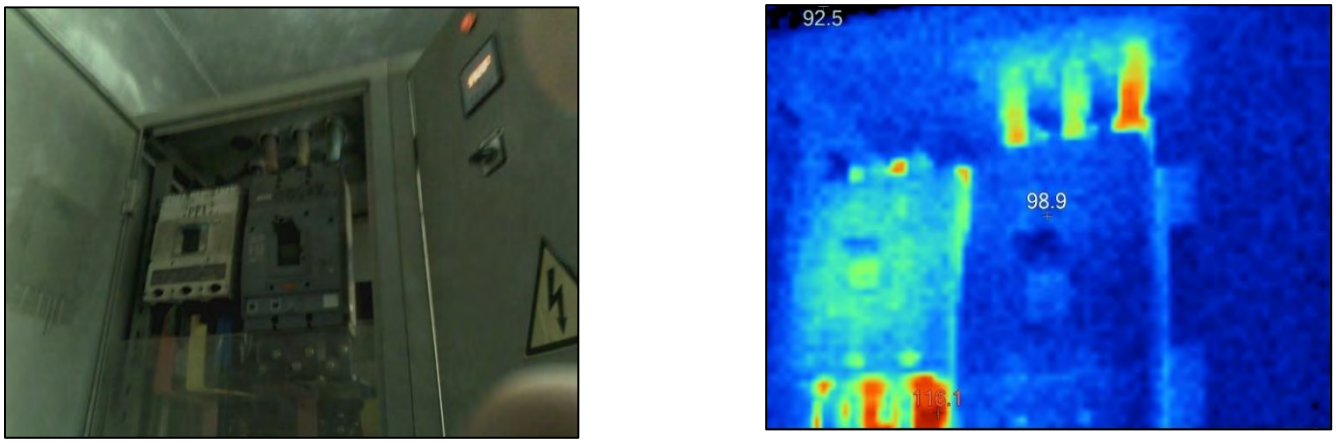

(a) **(b)**

Figure 101*: (a) Visible and (b) Thermal representation of sample Image-11*

Here, visible image shows the electrical component and thermal image shows the heat signatures on the component.

(i) Location

This Transformer is located at the Main Distribution Board (MDB) of the factory-3.

(ii) Defect

Load difference between the phases R, Y & B.
Phase B is the higher load phase and that is why it was showing more heat signature.

(iii) Defect Classification

Table 2.7: *Defect classification of Image-11 according to the "NETA" Standards*

Sl. No.	Temperature from normal heat signature area of components (Celsius)	Temperature from highest heat signature area of components (Celsius)	ΔT between similar components under similar load (Celsius)	Recommended Action/Classification
1	40.8	44.72	3.92	Indicates probable deficiency repair as time permits

(iv) Graph

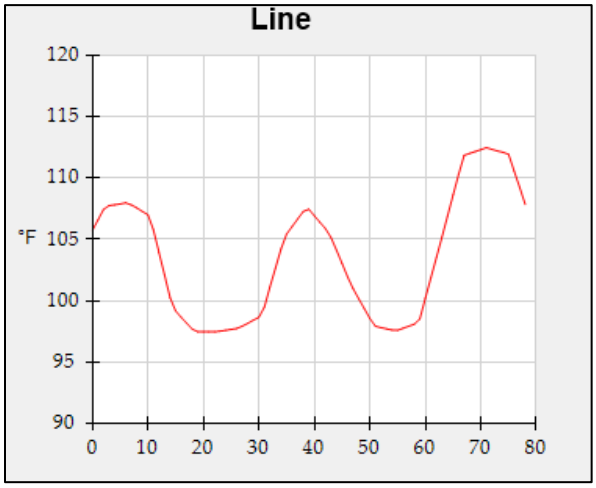

(c)

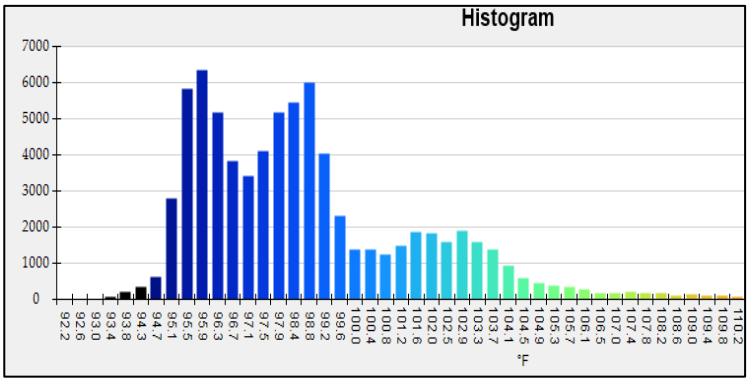

(d)

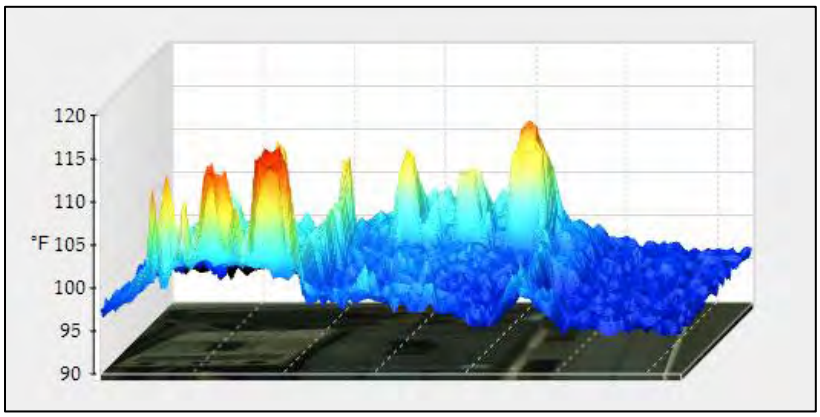

(e)

Figure 2.22*: (a) Line diagram, (b) Histogram and (c) 3D IR Graph of sample Image-11*

Therefore; line diagram, histogram and IR graph show the temperature difference between three different phases of the component.

2.3.12 Report of Thermal Image-12

Name of the equipment: Circuit Breaker

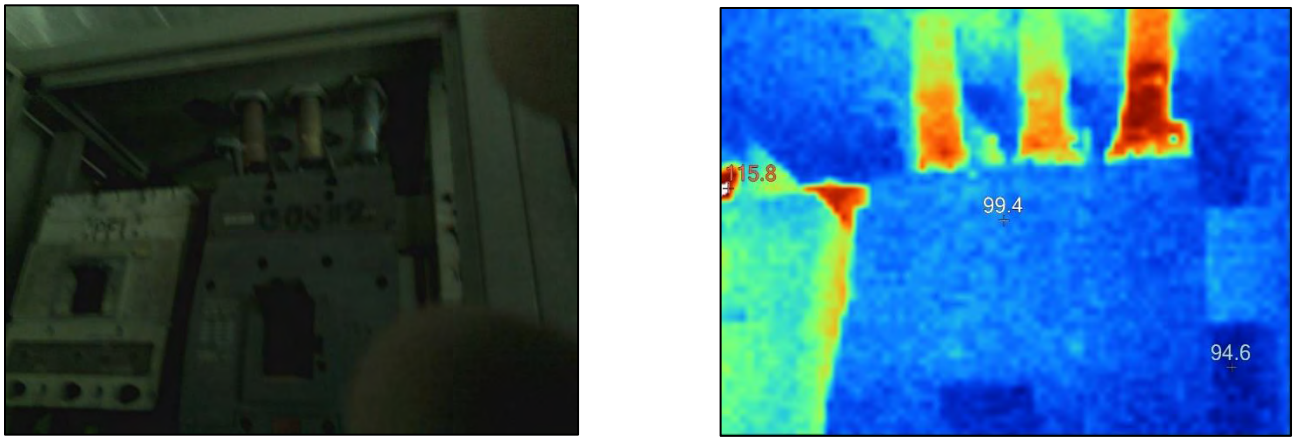

(a) **(b)**

***Figure 2.23**: (a) Visible and (b) Thermal representation of sample Image-12*

Here, visible image shows the electrical component and thermal image shows the heat signatures on the component.

(i) Location

This Transformer is located at the Main Distribution Board (MDB) of the factory-3.

(ii) Defect

Load difference between the phases R, Y & B.
Phase B is the higher load phase and that is why it was showing more heat signature.

(iii) Defect Classification

***Table 2.8:** Defect classification of Image-12 according to the "NETA" Standards*

Sl. No.	Temperature from normal heat signature area of components (Celsius)	Temperature from highest heat signature area of components (Celsius)	ΔT between similar components under similar load (Celsius)	Recommended Action/Classification
1	41.8	44.8	3	Possible deficiency warrants investigation

(iv) Graph

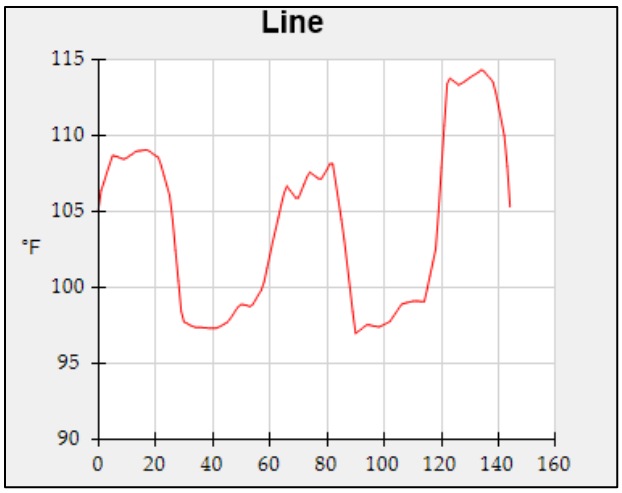

(c)

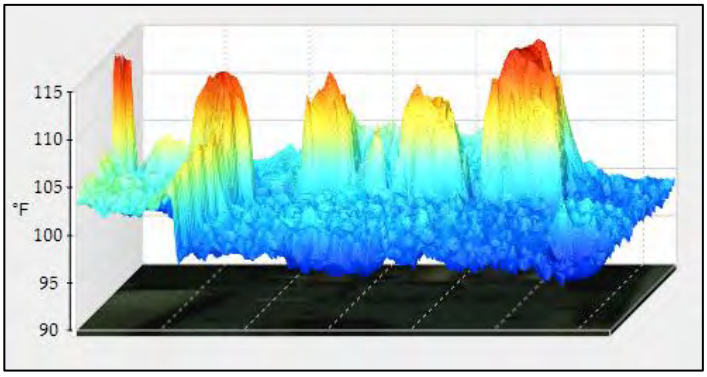

(d)

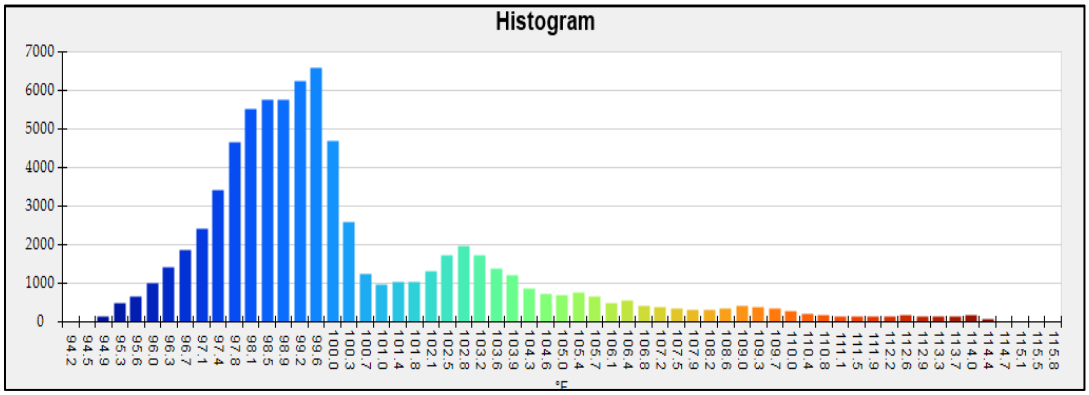

(e)

Figure 11*: (a) Line diagram, (b) Histogram and (c) 3D IR Graph of sample Image-12*

Therefore; line diagram, histogram and IR graph show the temperature difference between three different phases of the component.

2.3.13 Report of Thermal Image-13

Name of the equipment: Circuit Breaker

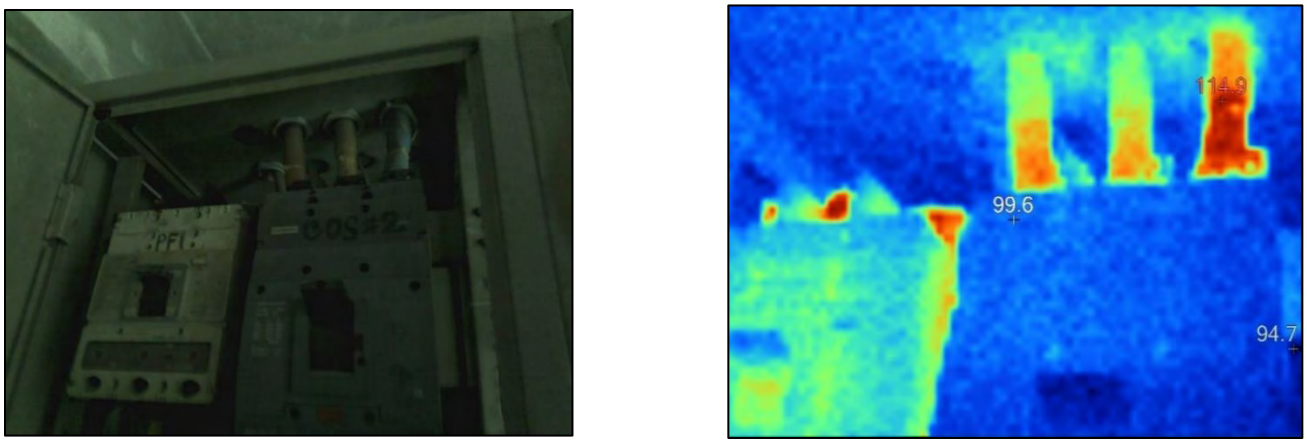

(a) **(b)**

***Figure 2.25**: (a) Visible and (b) Thermal representation of sample Image-13*

Here, visible image shows the electrical component and thermal image shows the heat signatures on the component.

(i) Location

This Transformer is located at the Main Distribution Board (MDB) of the Factory-3.

(ii) Defect

Load difference between the phases R, Y & B.
Phase B is the higher load phase and that is why it was showing more heat signature.

(iii) Defect Classification

***Table 2.9:** Defect classification of Image-13 according to the "NETA" Standards*

Sl. No.	Temperature from normal heat signature area of components (Celsius)	Temperature from highest heat signature area of components (Celsius)	ΔT between similar components under similar load (Celsius)	Recommended Action/Classification
1	40.8	46.06	5.26	Indicates probable deficiency repair as time permits

(iv) Graph

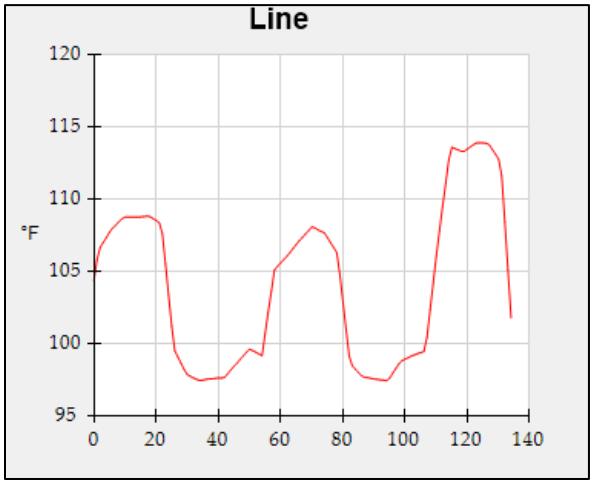

(c)

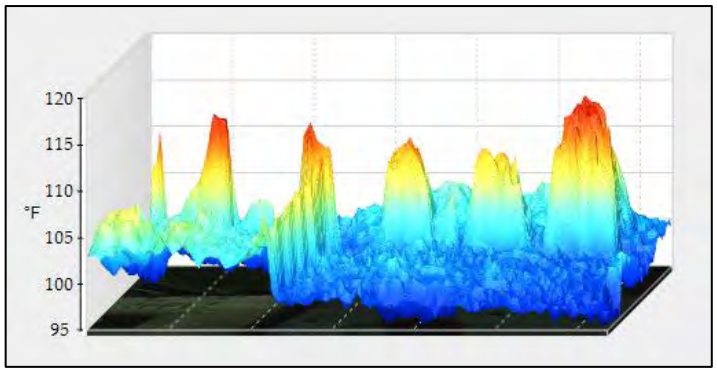

(d)

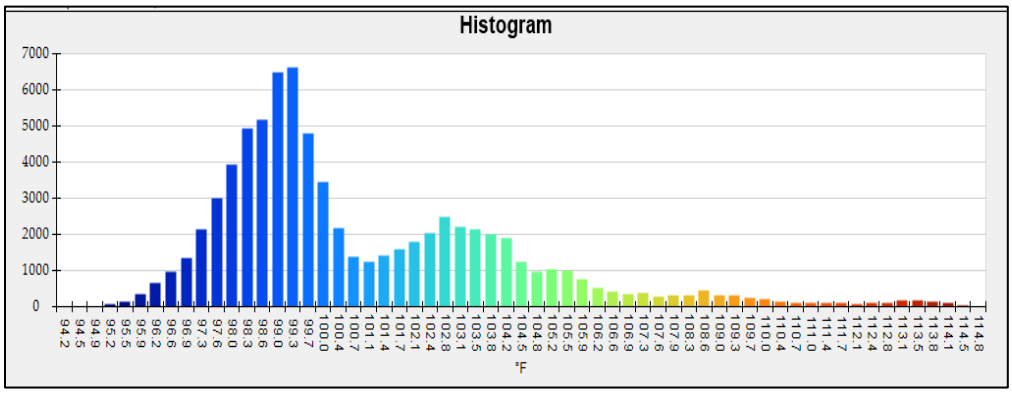

(e)

Figure 12*: (a) Line diagram, (b) Histogram and (c) 3D IR Graph of sample Image-13*

Therefore; line diagram, histogram and IR graph show the temperature difference between three different phases of the component.

2.3.14 Report of Thermal Image-14

Name of the equipment: PFI Board

(a) **(b)**

***Figure 2.27**: (a) Visible and (b) Thermal representation of sample Image-14*

Here, visible image shows the electrical component and thermal image shows the heat signatures on the component.

(i) Location

This PFI Board is located at the Main Distribution Board (MDB) of the factory-3.

(ii) Defect

The factory was full of inductive load. To maintain the power factor the capacitors are injecting apparent power that causes heating.

(iii) Defect Classification

***Table 2.10:** Defect classification of Image-14 according to the "NETA" Standards*

Sl. No.	Temperature from normal heat signature area of components (Celsius)	Temperature from highest heat signature area of components (Celsius)	ΔT between similar components under similar load (Celsius)	Recommended Action/Classification
1	38.11	56.94	18.83	Major discrepancy; repair immediately

(iv) Graph

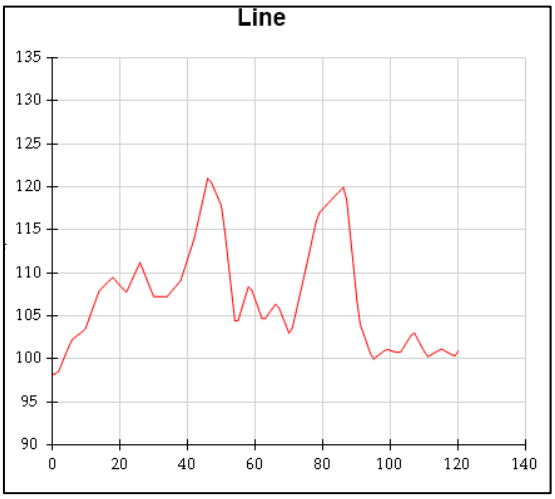

(c)

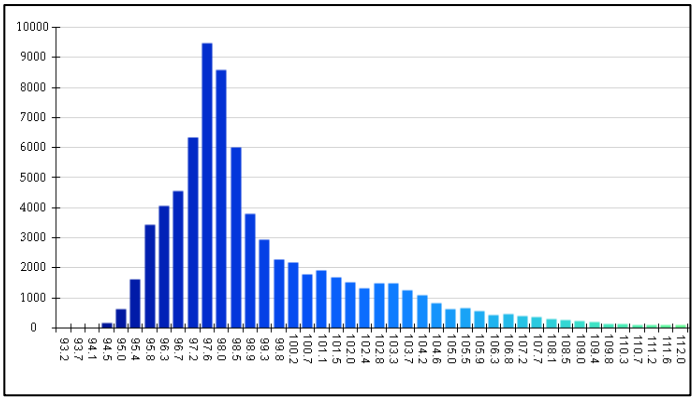

(d)

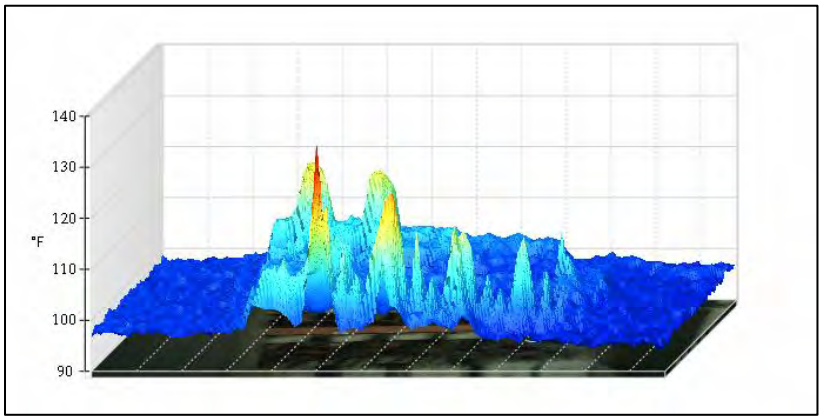

(e)

Figure 2.28*: (a) Line diagram, (b) Histogram and (c) 3D IR Graph of sample Image-14*

Therefore; line diagram, histogram and IR graph show the temperature difference between three different phases of the component.

2.3.15 Report of Thermal Image-15

Name of the equipment: Circuit breaker

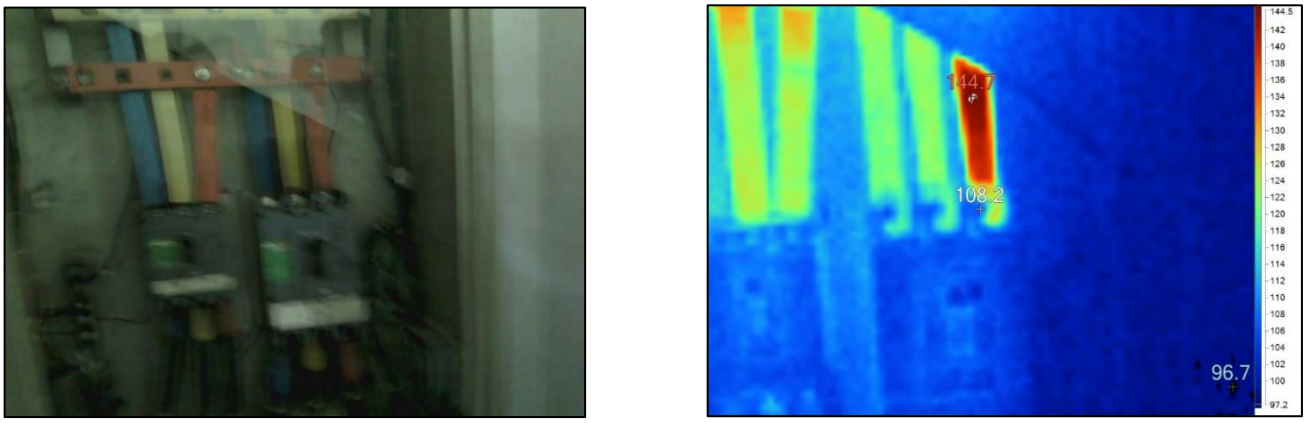

(a) **(b)**

***Figure 2.29**: (a) Visible and (b) Thermal representation of sample Image-15*

Here, visible image shows the electrical component and thermal image shows the heat signatures on the component.

(i) Location

This circuit breaker is located at the Main Distribution Board (MDB) of the factory-3.

(ii) Defect

The R phase heating due to phase imbalance. All the phase is not carrying same current.

(iii) Defect Classification

***Table 2.11:** Defect classification of Image-15 according to the "NETA" Standards*

Sl. No.	Temperature from normal heat signature area of components (Celsius)	Temperature from highest heat signature area of components (Celsius)	ΔT between similar components under similar load (Celsius)	Recommended Action/Classification
1	41.33	62.61	20.28	Major discrepancy; repair immediately

(iv) Graph

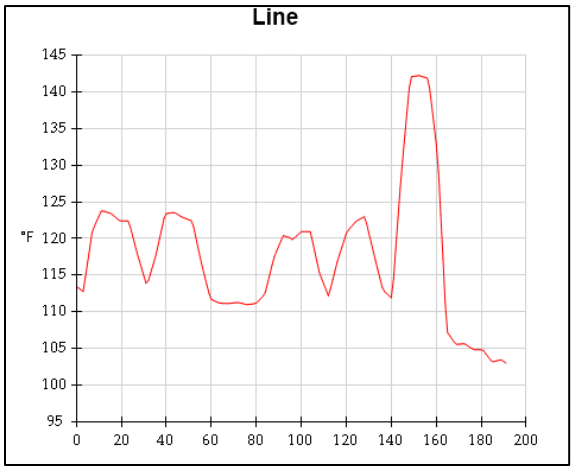

(c)

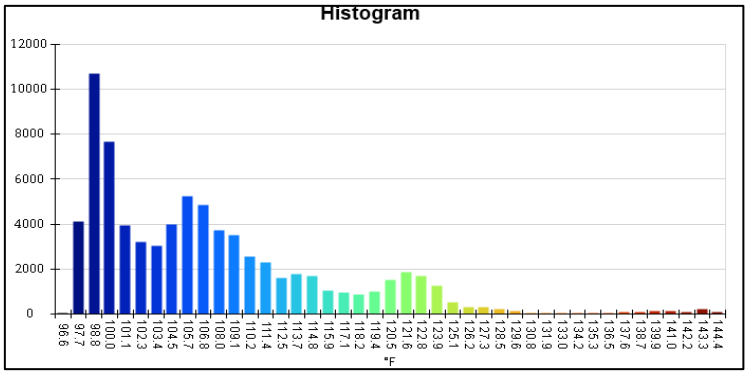

(d)

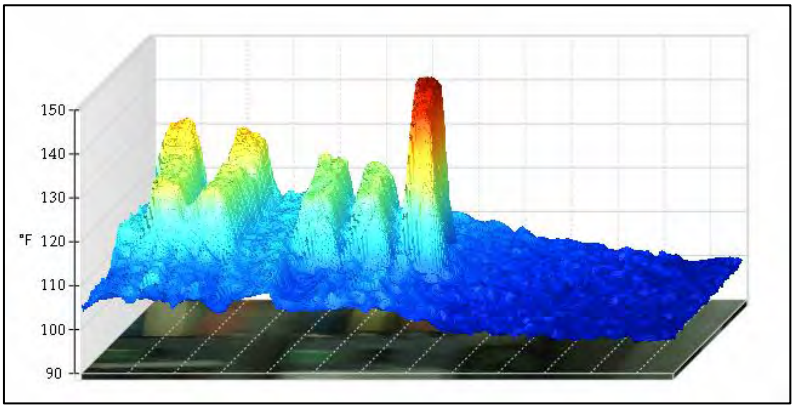

(e)

Figure 2.30*: (a) Line diagram, (b) Histogram and (c) 3D IR Graph of sample Image-15*

Therefore; line diagram, histogram and IR graph show the temperature difference between three different phases of the component.

2.3.16 Report of Thermal Image-16

Name of the equipment: Circuit breaker

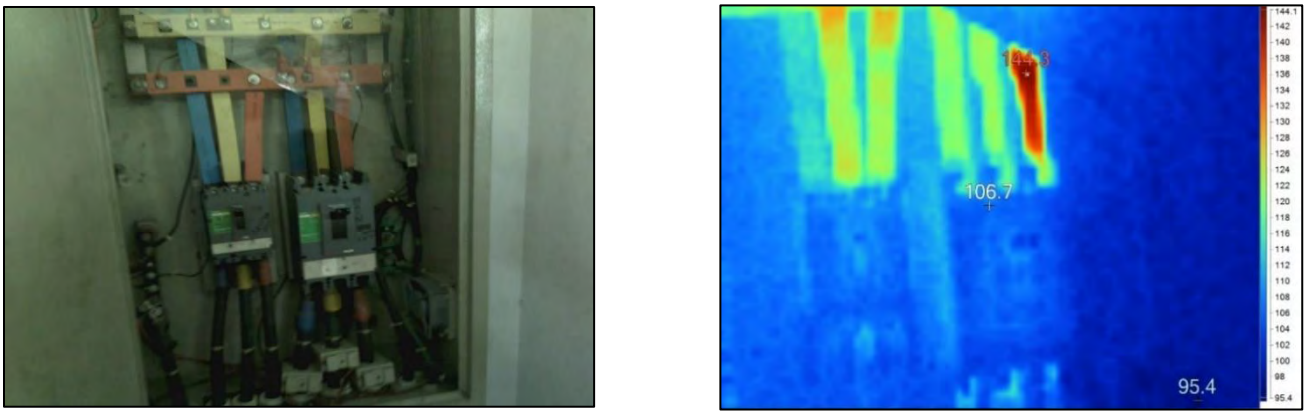

(a) **(b)**

Figure 2.31*: (a) Visible and (b) Thermal representation of sample Image-16*

Here, visible image shows the electrical component and thermal image shows the heat signatures on the component.

(i) Location

This circuit breaker is located at the Main Distribution Board (MDB) of the Factory-3.

(ii) Defect

The R phase heating due phase imbalance. All the phase is not carrying same current

(iii) Defect Classification

Table 2.12: *Defect classification of Image-16 according to the "NETA" Standards*

Sl. No.	Temperature from normal heat signature area of components (Celsius)	Temperature from highest heat signature area of components (Celsius)	ΔT between similar components under similar load (Celsius)	Recommended Action/Classification
1	41.5	62.38	20.88	Major discrepancy; repair immediately

(iv) Graph

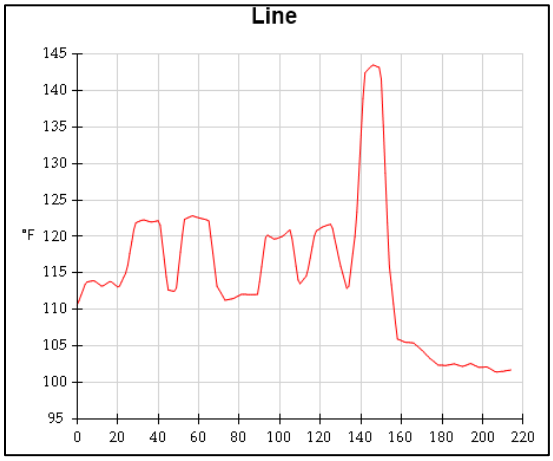

(c)

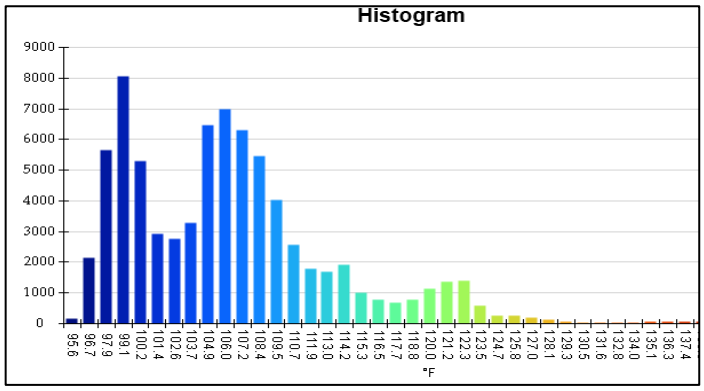

(d)

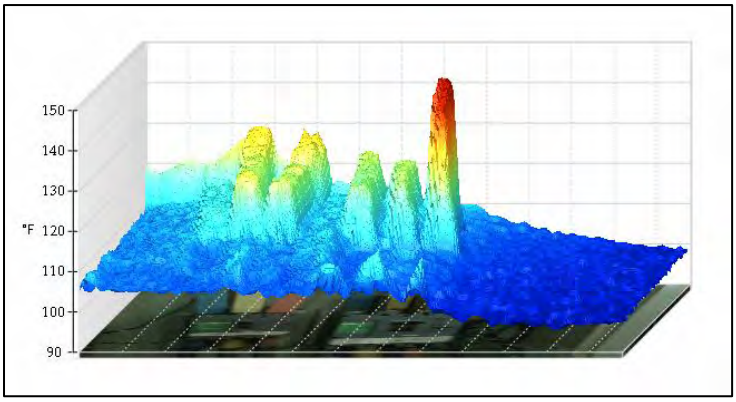

(e)

Figure 2.32*: (a) Line diagram, (b) Histogram and (c) 3D IR Graph of sample Image-16*

Therefore; line diagram, histogram and IR graph show the temperature difference between three different phases of the component.

2.3.17 Report of Thermal Image-17

Name of the equipment: Ceiling fan

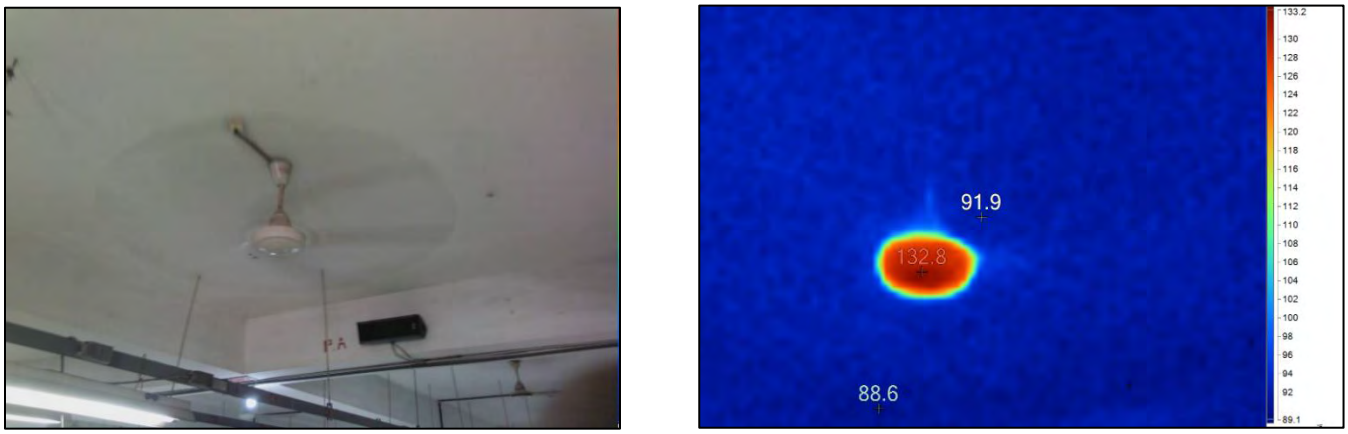

(a) **(b)**

***Figure 2.33**: (a) Visible and (b) Thermal representation of sample Image-17*

Here, visible image shows the electrical component and thermal image shows the heat signatures on the component.

(i) Location

This fan is located on cutting section of the Factory-3.

(ii) Defect

The fan is heating.

(iii) Defect Classification

***Table 2.13:** Defect classification of Image-17 according to the "NETA" Standards*

Sl. No.	Temperature from normal heat signature area of components (Celsius)	Temperature from highest heat signature area of components (Celsius)	ΔT between similar components under similar load (Celsius)	Recommended Action/Classification
1	33.22	56	23.67	Major discrepancy; repair immediately

(iv) Graph

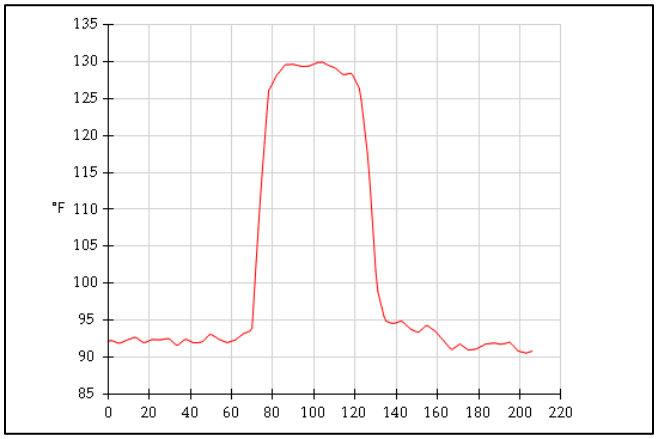

(c)

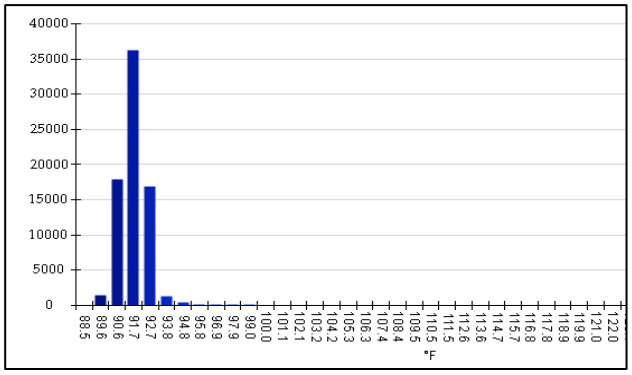

(d)

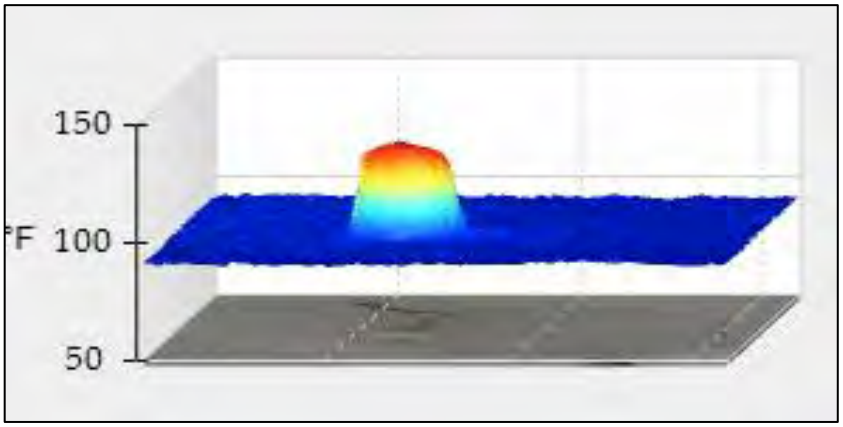

(e)

Figure 2.34*: (a) Line diagram, (b) Histogram and (c) 3D IR Graph of sample Image-17*

Therefore; line diagram, histogram and IR graph show the temperature difference between three different phases of the component.

2.3.18 Report of Thermal Image-18

Name of the equipment: Motor

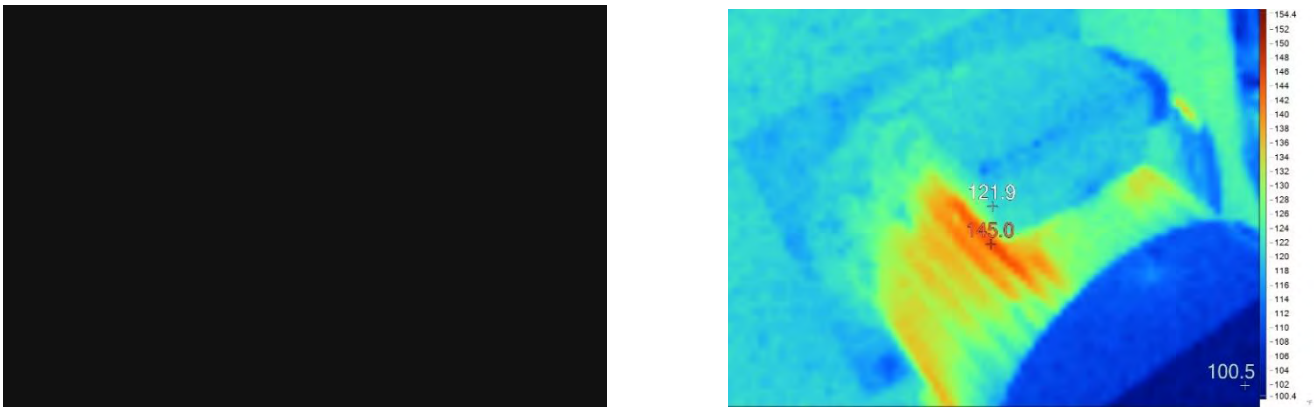

(a) **(b)**

***Figure 13**: (a) Visible and (b) Thermal representation of sample Image-18*

Here, visible image shows the electrical component and thermal image shows the heat signatures on the component.

(i) Location

This motor is located at the Factory-3 For Water Supply.

(ii) Defect

Motor is heating up due to excessive current in it.

(iii) Defect Classification

***Table 2.14:** Defect classification of Image-18 according to the "NETA" Standards*

Sl. No.	Temperature from normal heat signature area of components (Celsius)	Temperature from highest heat signature area of components (Celsius)	ΔT between similar components under similar load (Celsius)	Recommended Action/Classification
1	49.44	62.77	13.33	Indicates probable deficiency; repair as time permits

(iv) Graph

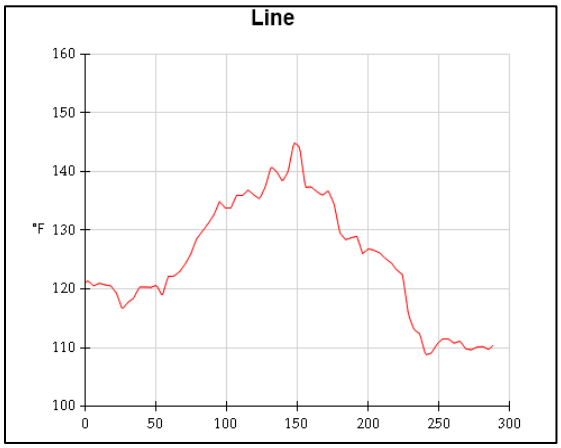

(c)

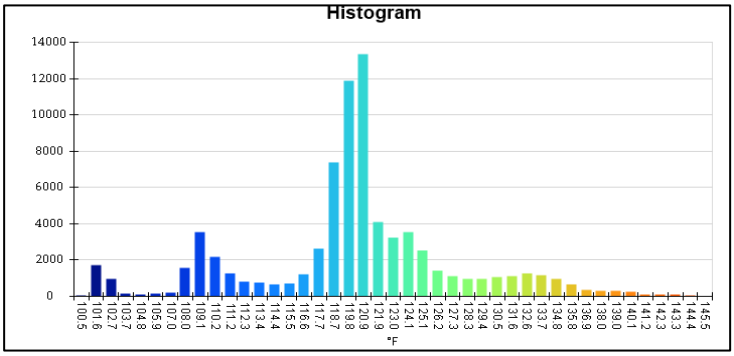

(d)

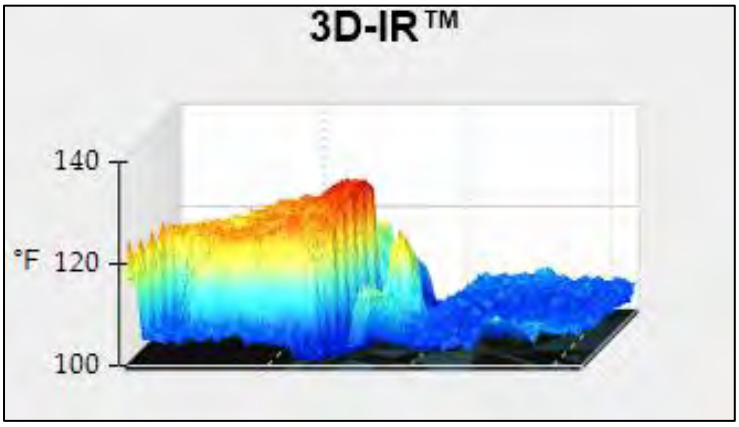

(e)

Figure 2.36*: (a) Line diagram, (b) Histogram and (c) 3D IR Graph of sample Image-18*

Therefore; line diagram, histogram and IR graph show the temperature difference between three different phases of the component.

2.3.19 Report of Thermal Image-19

Name of the equipment: Induction motor

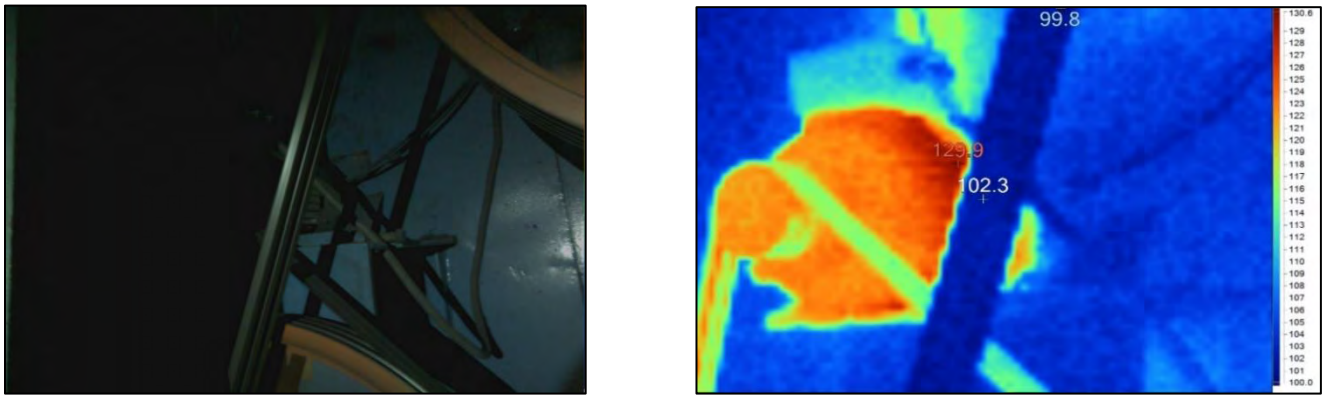

(a) **(b)**

Figure 14*: (a) Visible and (b) Thermal representation of sample Image-19*

Here, visible image shows the electrical component and thermal image shows the heat signatures on the component.

(i) Location

This motor is located at the Factory-3 production Line.

(ii) Defect

The motor is heating and drawing energy. Huge amount of current is flowing through it.

(iii) Defect Classification

Table 2.15: *Defect classification of Image-19 according to the "NETA" Standards*

Sl. No.	Temperature from normal heat signature area of components (Celsius)	Temperature from highest heat signature area of components (Celsius)	ΔT between similar components under similar load (Celsius)	Recommended Action/Classification
1	38.88	53.88	15	Major discrepancy; repair immediately

(iv) Graph

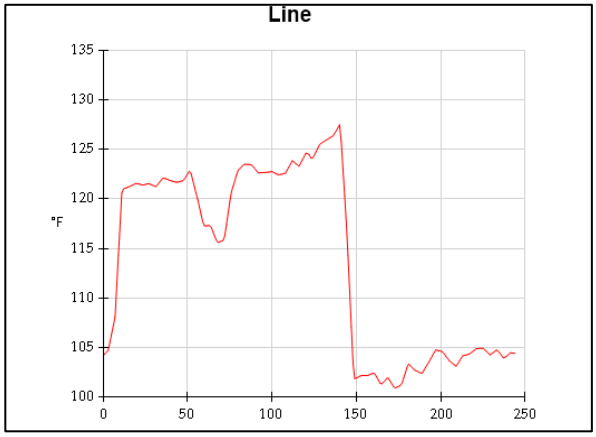

(c)

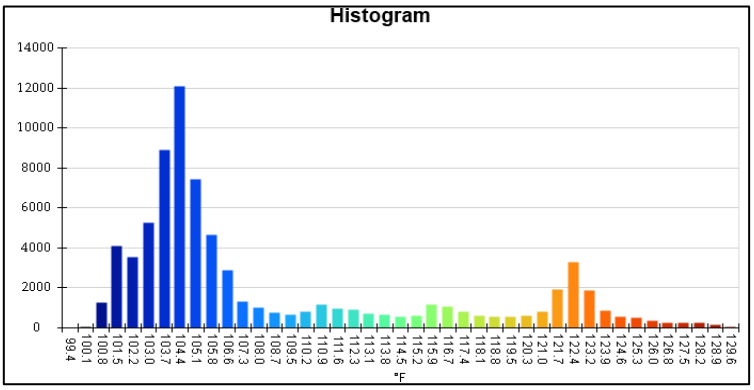

(d)

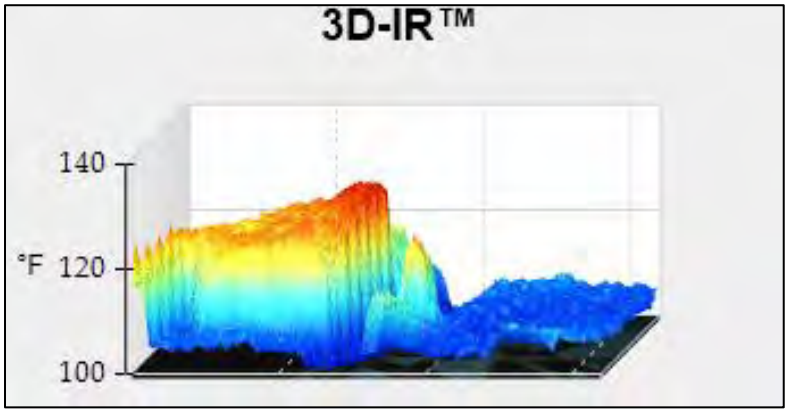

(e)

Figure 2.38*: (a) Line diagram, (b) Histogram and (c) 3D IR Graph of sample Image-19*

Therefore; line diagram, histogram and IR graph show the temperature difference between three different phases of the component.

2.3.20 Report of Thermal Image-20

Name of the equipment: Induction Motor

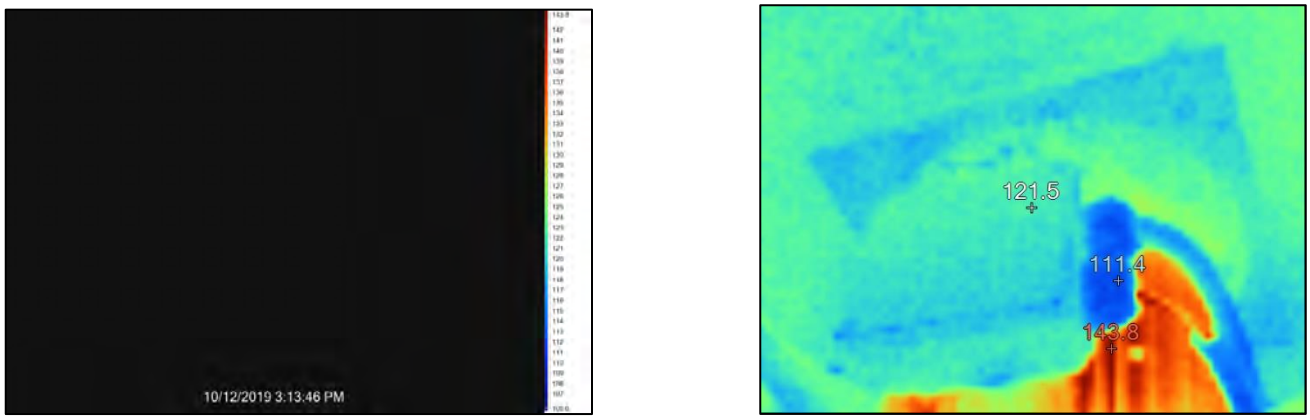

(a) **(b)**

***Figure 15**: (a) Visible and (b) Thermal representation of sample Image-20*

Here, visible image shows the electrical component and thermal image shows the heat signatures on the component.

(i) Location

This motor is located at the Factory-3 production Line.

(ii) Defect

The motor is heating and drawing energy. Huge amount of current is flowing through it.

(iii) Defect Classification

***Table 2.16:** Defect classification of Image-20 according to the "NETA" Standards*

Sl. No.	Temperature from normal heat signature area of components (Celsius)	Temperature from highest heat signature area of components (Celsius)	ΔT between similar components under similar load (Celsius)	Recommended Action/Classification
1	44.11	62	17.11	Major discrepancy; repair immediately.

(iv) Graph

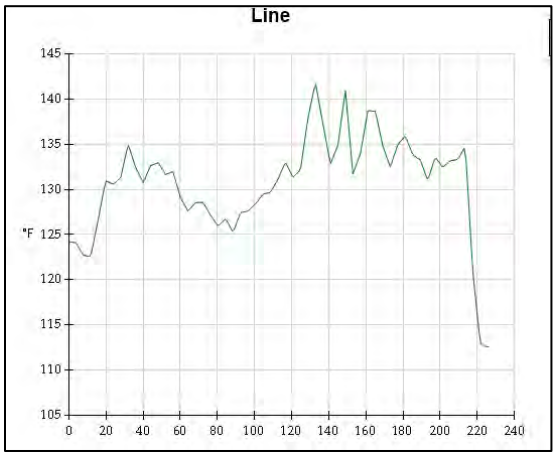

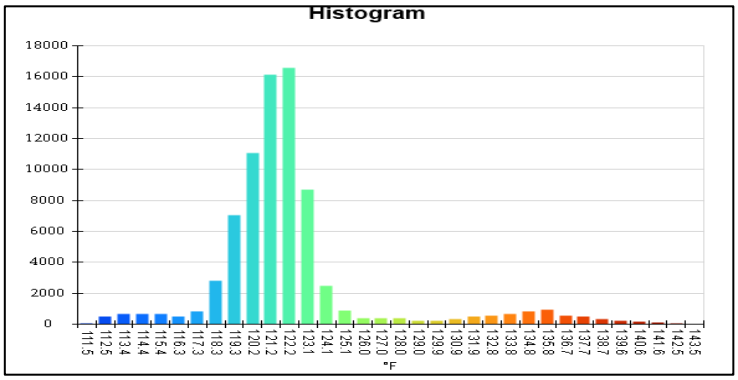

(c) **(d)**

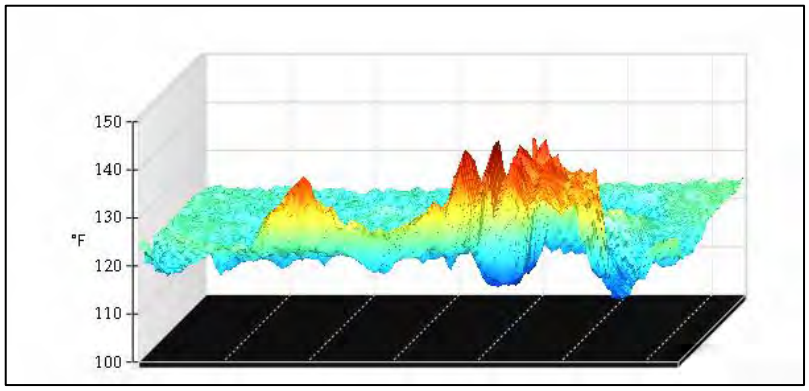

(e)

Figure 2.40*: (a) Line diagram, (b) Histogram and (c) 3D IR Graph of sample Image-20*

Therefore; line diagram, histogram and IR graph show the temperature difference between three different phases of the component.

2.3.21 Report of Thermal Image-21

Name of the equipment: Circuit Breaker

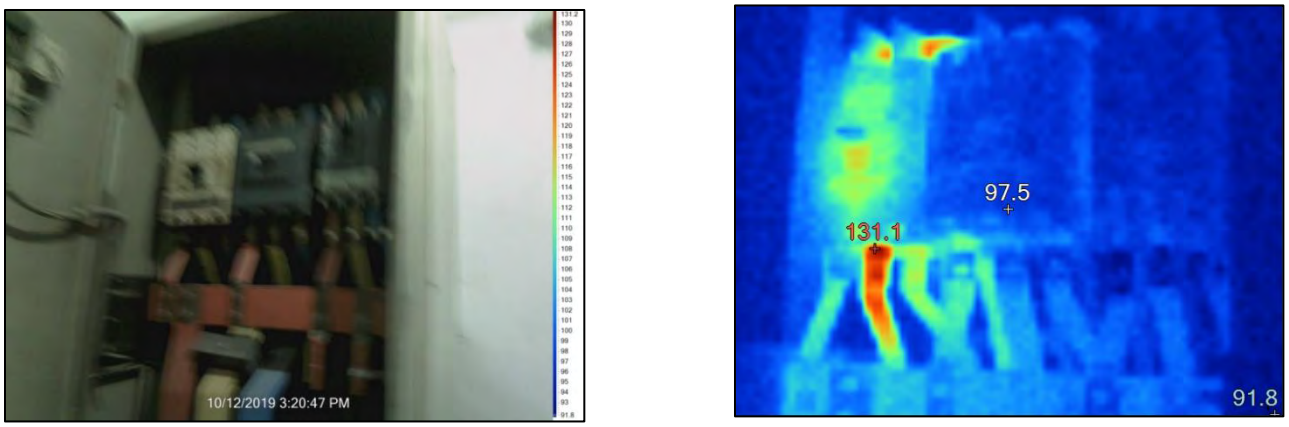

(a) **(b)**

Figure 2.41*: (a) Visible and (b) Thermal representation of sample Image-21*

Here, visible image shows the electrical component and thermal image shows the heat signatures on the component.

(i) Location
This circuit breaker is located at the Factory 2 distribution board.

(ii) Defect
Load difference between the phases R, Y & B. Phase Y is the higher load phase

(iii) Defect Classification

Table 2.17: *Defect classification of Image-21 according to the "NETA" Standards*

Sl. No.	Temperature from normal heat signature area of components (Celsius)	Temperature from highest heat signature area of components (Celsius)	ΔT between similar components under similar load (Celsius)	Recommended Action/Classification
1	36.4	55.1	18.7	Major discrepancy; repair immediately

(iv) Graph

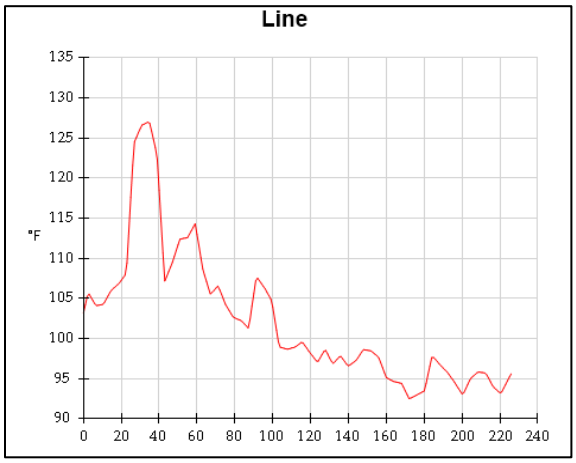

(c)

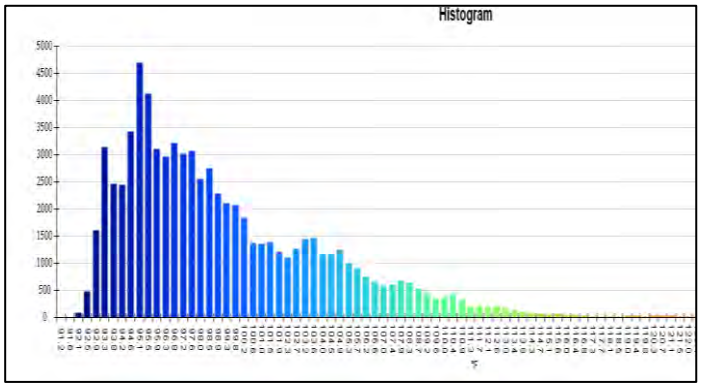

(d)

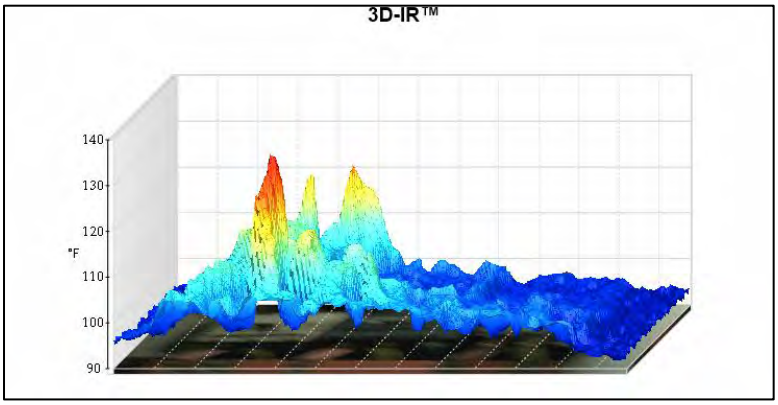

(e)

Figure 2.42*: (a) Line diagram, (b) Histogram and (c) 3D IR Graph of sample Image-21*

Therefore; line diagram, histogram and IR graph show the temperature difference between three different phases of the component.

2.3.22 Report of Thermal Image-22

Name of the equipment: Transformer

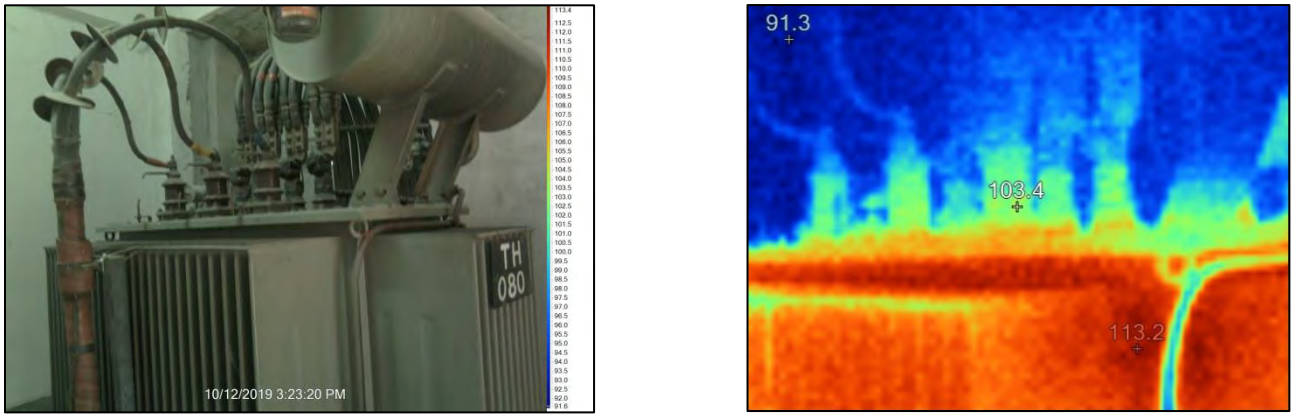

(a) **(b)**

***Figure 2.43**: (a) Visible and (b) Thermal representation of sample Image-22*

Here, visible image shows the electrical component and thermal image shows the heat signatures on the component.

(i) Location
This transformer is located at the Factory 2.

(ii) Defect
Transformer core is showing excessive heat that indicates transformer is unable to dissipate heat as higher current is flowing through the transformer coil.

(iii) Defect Classification

***Table 2.18:** Defect classification of Image-22 according to the "NETA" Standards*

Sl. No.	Temperature from normal heat signature area of components (Celsius)	Temperature from highest heat signature area of components (Celsius)	ΔT between similar components under similar load (Celsius)	Recommended Action/Classification
1	39.7	45.1	5.4	Indicates probable deficiency; repair as time permits

(iv) Graph

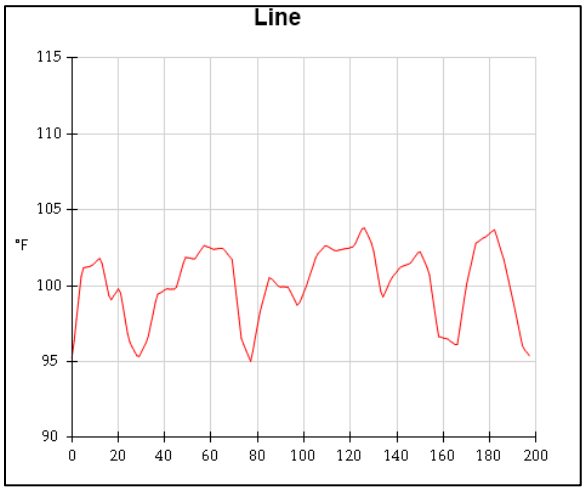

(c)

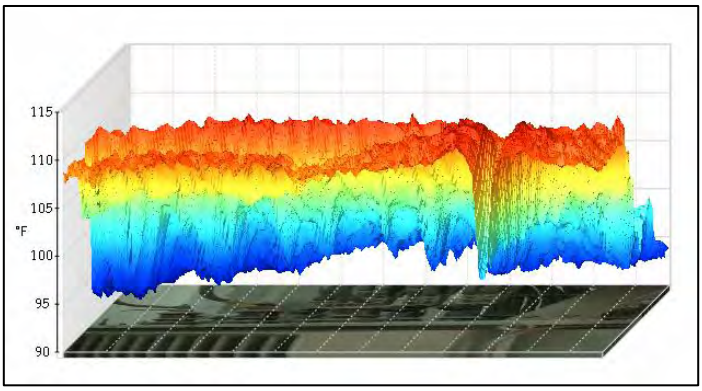

(e)

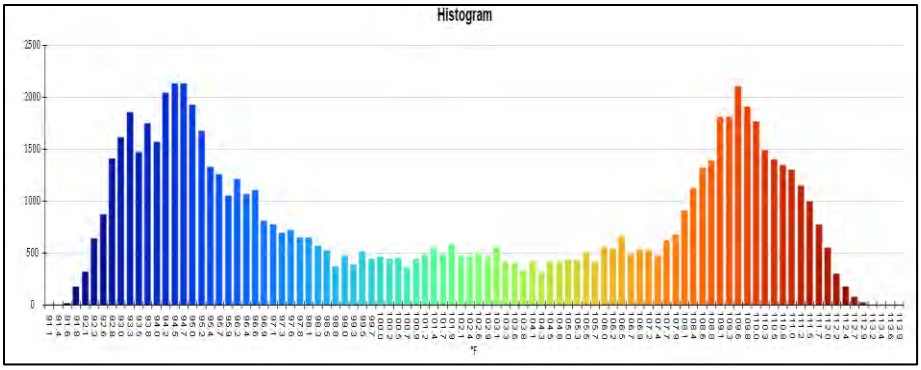

(d)

Figure 16*: (a) Line diagram, (b) Histogram and (c) 3D IR Graph of sample Image-22*

Therefore; line diagram, histogram and IR graph show the temperature difference between three different phases of the component.

2.3.23 Report of Thermal Image-23

Name of the equipment: Transformer

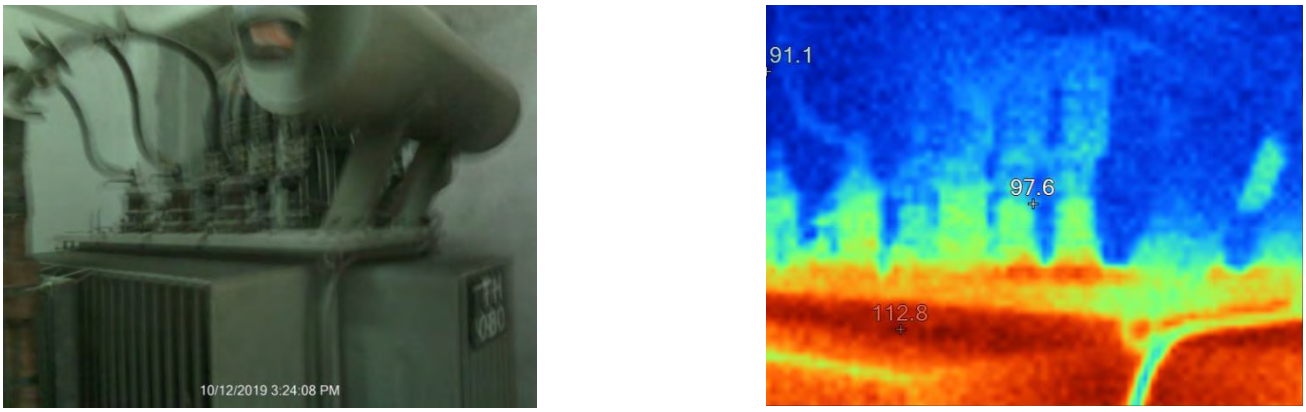

(a) **(b)**

Figure 2.45*: (a) Visible and (b) Thermal representation of sample Image-23*

Here, visible image shows the electrical component and thermal image shows the heat signatures on the component.

(i) Location
This transformer is located at the Factory-2.

(ii) Defect
Transformer core is showing excessive heat that indicates transformer is unable to dissipate heat as higher current is flowing through the transformer coil.

(iii) Defect Classification

Table 2.19: *Defect classification of Image-23 according to the "NETA" Standards*

Sl. No.	Temperature from normal heat signature area of components (Celsius)	Temperature from highest heat signature area of components (Celsius)	ΔT between similar components under similar load (Celsius)	Recommended Action/Classification
1	36.4	44.9	8.5	Indicates probable deficiency; repair as time permits

(iv) Graph

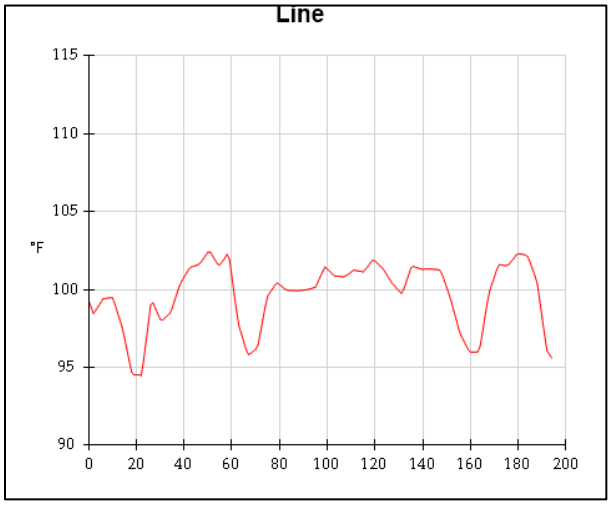

(c)

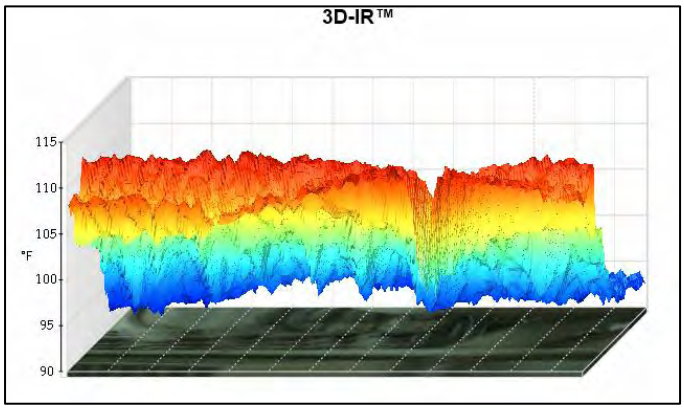

(e)

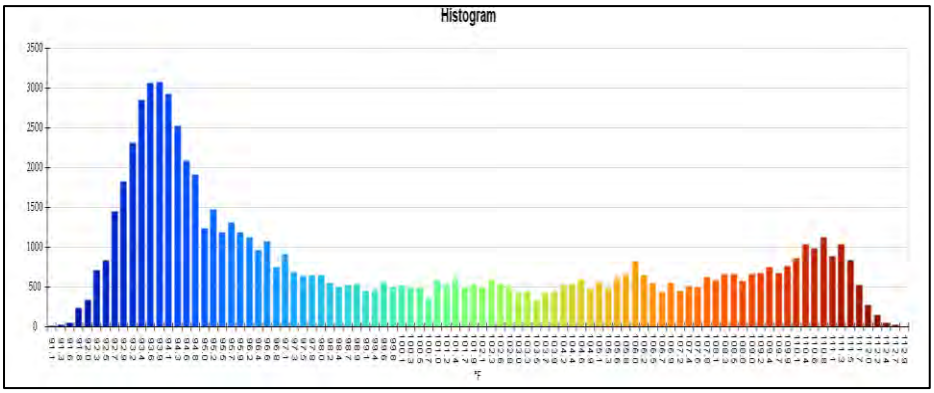

(d)

Figure 2.46*: (a) Line diagram, (b) Histogram and (c) 3D IR Graph of sample Image-23*

Therefore; line diagram, histogram and IR graph show the temperature difference between three different phases of the component.

2.3.24 Report of Thermal Image-24

Name of the equipment: Circuit Breaker

(a)

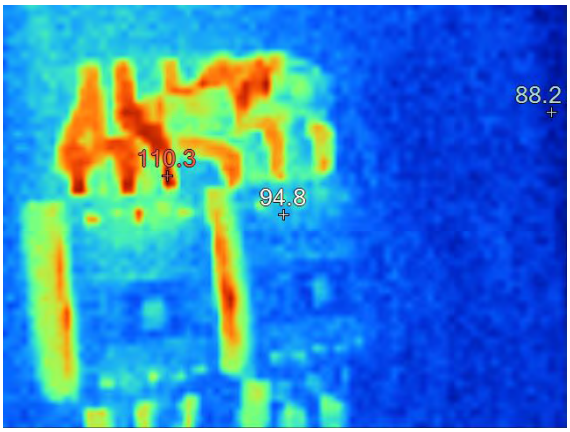

(b)

Figure 2.47*: (a) Visible and (b) Thermal representation of sample Image-24*

Here, visible image shows the electrical component and thermal image shows the heat signatures on the component.

(i) Location
This circuit breaker is situated at the factory-2 distribution board of compressor.

(ii) Defect
Due to corrosion in the incoming contact of the circuit breaker, current flow is hampered that's why producing abnormal heat.

(iii) Defect Classification

Table 2.20*: Defect classification of Image-24 according to the "NETA" Standards*

Sl. No.	Temperature from normal heat signature area of components (Celsius)	Temperature from highest heat signature area of components (Celsius)	ΔT between similar components under similar load (Celsius)	Recommended Action/Classification
1	34.9	43.5	8.6	Indicates probable deficiency; repair as time permits

(iv) Graph

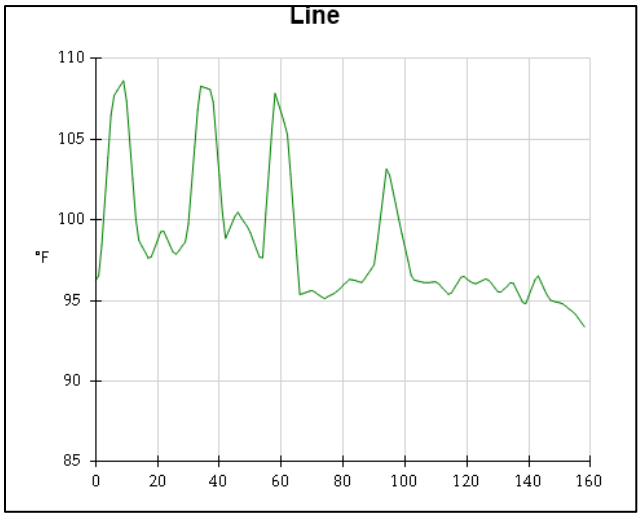

(c)

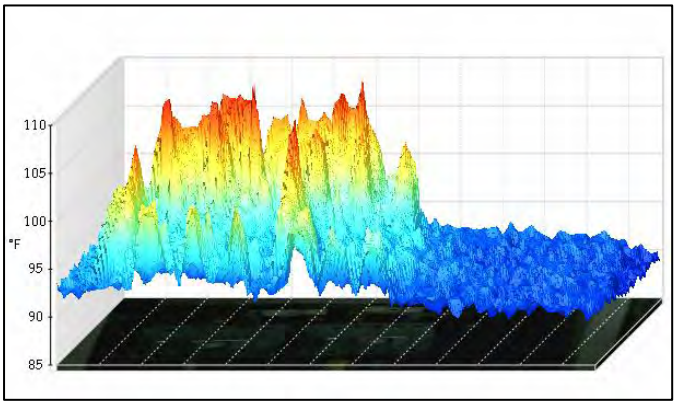

(e)

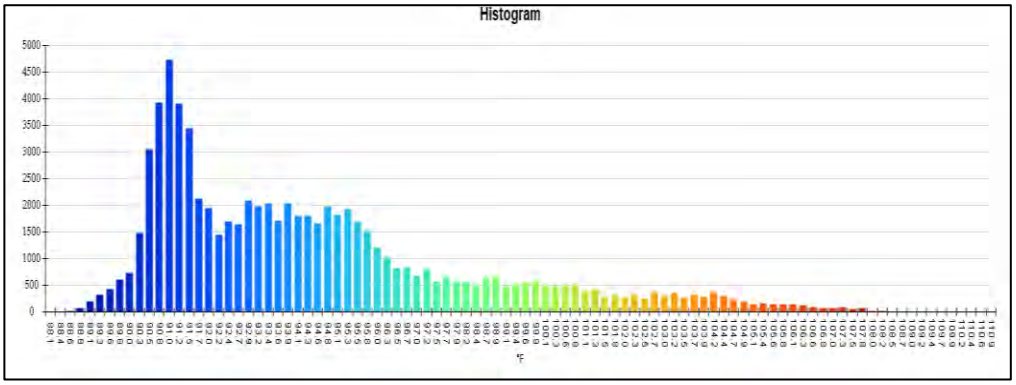

(d)

Figure 17*: (a) Line diagram, (b) Histogram and (c) 3D IR Graph of sample Image-24*

Therefore; line diagram, histogram and IR graph show the temperature difference between three different phases of the component.

Chapter 3

Thresholding Techniques

3.1 Basic principles of Thresholding

Thresholding is one of the most important methods of image segmentation. It targets to segment the provided image into two categories, known as pixels belong to the object and pixels belong to the background. If the gray level values of object pixels are lower than the given threshold or equal to it, then the gray level values of background pixels are higher than the threshold, so does the opposite way [5]. On the other perspective it could be said image segmentation is used to separate object from background according to threshold value. In actual system although the grey levels of object and image background is not entirely different, and the intensity of both varies with illumination angle. So, it's important to determine threshold correctly, and this has direct influence on segmentation precision and accuracy of image analysis [6]. Segmentation is important on our experiment since we are comparing several thresholding techniques to find the best or most accurate one in case of hotspot detection. The performance of segmentation will further be evaluated in terms of five parameters namely true positive rate (*TPR*), false positive rate (*FPR*), the Jaccard index (J), Dice similarity (*DS*) index and the absolute error [7]. Segmentation can be categorized based on the approaches of segmentation method. According to T. Zouagui., H. Benoit-Cattin and C. Odet [8], most of the segmentation techniques can be roughly categorized into two approaches: Boundary based methods and region-based methods. So, we need to find the accurate thresholding value to segment the image. To find the thresholding value multiple methods can be applied to find that value. According to M Sezgin and B Sankur [9], the thresholding techniques are sorted based on the information exploited, such as histogram shape, measurement of space clustering, entropy, object attributes, spatial correlation, and local gray-level surface.

From the other viewpoint, there are two kinds of thresholding namely, Global Thresholding it could be point dependent or region dependent and Local Thresholding. The Global Thresholding means a single threshold value is used to threshold the whole image, whereas the Local Thresholding divides the whole image into sub-images and determines the threshold value for corresponding images [10]. These are sometimes mentioned as automatic thresholding techniques. Global thresholding is quite simple and easy to implement but it depends on uniform illumination however, local thresholding methods can work with non-uniform illumination but this process is slow and complicated. In case of automated visual inspection application non-uniform illumination is not considered as an issue and that's why global thresholding is widely used for its simplicity and speed [11]. For our work we choose seven thresholding techniques namely IsoData Thresholding techniques, MaxEntropy/Kapur Thresholding techniques, MET Thresholding techniques, OTSU Thresholding techniques, Moments Thresholding techniques, RenyiEntropy Thresholding techniques, Yen Thresholding techniques.

In next sections the process of these thresholding techniques and the algorithm will be discussed to compare the thresholding techniques to evaluate the thresholding value to find the hotspot.

3.2 IsoData Thresholding Technique

IsoData thresholding could be a way to automatically detect a threshold for a given gray value image f. An iterative strategy for threshold selection has been proposed by Ridler and Calvard [12] for object-background separation through choosing a starting threshold value from the grey level histogram, at each iteration we get a new threshold within the following way,

Suppose for a threshold t_i at a random object within the range of gray values in the image, we can assume the mean of all of the pixels within the image with a gray value is M.

$$\begin{cases} M \leq t_i = M_L \\ M \geq t_i = M_H \end{cases}$$

The new threshold value t_{i+1} can be found by taking average of M_L and M_H. Both M_L and M_H are function of t_i

$$t_{i+1} = \frac{M_L(t_i) + M_H(t_i)}{2}$$

$$=\mathrm{M}\,(t_i)$$

t_{i+1} Should be a better threshold than t_i for object-background discrimination. The process terminates as soon as we have $t_i = t_{i+!}$. This method is applied to threshold a low-contrast image. The basic ISODATA algorithm is a procedure for classifying a set of sample vectors into c distinct classes [13].

Algorithm I-Basic ISODATA

1) Choose some initial values for the means

Loop

2) Classify the m samples by assigning them to the class having the closest mean.

3) Recomputed the means as the averages of the samples in each class.

4) If any mean has changed value, go to loop otherwise, stop.

Each image has grey level integer value, considering the interval to be [0, L], each sample is a point of the image. According to histogram h we divide the grey level where {h(0), h(l),- - - , h(L)}

are the numbers of grey. Considering smallest interval of all nonzero value to be [L, H]. In this one-dimensional case, the ISODATA algorithm may be rewritten as,

Algorithm I-Basic ISODATA

1) Choose some initial values for the means such that $(m_1, m_2, \ldots, m_c)$, where,

$$L \leq m_1 < m_2 \ldots \ldots < m_c < H$$

Loop

2) Calculate thresholds $t_1, t_2, \ldots, t_{c-1}$by the formula

$$t_i = \frac{m_i + m_{i+1}}{2} \quad where\ 1 \leq i < c$$

All gray levels are in the interval $I_i = [t_{i-1} + 1, t_i]$, defined that $t_0 = L\ and\ t_c = H$

3) Recompute the means: for every i make m_i the nearest gray level to,

$$\frac{\sum_{j \in I_i} j.h(j)}{\sum_{j \in I_i} h(j)} \qquad \text{Where } 1 \leq i \leq c$$

4) If any mean has changed value, go to loop; otherwise,

Stop

In step 3) of the algorithm, if it happens that $\sum_{j \in I_i} h(j) = 0$ for some i, in other words, there is no point whose gray level falls in the interval I_i, one should suppress class i and consider just the remaining classes [14].

3.4 MaxEntropy/Kapur Thresholding Technique

Kapur's Thresholding technique employments a comprehensive look to assess the criterion for maximizing the between-class entropy. Kapur considered the image foreground and background as two distinctive signal sources. The method portrays a gray-level thresholding strategy utilizing the entropy of signal sources. When the entirety of the two class entropies comes to its maximum, the picture is said to be ideally thresholded [15]. It could be categorized into single threshold and multiple thresholds.

I. Single Threshold

If the number of pixels with gray level i is denoted by h (i). Typically, i takes integer values from 0 to 255. We assume that h(i) is normalized, that is:

$$\sum_{i=0}^{L} h(i) = 1$$

The pixels are distributed into two classes, Cf with gray levels [0-t] and Cb with gray levels [t-L], where t is the threshold value and Cf and Cb normally correspond to foreground and background, respectively [16].

Using discriminate analysis, Kapur [1] defined the between-class entropy of the thresholded image as

$$f_1(t) = H_f(t) + H_b(t)$$

the optimal threshold, t*, is chosen so that the between-class entropy $f_1(t)$ is maximized [1]; that is,

$$t^* = Arg_{0\le t\le L}\max\{f_1(t)\} \qquad (1)$$

And verified,

Entropy of foreground pixels,

$$H_f(t) = -\sum_{i=0}^{t} \frac{h(i)}{\sum_{j=0}^{t} h(j)} \log \frac{h(i)}{\sum_{j=0}^{t} h(j)}$$

Entropy of background pixels,

$$H_b(t) = -\sum_{i=t+1}^{L} \frac{h(i)}{\sum_{j=t+1}^{L} h(j)} \log \frac{h(i)}{\sum_{j=t+1}^{L} h(j)}$$

II. Multiple Threshold

Above formulation can be easily converted to multilevel thresholding of an image [1]. Assuming that there are n thresholds, {t1, t2, …, tn}, which divide the original image into m classes: C0 for [0-t1], C1 for [t1- t2], … , Cm for [tm-L], the optimal thresholds {t1*, t2*, …, tn*} are chosen by maximizing fm(t1, t2 ,..., tn) as follows [1]

$$f_m(t_1, t_2, \ldots\ldots, t_n) = H(0, t_1) + H(t_1, t_2) + \cdots + H(t_n, L)$$

$$= \sum_{i=0}^{n} H(t_i, t_{i+1})$$

For multiple thresholds if we want to find optimal n number of thresholds, the Equation (1) can be generalized from one threshold to *n* threshold as, [1]

$$f_m(t_1^*, t_2^*, \ldots\ldots, t_n^*) = Arg_{0 \le 0 \ldots\ldots t_n \le L} \max\{f_m(t_1, t_2, \ldots\ldots, t_n)\}$$

Where,

$$H(t_i, t_{i+1}) = -\sum_{i=t_i}^{t_{i+1}} \frac{h(i)}{\sum_{j=t_i}^{t_{i+1}} h(j)} \log \frac{h(i)}{\sum_{j=t_i}^{t_{i+1}} h(j)}$$

3.5 MET Thresholding Technique

In the minimum error method according to Kittler and Illingworth's [25] minimum error algorithm, the gray level histogram h(g) is viewed as an estimate of the probability density function P(g) of the mixture population comprising of the gray levels of the object and background pixels. It is usually assumed that each of the two components $P(g|i)$ of the mixture is normally distributed with meanμ_i and standard deviation σ_i and a priori probability p_i, that is

$$P(g) = \sum_{i=1}^{2} P_i P(g|i)$$

Where,

$$P(g|i) = \frac{1}{\sqrt{2\pi}\sigma_i} \exp(-\frac{(g-\mu_i)}{2{\sigma_i}^2})$$

The threshold value can be selected by solving the quadratic equation

$$\frac{(g-\mu_1)^2}{{\sigma_1}^2} + \log_e {\sigma_1}^2 - 2\log_e P_1 = \frac{(g-\mu_2)^2}{{\sigma_2}^2} + \log_e {\sigma_2}^2 - 2\log_e P_2$$

However, the parameters μ_i, σ_i and P_i (i = 1,2) of the mixture density p(g) associated with an image to be threshold are not usually known. To overcome the difficulty of estimating these unknown parameters, Kittler and Illingworth introduced a criterion function J(t), which is given by,

$$J(t) = 1 + 2\{P_1(t)\log_e \sigma_1(t) + P_2(t)\log_e \sigma_2(t)\} - 2\{P_1(t)\log_e P_1(t) + P_2(t)\log_e P_2(t)\}$$

Where,

$$P_1(t) = \sum_{g=0}^{t} h(g)$$

$$P_2(t) = \sum_{g=t+1}^{L-1} h(g)$$

$$\mu_1(t) = \frac{\{\sum_{g=0}^{t} h(g)g\}}{P_1(t)}$$

$$\mu_2(t) = \frac{\{\sum_{g=t+1}^{L-1} h(g)g\}}{P_2(t)}$$

$${\sigma_1}^2(t) = \frac{\sum_{g=0}^{t}[g - \mu_1(t)]^2 h(g)}{P_1(t)}$$

$${\sigma_2}^2(t) = \frac{\sum_{g=t+1}^{L-1}[g - \mu_2(t)]^2 h(g)}{P_2(t)}$$

The optimal threshold is obtained by minimizing J(t), that is by finding,

$$t^* = Arg_{0 \le t < L-1} \min J(t)$$

3.6 Otsu Thresholding Technique

Otsu [17] recommended minimizing the weighted entirety of within-class changes of the frontal area and foundation pixels to set up an ideal threshold. Review that minimization of inside class changes is commensurate to the maximization of between-class scramble. Satisfactory results can be extracted when the numbers of pixels in each class are close to each other. The Otsu method still remains one of the most referenced thresholding methods. It is one of the Clustering-Based Thresholding Methods [9].

In this section, we rewrite Otsu method [17] as follows,

In bi-level thresholding, the pixel whose gray level is less than the threshold will be assigned to the background, else to the foreground. Assuming an image is divided in L gray levels

[0, 1,…L-1]. The number of pixels at level *i* is denoted by n_i, and the total amount of pixels is denoted by, $N = n_1 + n_2 + \cdots + n_L$. The probability of gray level *i* is denoted by,

$$P_i = \frac{n_i}{N} \qquad where, \qquad P_i \geq 0$$

$$\sum_{0}^{L-1} P_i = 1$$

Pixels are distributed into two classes C_1 with gray levels [0,1,…t] and C_2 with gray levels [t+1,…..,L-1] by the threshold *t*, in the bi-level thresholding method. The gray level probability distributions for the two classes are,

$$w_1 = \Pr(C_1) = \sum_{i=0}^{t} P_i$$

$$w_2 = \Pr(C_2) = \sum_{i=t+1}^{L-1} P_i$$

The means of classes C_1 and C_2 are,

$$u_1 = \sum_{i=0}^{t} \frac{iP_i}{w_1}$$

$$u_2 = \sum_{i=t+1}^{L-1} \frac{iP_i}{w_2}$$

The total mean of gray levels is denoted by u_T,

$$u_T = w_1 u_1 + w_2 u_2$$

The class variances are,

$$\sigma_1{}^2 = \sum_{i=0}^{t} (i - u_1)^2 \frac{P_i}{w_1}$$

$$\sigma_2{}^2 = \sum_{i=t+1}^{L-1} (i - u_2)^2 \frac{P_i}{w_2}$$

The within -class variance is,

$$\sigma_w{}^2 = \sum_{K=1}^{M} w_K \, \sigma_k{}^2$$

The between-class variance is,

$$\sigma_B{}^2 = w_1(u_1 - u_T)^2 + w_2(u_2 - u_T)^2$$

The total variance of gray levels is,

$$\sigma_T{}^2 = \sigma_w{}^2 + \sigma_B{}^2$$

Otsu method chooses the ideal threshold t by maximizing the between-class change, which is proportionate to minimizing the within-class change, since the overall fluctuation is steady for distinctive allotments,

$$t = arg_{0 \le t \le L-1}[\max\{\sigma_B{}^2(t)\}] = arg_{0 \le t \le L-1}[\min\{\sigma_w{}^2(t)\}]$$

Otsu method can be extended to multilevel thresholding method. Assuming that there are M-1 thresholds $\{t_1, t_2, \ldots, t_{M-1}\}$ that divide the pixels in the image to M classes $\{C_1, C_2, \ldots, C_M\}$

$$\{t_1, t_2, \ldots, t_{M-1}\} = arg_{0 \le t \le L-1}[\max\{\sigma_B{}^2(t_1, t_2, \ldots, t_{M-1})\}]$$

$$= arg_{0 \le t \le L-1}[\min\{\sigma_w{}^2(t_1, t_2, \ldots, t_{M-1})\}]$$

Where,

$$w_j = \sum_{i=t_{j-1}+1}^{t_j} P_i$$

$$u_j = \sum_{i=t_{j-1}+1}^{t_j} \frac{iP_i}{w_j}$$

$${\sigma_j}^2 = \sum_{i=t_{j-1}+1}^{t_j} (i-u_j)^2 \frac{P_i}{w_j}$$

$${\sigma_w}^2 = \sum_{j=1}^{M} w_j \, {\sigma_j}^2$$

$${\sigma_B}^2 = w_j(u_j - u_T)^2$$

3.7 Moments Thresholding Technique

Moment is a mathematical feature of arbitrary variable. Moment strategy is a calculation of parameter point estimation put forward by Karl Pearson in 1894. Its fundamental theory is as takes after: the moment of sample reflects population moment in a few degrees, so the moment function estimation of sample can be seen as estimation of population moment function. Moment strategy is one of compelling normality review. It has sample moment as corresponsive population moment, and sample moment function as estimation of the same population moment function. Its most well-known application is to assess population mathematical expectation with sample average [18].

Before thresholding, we compute the gray-level moments of the input image. The thresholds are at that point chosen in such a way that the moments of the thresholded picture are kept unchanged. This approach may be regarded as a moment-preserving image transformation which recovers a

perfect image from a blurred form. The approach can automatically and deterministically select multiple thresholds without iteration or search. In expansion, a representative gray value can moreover be obtained for each thresholded class [19].

Considering an image *f* containing n pixels whose gray value at pixel (x, y) is denoted by f (x, y), we need to threshold f into two-pixel classes, the below-threshold pixels and the above-threshold ones. The ith moment m_i of f is defined as,

$$m_i = (\frac{1}{n}) \sum_x \sum_y f^i (x, y)$$

$$i = 1,2,3, \dots \dots \dots$$

Moments can moreover be obtained from the histogram of an image *f*.

$$m_i = \frac{1}{n} \sum_j n_j (z_j)^i$$

$$= \sum_j P_j (z_j)^i$$

Where n_j is the total number of the pixels in f with gray value z_j and $P_j = {}^{n_j}/_{n}$. We also define m_0 to be 1. Image f can be considered as a obscured adaptation of an perfect bi-level image which comprises of pixels with as it were two gray values z_0 and z_1, where $z_0 < z_1$. The proposed moment-preserving thresholding is to choose a threshold esteem such that in case all below-threshold gray values in f are supplanted by z_0 , and all above-threshold replaced by z_1, at that point the primary three moments of image f are preserved within the resulting bi-level image g. Image g so obtained may be respected as an perfect unblurred adaptation of f.

Let P_0 and P_1 denote the fractions of the below-threshold pixels and the above-threshold pixels in f, respectively, then the first three moments of g are just

$$m_i' = \sum_{j=0}^{1} P_j (z_j)^i$$

$$i = 1,2,3, \ldots ..$$

And preserving the first three moments in g means the following equalities:

$$m_i' = m_i \qquad i = 1,2,3, \ldots \ldots$$

Note that

$$P_0 + P_1 = 1$$

The four equalities

$$P_0 {z_0}^0 + P_1 {z_1}^0 = m_0$$

$$P_0 {z_0}^1 + P_1 {z_1}^1 = m_1$$

$$P_0 {z_0}^2 + P_1 {z_1}^2 = m_2$$

$$P_0 {z_0}^3 + P_1 {z_1}^3 = m_3$$

Where m_i with i=1,2,3 is computed and $m_0 = 1$. To find the desired threshold value we need to solve above 4 equations to obtain P_0 and P_1 then proper *t* can be selected from histogram of the original image to satisfy

$$P_0 = \sum_{i \le t} P_i$$

Then the *t* is just the wanted. If precise gray value can't be found, the closest can be chosen.

3.8 RenyiEntropy Thresholding Technique

Consider that a digital image of size $M \times N$ has L grey levels denoted by $G = \{0, 1,..., L-1\}$. Let $f(x, y)$ be the grey level of the pixel located at the location (x, y). Then the image can be represented by $F = f(x, y)$ where, $x = [0,1,2,...,M-1,]$ and $y = [0,1,2,...,N-1]$.

Let g(x; y) be the average of the neighborhood of the pixel located at the point (x, y). The average gray value for the W × W neighborhood of each pixel is calculated as [20]

$$g(x,y) = Round\left(\frac{1}{w^2}\sum_{j=-\frac{(w-1)}{2}}^{\frac{(w-1)}{2}}\sum_{j=-\frac{(w-1)}{2}}^{\frac{(w-1)}{2}} f(x+i, y+j)\right)$$

Where *Round* (μ) denotes the integer part of μ. Using the pixel's gray value $f(x, y)$ and the average gray value $g(x,y)$ as a pair vector (t, s) frequency of occurrence of the pair vectors can be found from, [21]

$$h(i,j) = \frac{1}{MN}\sum_{x=0}^{M}\sum_{y=0}^{n}\delta(i,j)$$

Where,

$$\delta(i,j) = \begin{cases} 1, & f(x,y) = i \ \ and \ \ g(x,y) = j, \\ 0, & Otherwise \end{cases}$$

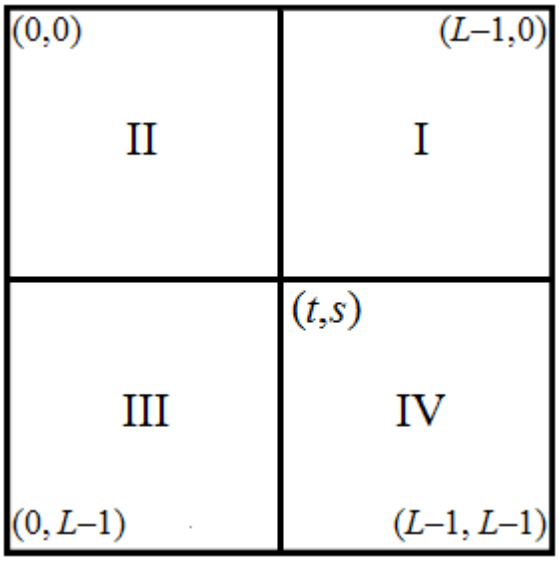

***Figure 18.1**: 2-D Histogram*

From above histogram it can be defined that matrix with horizontal axes for the gray value and vertical axes for the local average gray value. If we consider the combination (t, s) as a threshold vector, the space of the histogram is partitioned into four quadrants, these four can be classified into inclining quadrants II and IV, and off-diagonal quadrants I and III. Depending on the distinction between the gray-levels and the neighborhood normal gray levels, the corner to corner quadrants, which have little gray-level varieties, are characterized as containing question and foundation, and the off-diagonal quadrants, which have expansive varieties, are respected as edges [21].

$$P_{II}(t,s) = \sum_{i=0}^{t}\sum_{j=0}^{s} P(i,j),$$

$$P_{IV}(t,s) = \sum_{i=t+1}^{L-1}\sum_{j=s+1}^{L-1} P(i,j)$$

The total number of occurrences, $n_{(i,j)}$ of the pair (i, j), divided by the total number of pixels, N ×M defines a joint probability mass function, $P_{(i,j)}$ [1]

$$P_{(i,j)} = \frac{n_{(i,j)}}{\mathrm{N} \times \mathrm{M}}$$

Using these two-probability distributions Sahoo [1] defined the Renyi's entropies associated with the object and background classes as follows,

$$H_O{}^{\alpha}(t,s) = \frac{1}{1-\alpha} \ln \sum_{j=0}^{s} \sum_{i=0}^{t} \left(\frac{P_{(i,j)}}{P_{II}(t,s)} \right)^{\alpha}$$

$$H_B{}^{\alpha}(t,s) = \frac{1}{1-\alpha} \ln \sum_{j=s+1}^{L-1} \sum_{i=t+1}^{L-1} \left(\frac{P_{(i,j)}}{P_{IV}(t,s)} \right)^{\alpha}$$

Where order-α is a positive real number and not equal to 1

Finally, the optimal threshold pair ($t^*(\alpha)$, $s^*(\alpha)$) can be obtained by solving the following maximization problem,

$$(t^*(\alpha), s^*(\alpha)) = arg_{(t,s)\epsilon L \times L} max\left(H_B{}^{\alpha}(t,s) + H_O{}^{\alpha}(t,s) \right)$$

3.9 Yen Thresholding Technique

[22] Consider an image $f(x,y)$ of size N x N pixels that are represented by m gray-levels, where G_m = {0,1,. . . , (m - l)} denote the set of gray-levels and f_i, $\boldsymbol{i} \in G_m$ be the observed gray-level frequencies of the image ***f.*** The probability of the gray-level i in the image f can be calculated as,

$$P_i = \frac{f_i}{N \text{ x } N}$$

Hence a distribution is obtained. For a given grey level s, if $0 < \sum_{i=0}^{s-1} P_i < 1$ then the following two distributions can be derived from this distribution after normalization;

$$A \equiv \left\{ \frac{P_0}{P(s)}, \frac{P_1}{P(s)}, \dots\dots, \frac{P_{s-1}}{P(s)} \right\}$$

$$B \equiv \left\{ \frac{P_s}{1-P(s)}, \frac{P_{s+1}}{1-P(s)}, \dots\dots, \frac{P_{m-1}}{1-P(s)} \right\}$$

In the maximum entropy criterion, the basic idea is to choose the threshold such that the total amount of information provided by the object and background is maximized the total amount of information provided by ***A*** and ***B*** is,

$$TE(s) = E_A(s) + E_B(s)$$

$$= -\sum_{i=0}^{s-1}\left(\frac{P_i}{P(s)}\right)\ln\left(\frac{P_i}{P(s)}\right) - \sum_{i=s}^{m-1}\left(\frac{P_i}{1-P(s)}\right)\ln\left(\frac{P_i}{1-P(s)}\right)$$

$$= \ln\{P(s)(1-P(s)\} - \frac{H(s)}{P(s)} - \frac{H'(s)}{1-P(s)}$$

Where,

$$P(s) = \sum_{i=0}^{s-1} P_i$$

$$H(s) = -\sum_{i=0}^{s-1} P_i \text{ x } \ln(P_i)$$

$$H'(s) = -\sum_{i=s}^{m-1} P_i \text{ x } \ln(P_i)$$

The **maximum entropy criterion (MEC)** [24] is to determine the threshold **s*** such that,

$$TE(s^*) = max_{s\in G_m} TE(s)$$

Chapter 4

Performance Evaluation

4.1 Terms used for Performance Evaluation

Thresholding techniques are part of image segmentation. So, performance evaluation is the measure of how well the different thresholding techniques do perform as segmenting the image as accurately as possible compare to the Ground Truth Image. Ground Truth Image is also a segmented image but it is done manually by comparing with the original thermal image ROI to get the most accurate segmentation. It is time consuming but it is best suited to compare any model or techniques to find out the accuracy in real life for automatic analysis. In order to find out the difference among Ground Truth (GT) and Segmented Image (SI), they are overlapped to find out the necessary evaluation terms like True Positive Rate (TPR), False Positive Rate (FPR), Accuracy, Precision, Matthews correlation coefficient (MCC), Dice Index, Jaccard index and Error Rate. To find out the True Positive Rate (TPR) & False Positive Rate (FPR) it is essential to calculate True Positive (TP), True Negative (TN), False Positive (FP), False Negative (FN).

True Positive (TP) means the overlapped region between GT & SI where the bright pixels are correctly matched and Predicted value and actual value are both 1. True Negative (TN) means the common black pixels are matched and Predicted value and actual value are both 0. False Positive (FP) means having the black pixels as bright pixels and False Negative (FN) means having the bright pixels as black pixels respectively. TPR & FPR are calculated as follows:

$$TPR = \frac{TP}{TP + FN}$$

And

$$FPR = \frac{FP}{TP + FP}$$

TPR value close to 1 means better segmentation and FPR value close to 0 means better Segmentation.

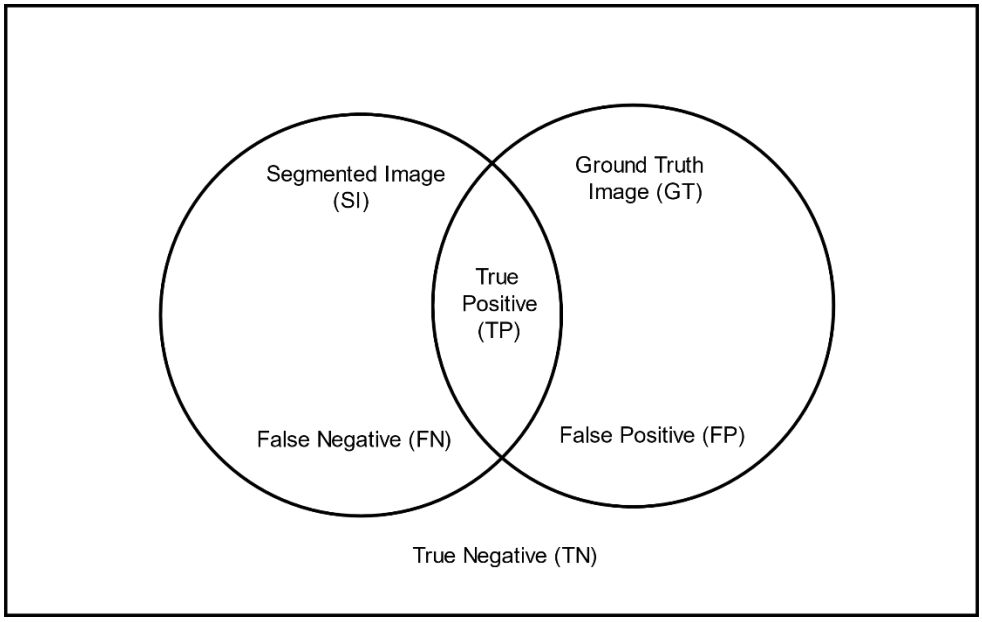

***Figure 19**: Overlapping of ground truth and segmented image*

Accuracy can be measured as:

$$Accuracy = \frac{TP + TN}{(FN + FP + TP + TN)}$$

Accuracy value close to 1 means better segmentation.

Precision can be measured as:

$$Precision = \frac{TP}{FP + TP}$$

Precision value close to 1 means better segmentation.

Matthews correlation coefficient (MCC) Formula:

$$MCC = \frac{(TP * TN) - (FP * FN)}{\sqrt{((TP + FP) * (TP + FN) * (TN + FP) * (TN + FN))}}$$

MCC value close to 1 means better segmentation.

Dice Index can be calculated as:

$$Dice\ Index = \frac{2 * TP}{2 * (TP + FP + FN)}$$

Jaccard Index can be calculated as:

$$Jaccard\ Index = \frac{Dice\ Index}{2 - Dice\ Index}$$

Dice & Jaccard Index value close to 1 means better segmentation.

Error is measured as the ratio between the absolute difference, $Ndiff$ between the bright pixels of Ground Truth & Segmented Image and the total pixels value of Ground Truth Image (N):

$$Error = \frac{abs(\ Ndiff\ )}{N} \times 100\%$$

4.2 Image Dataset of Segmentation

4.2.1 Image-01 Dataset

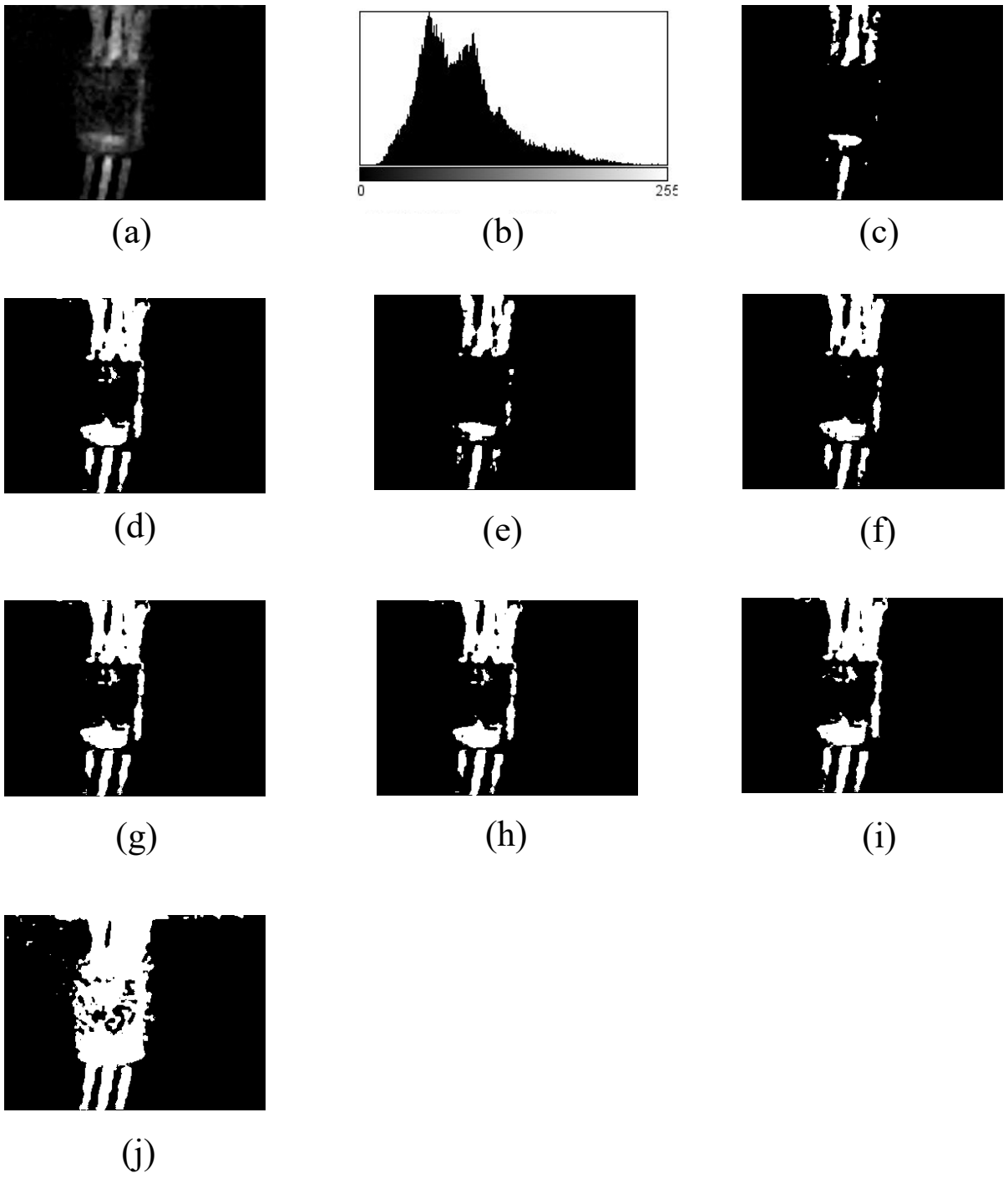

Figure 4.2*: Target hotspots extraction from Image-01 using Thresholding techniques (a) Enhanced Thermal Image (b) Histogram (c) Ground truth image (d) IsoData (e) MaxEntropy/Kapur (f) Moments*

4.2.2 Image-02 Dataset

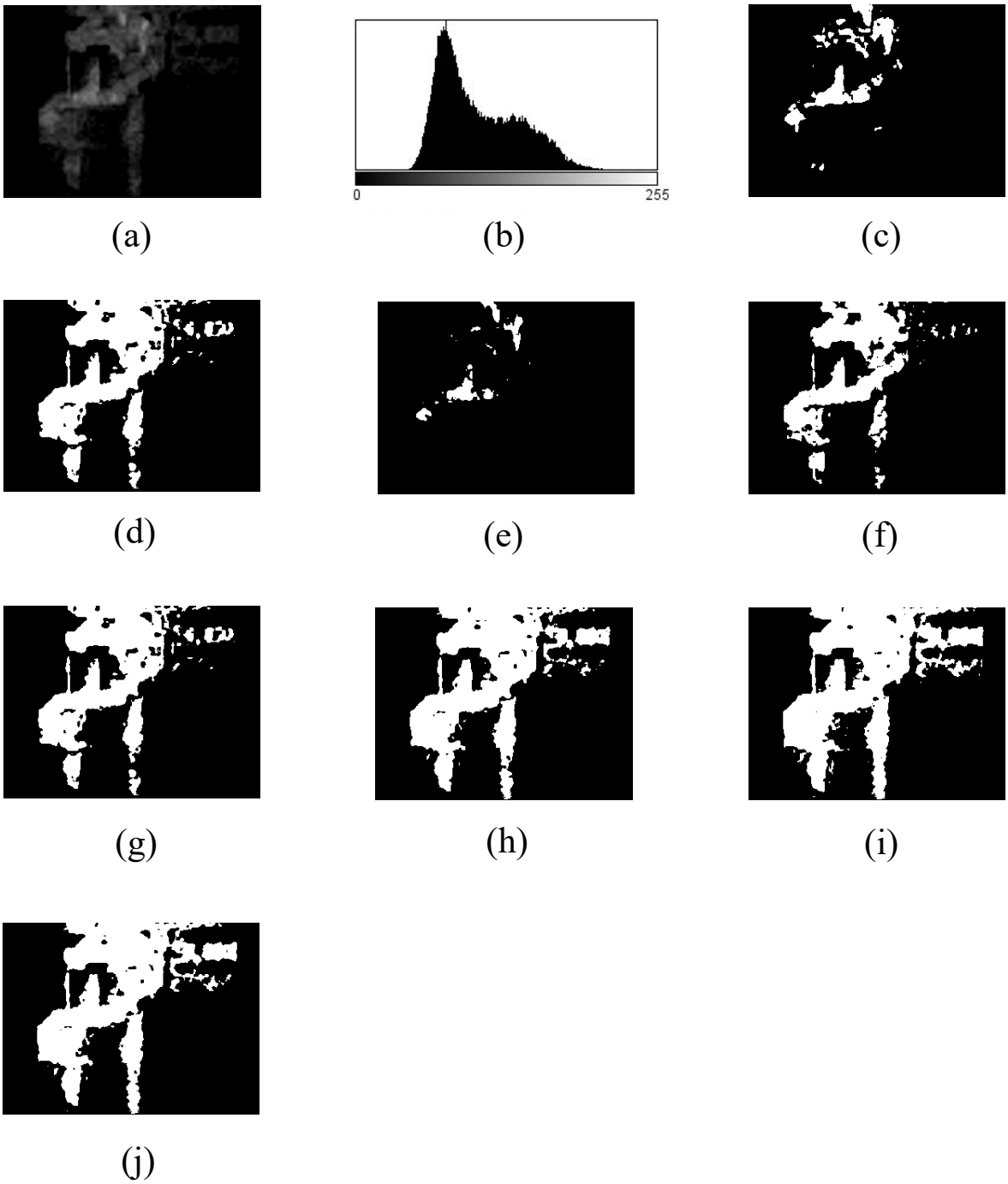

Figure 4.3*: Target hotspots extraction from Image-02 using Thresholding techniques (a) Enhanced Thermal Image (b) Histogram (c) Ground truth image (d) IsoData (e) MaxEntropy/Kapur (f) Moments*

4.2.3 Image-03 Dataset

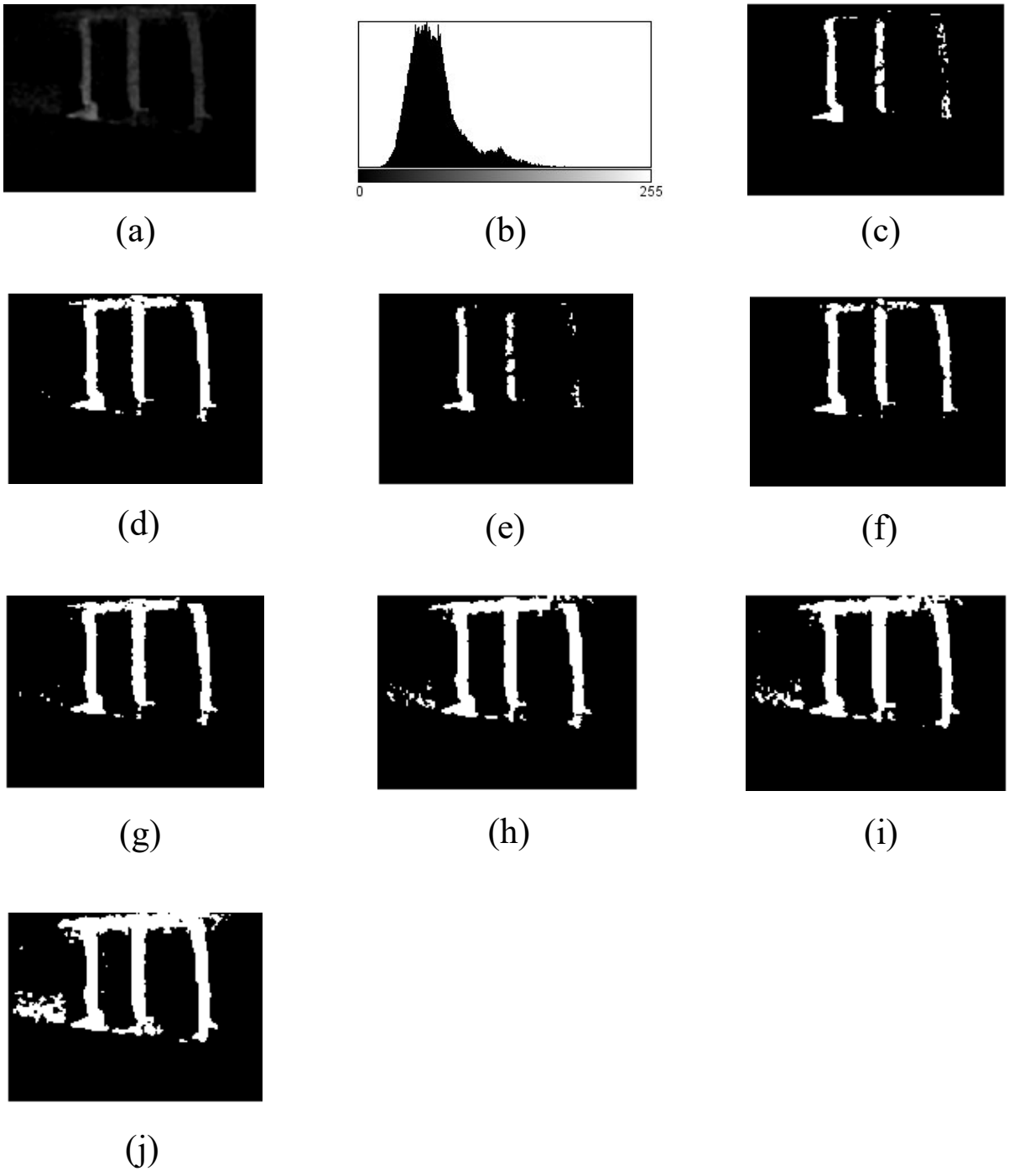

Figure 4.4*: Target hotspots extraction from Image-03 using Thresholding techniques (a) Enhanced Thermal Image (b) Histogram (c) Ground truth image (d) IsoData (e) MaxEntropy/Kapur (f) Moments*

4.2.4 Image-04 Dataset

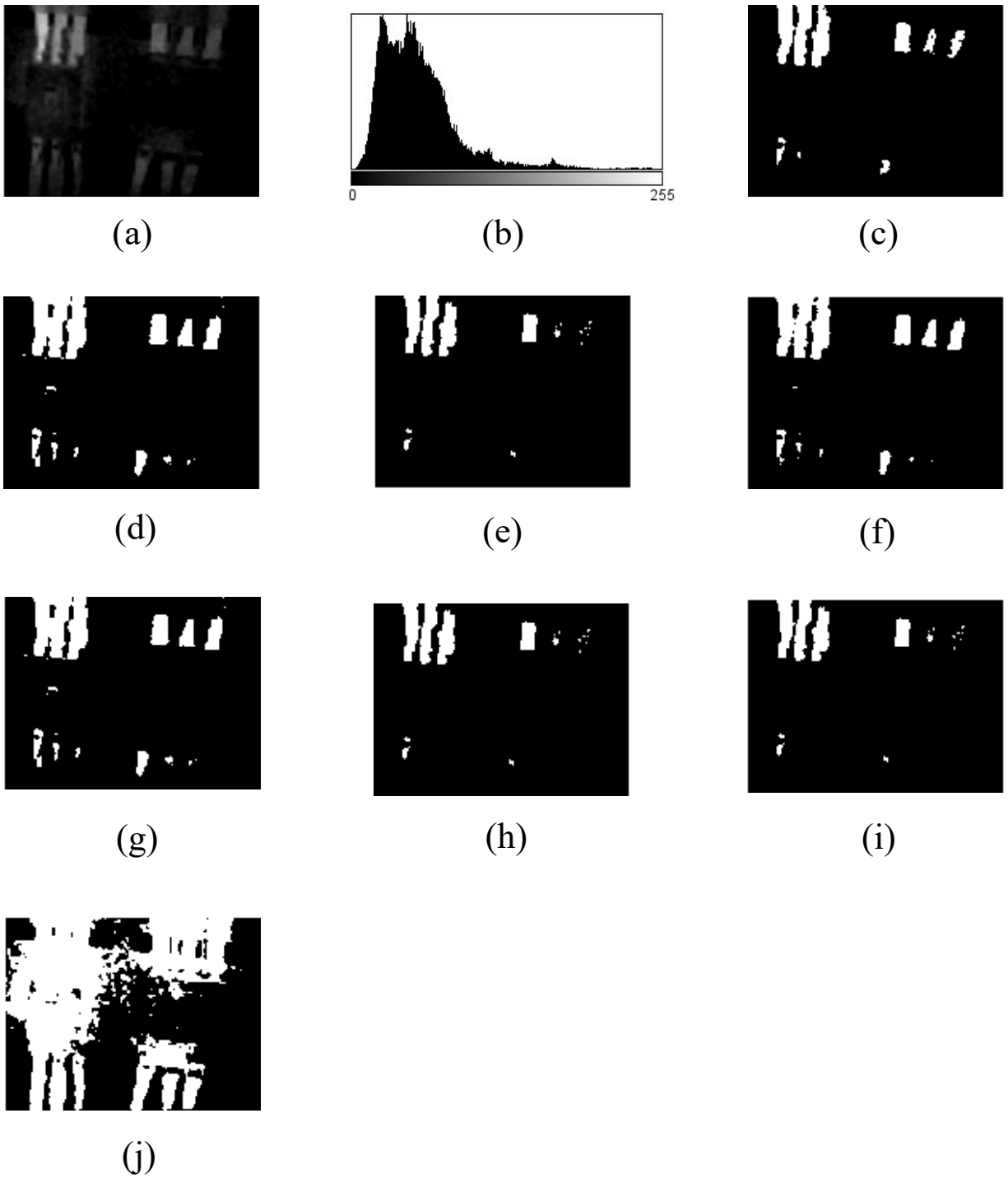

Figure 4.5*: Target hotspots extraction from Image-04 using Thresholding techniques (a) Enhanced Thermal Image (b) Histogram (c) Ground truth image (d) IsoData (e) MaxEntropy/Kapur (f) Moments*

4.2.5 Image-05 Dataset

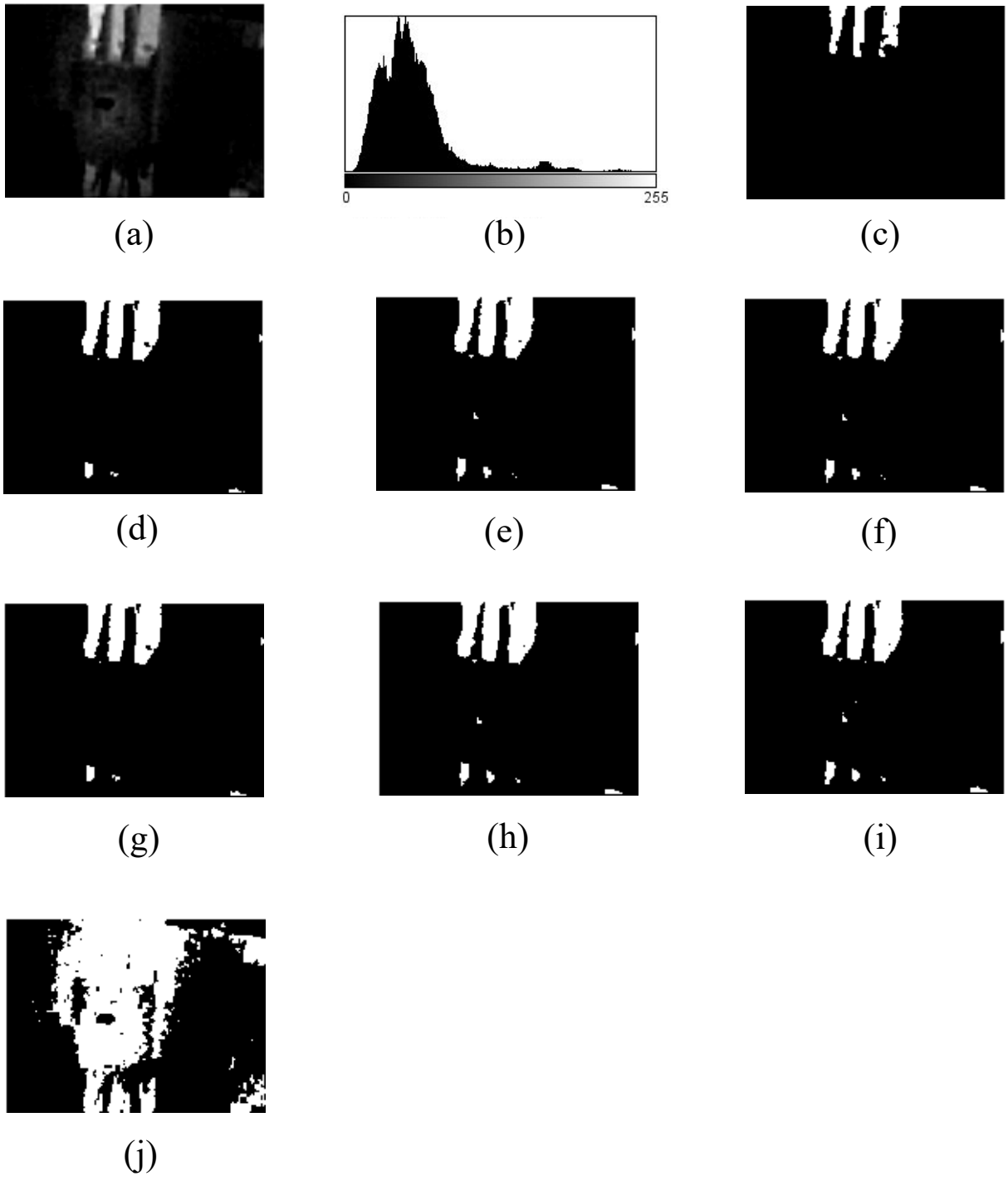

Figure 4.6*: Target hotspots extraction from Image-05 using Thresholding techniques (a) Enhanced Thermal Image (b) Histogram (c) Ground truth image (d) IsoData (e) MaxEntropy/Kapur (f) Moments*

4.2.6 Image-06 Dataset

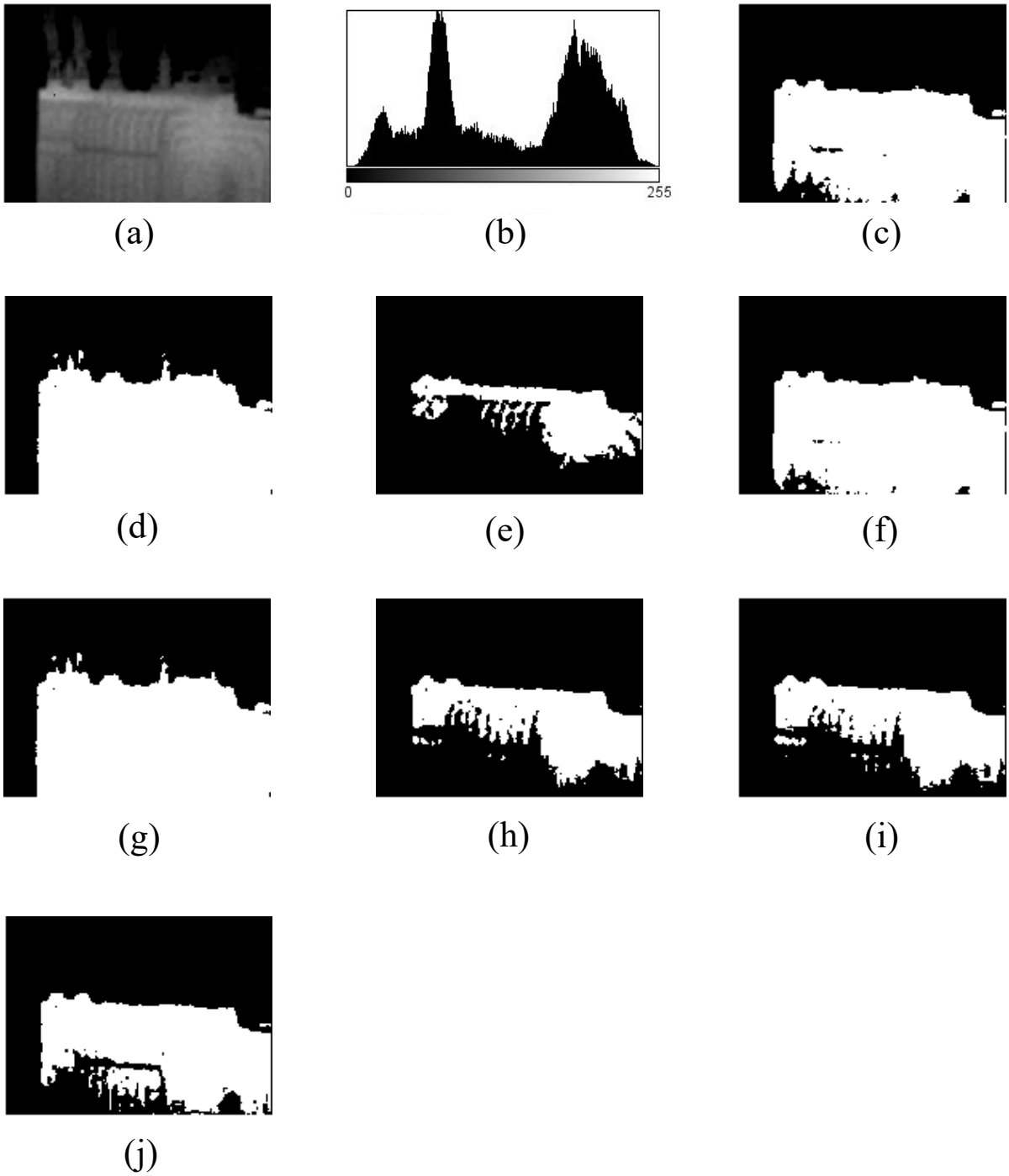

Figure 4.7*: Target hotspots extraction from Image-06 using Thresholding techniques (a) Enhanced Thermal Image (b) Histogram (c) Ground truth image (d) IsoData (e) MaxEntropy/Kapur (f) Moments*

4.2.7 Image-07 Dataset

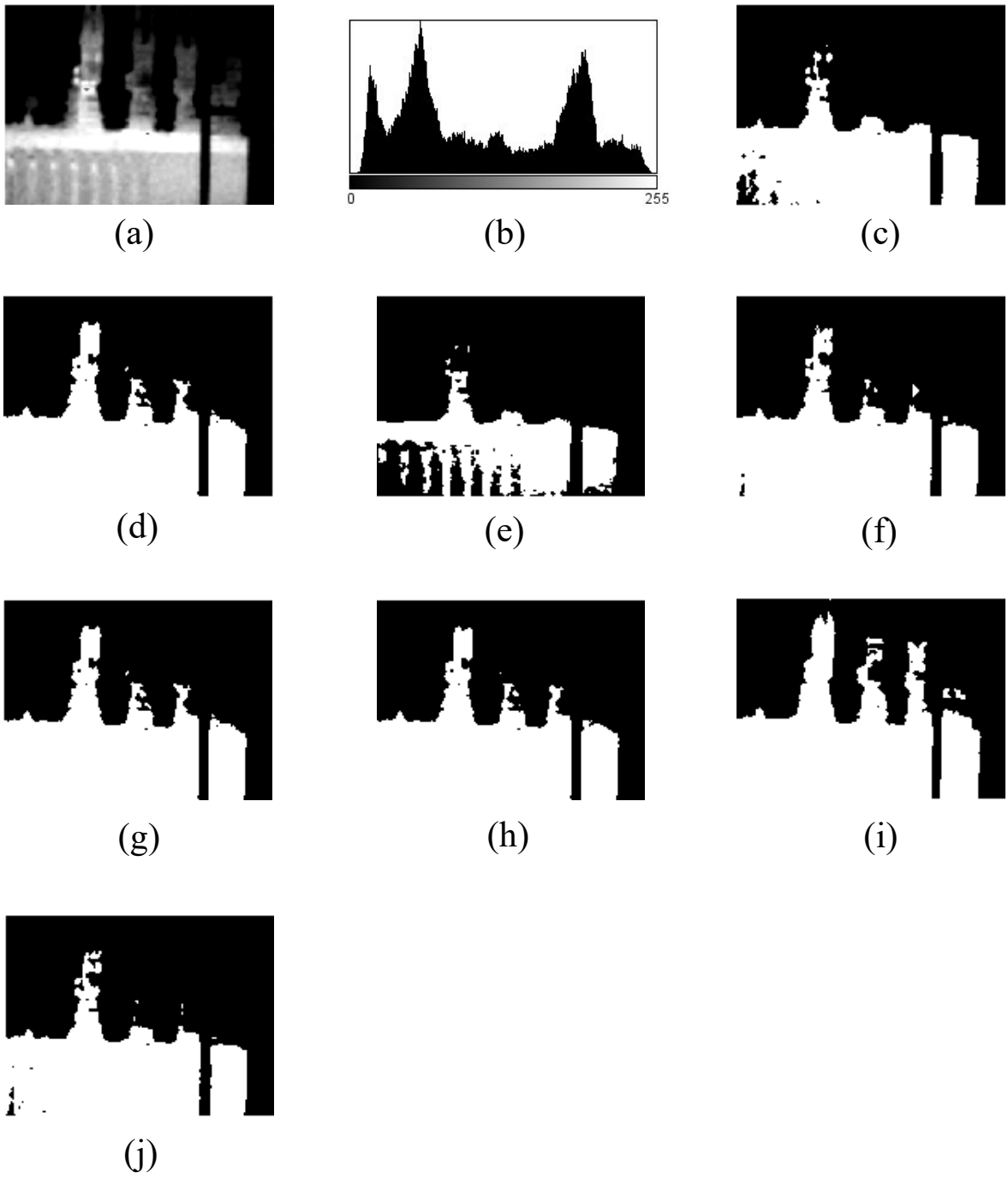

***Figure 4.8**: Target hotspots extraction from Image-07 using Thresholding techniques (a) Enhanced Thermal Image (b) Histogram (c) Ground truth image (d) IsoData (e) MaxEntropy/Kapur (f) Moments*

4.2.8 Image-08 Dataset

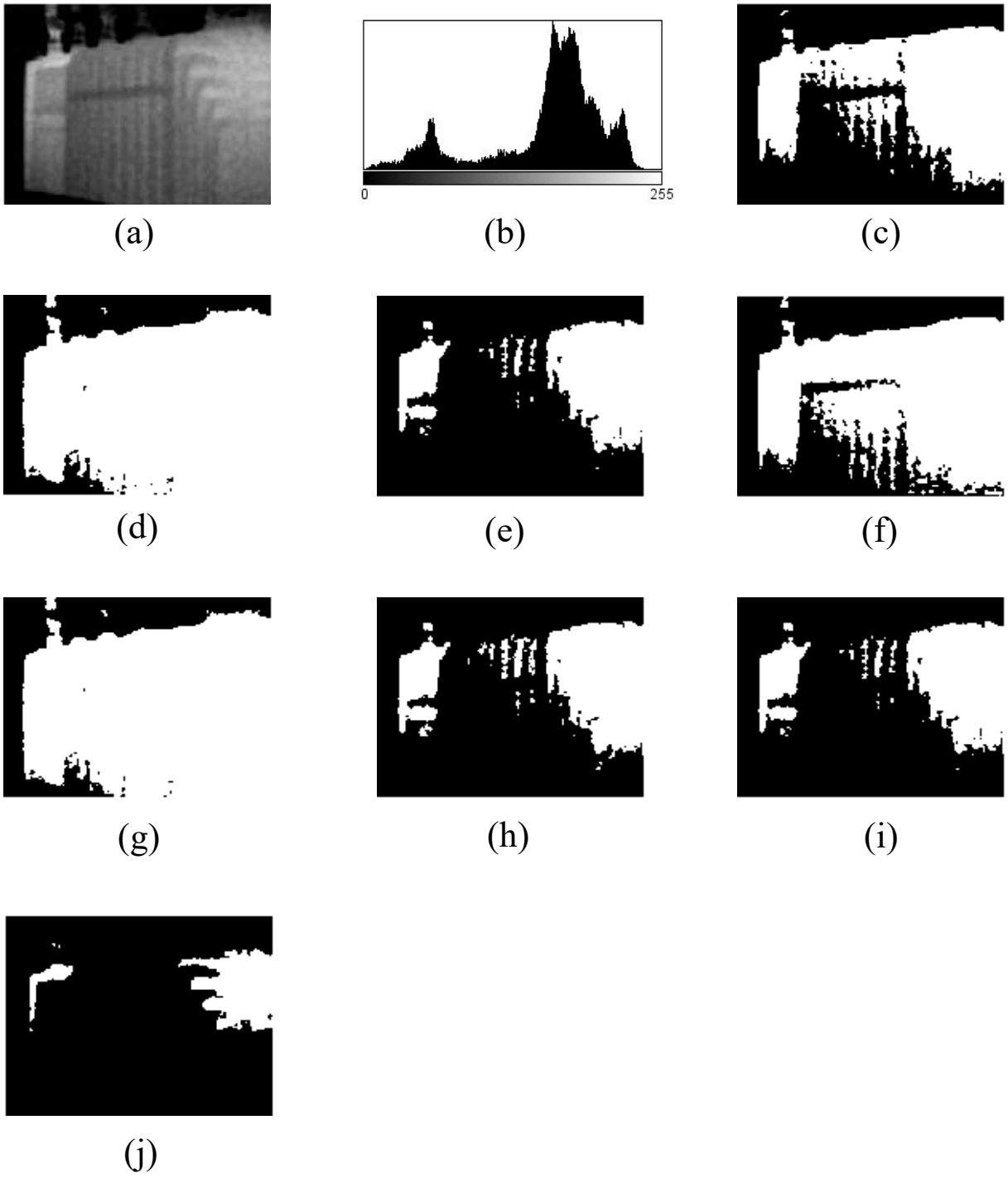

Figure 4.9*: Target hotspots extraction from Image-08 using Thresholding techniques (a) Enhanced Thermal Image (b) Histogram (c) Ground truth image (d) IsoData (e) MaxEntropy/Kapur (f) Moments*

4.2.9 Image-09 Dataset

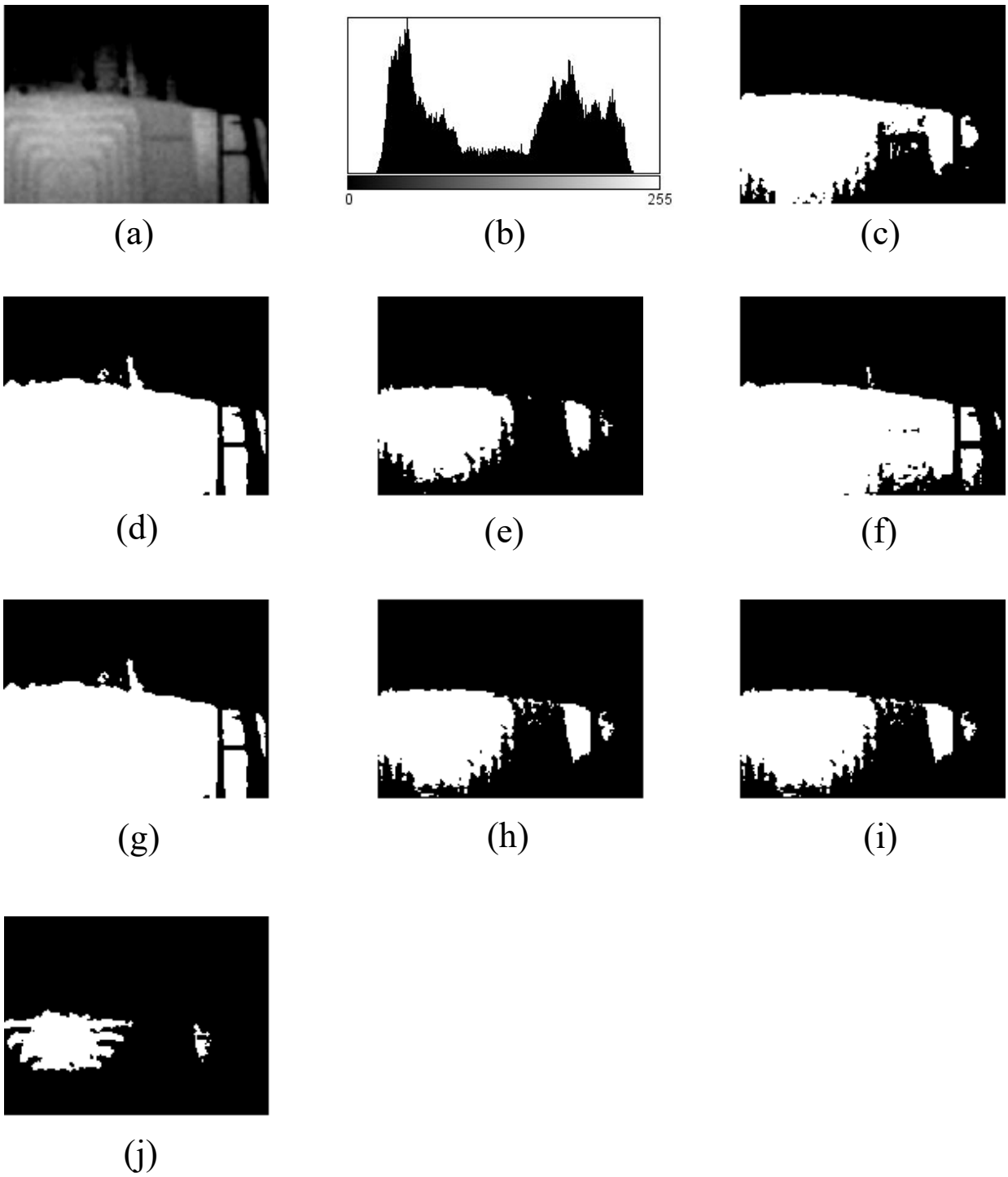

Figure 20*: Target hotspots extraction from Image-09 using Thresholding techniques (a) Enhanced Thermal Image (b) Histogram (c) Ground truth image (d) IsoData (e) MaxEntropy/Kapur (f) Moments*

4.2.10 Image-10 Dataset

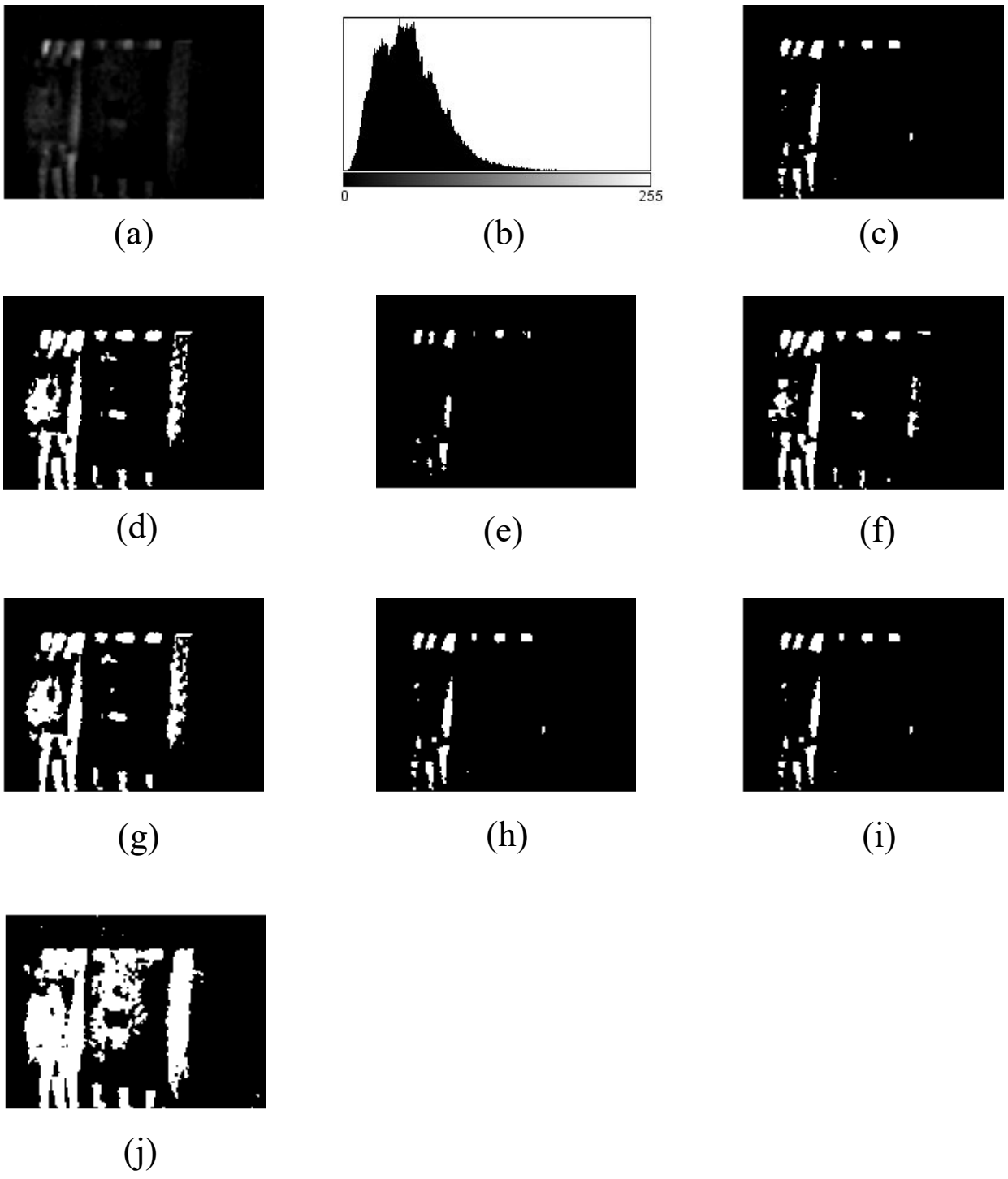

Figure 4.11*: Target hotspots extraction from Image-10 using Thresholding techniques (a) Enhanced Thermal Image (b) Histogram (c) Ground truth image (d) IsoData (e) MaxEntropy/Kapur (f) Moments*

4.2.11 Image-11 Dataset

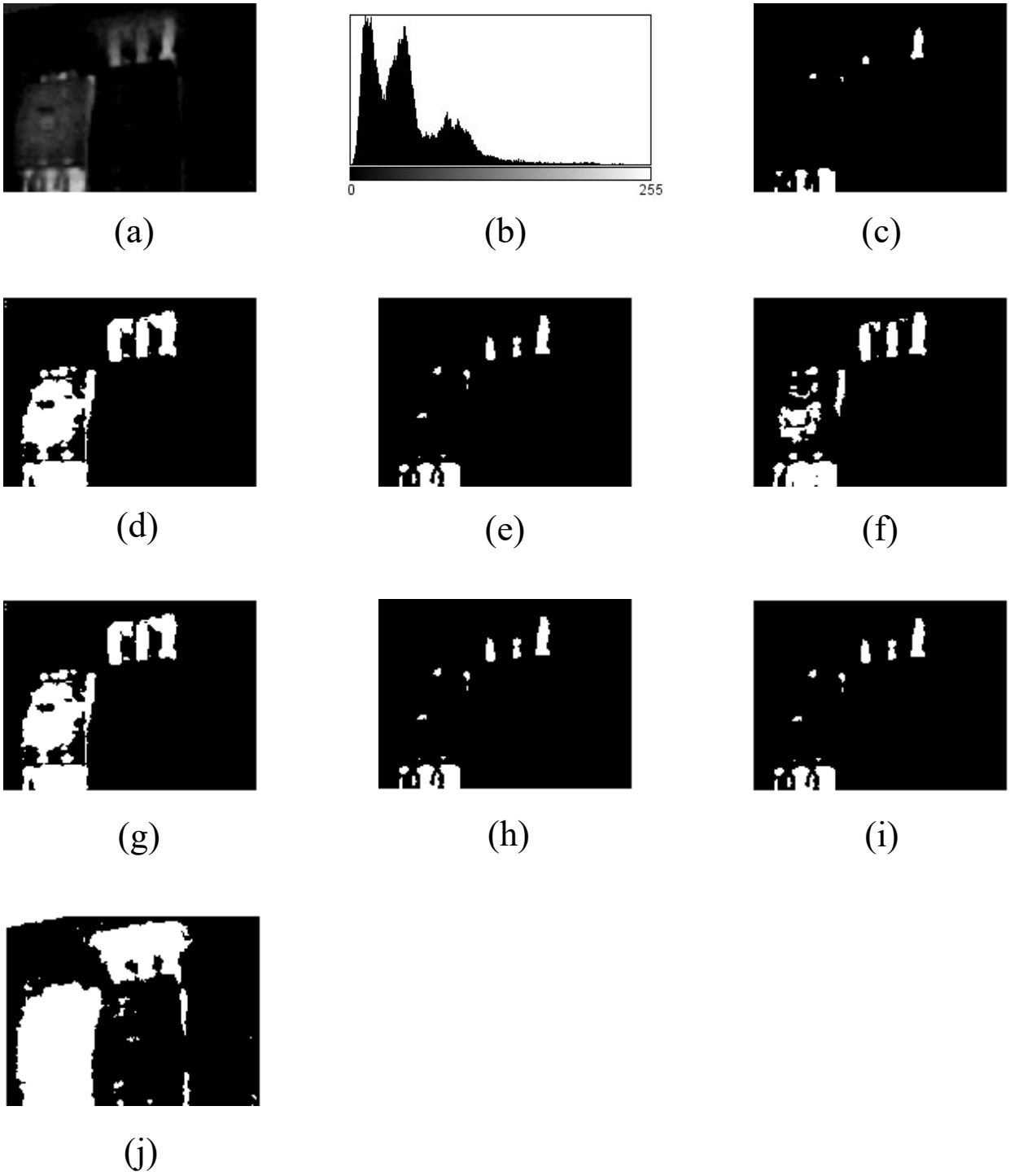

Figure 4.12*: Target hotspots extraction from Image-11 using Thresholding techniques (a) Enhanced Thermal Image (b) Histogram (c) Ground truth image (d) IsoData (e) MaxEntropy/Kapur (f) Moments*

4.2.12 Image-12 Dataset

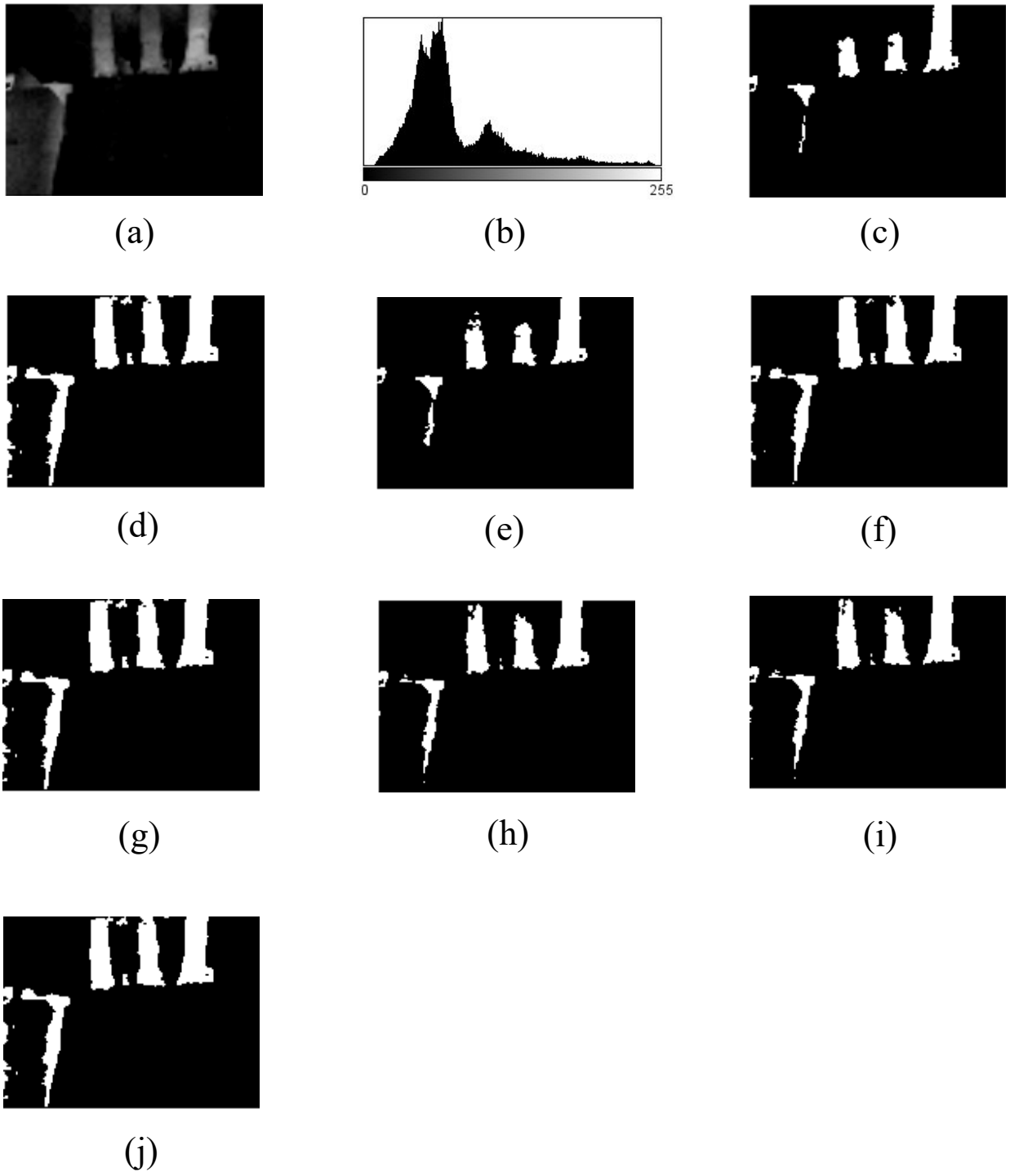

Figure 4.13*: Target hotspots extraction from Image-12 using Thresholding techniques (a) Enhanced Thermal Image (b) Histogram (c) Ground truth image (d) IsoData (e) MaxEntropy/Kapur (f) Moments*

4.2.13 Image-13 Dataset

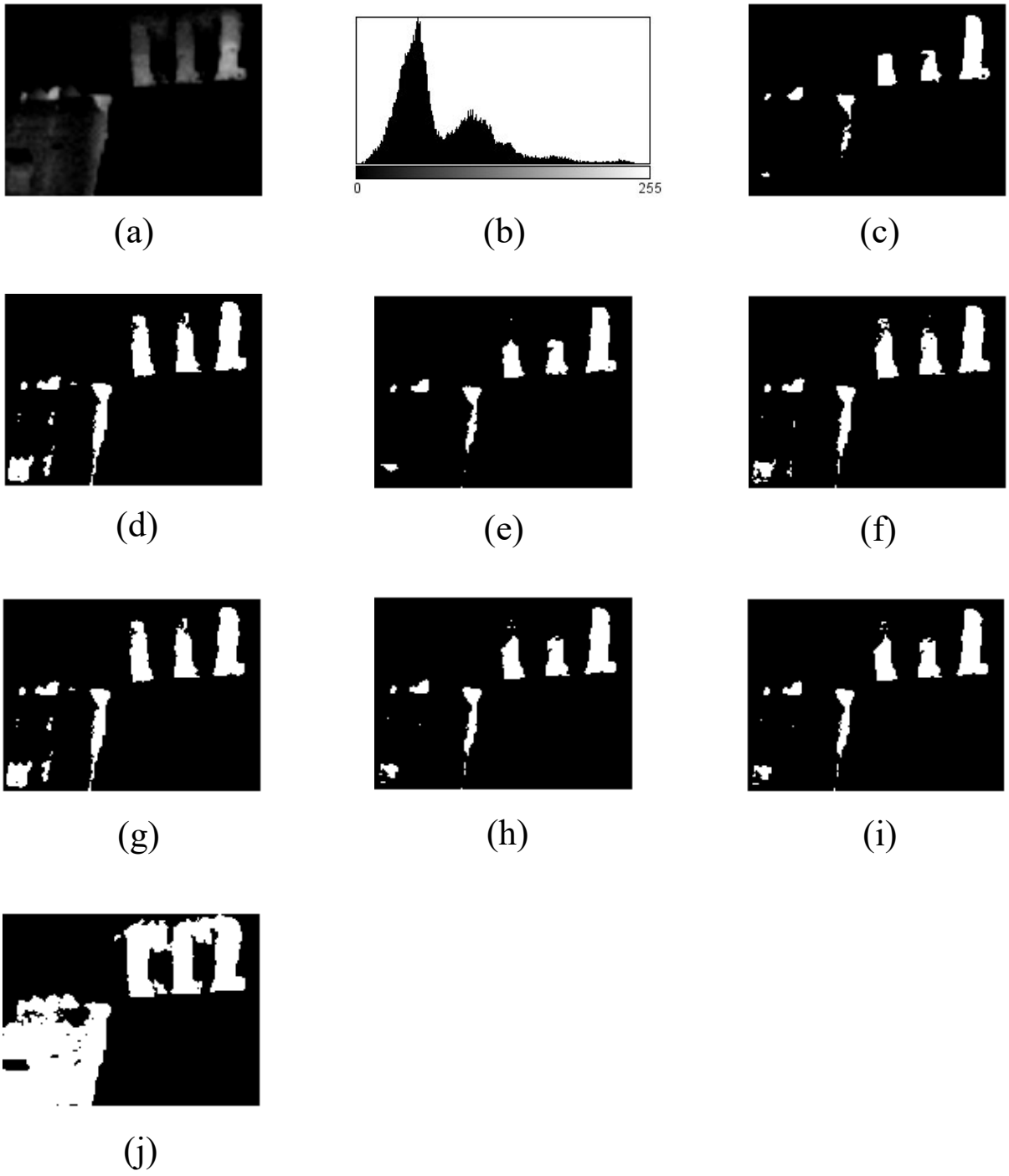

Figure 4.14*: Target hotspots extraction from Image-13 using Thresholding techniques (a) Enhanced Thermal Image (b) Histogram (c) Ground truth image (d) IsoData (e) MaxEntropy/Kapur (f) Moments*

4.2.14 Image-14 Dataset

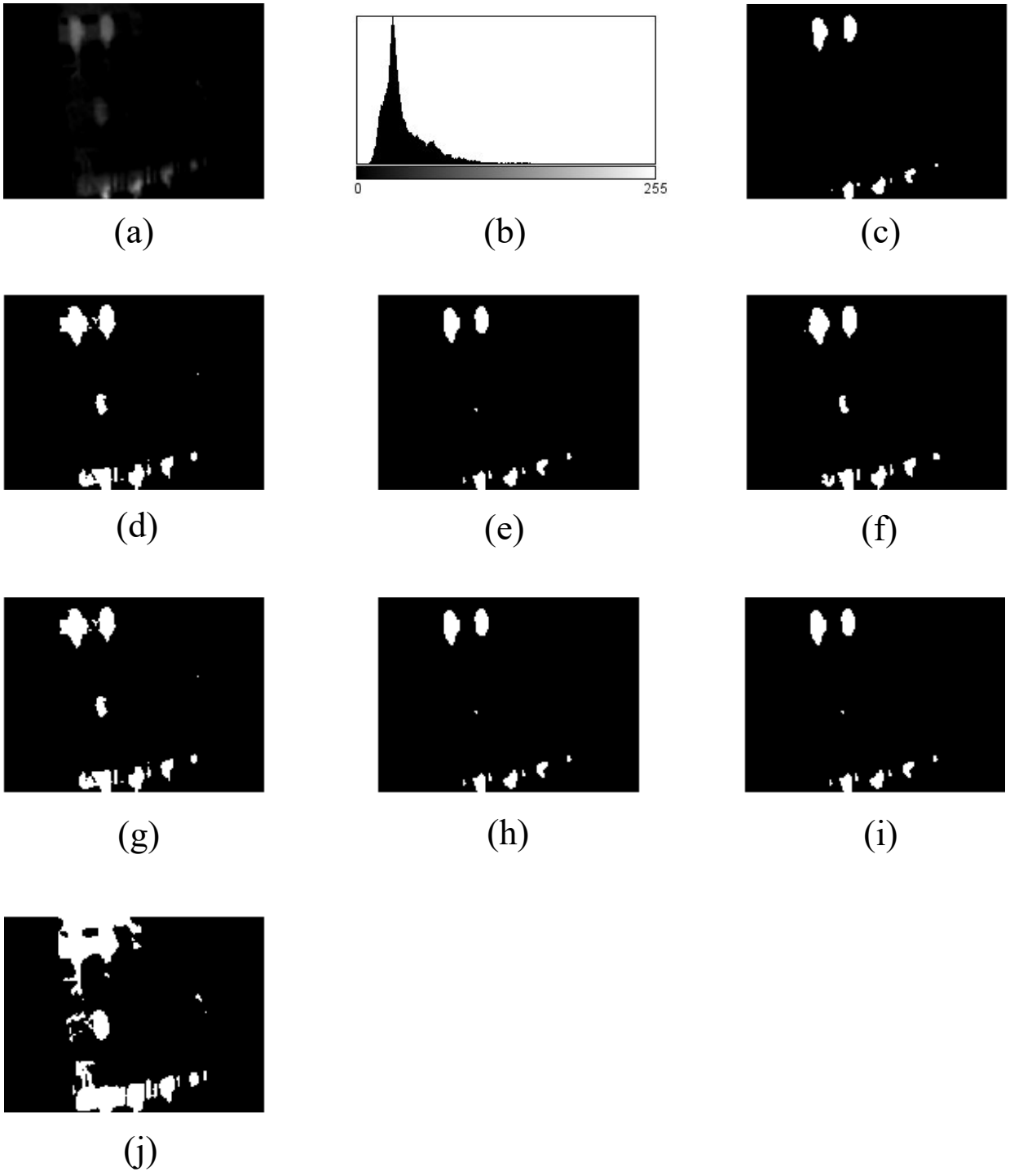

Figure 4.15*: Target hotspots extraction from Image-14 using Thresholding techniques (a) Enhanced Thermal Image (b) Histogram (c) Ground truth image (d) IsoData (e) MaxEntropy/Kapur (f) Moments*

4.2.15 Image-15 Dataset

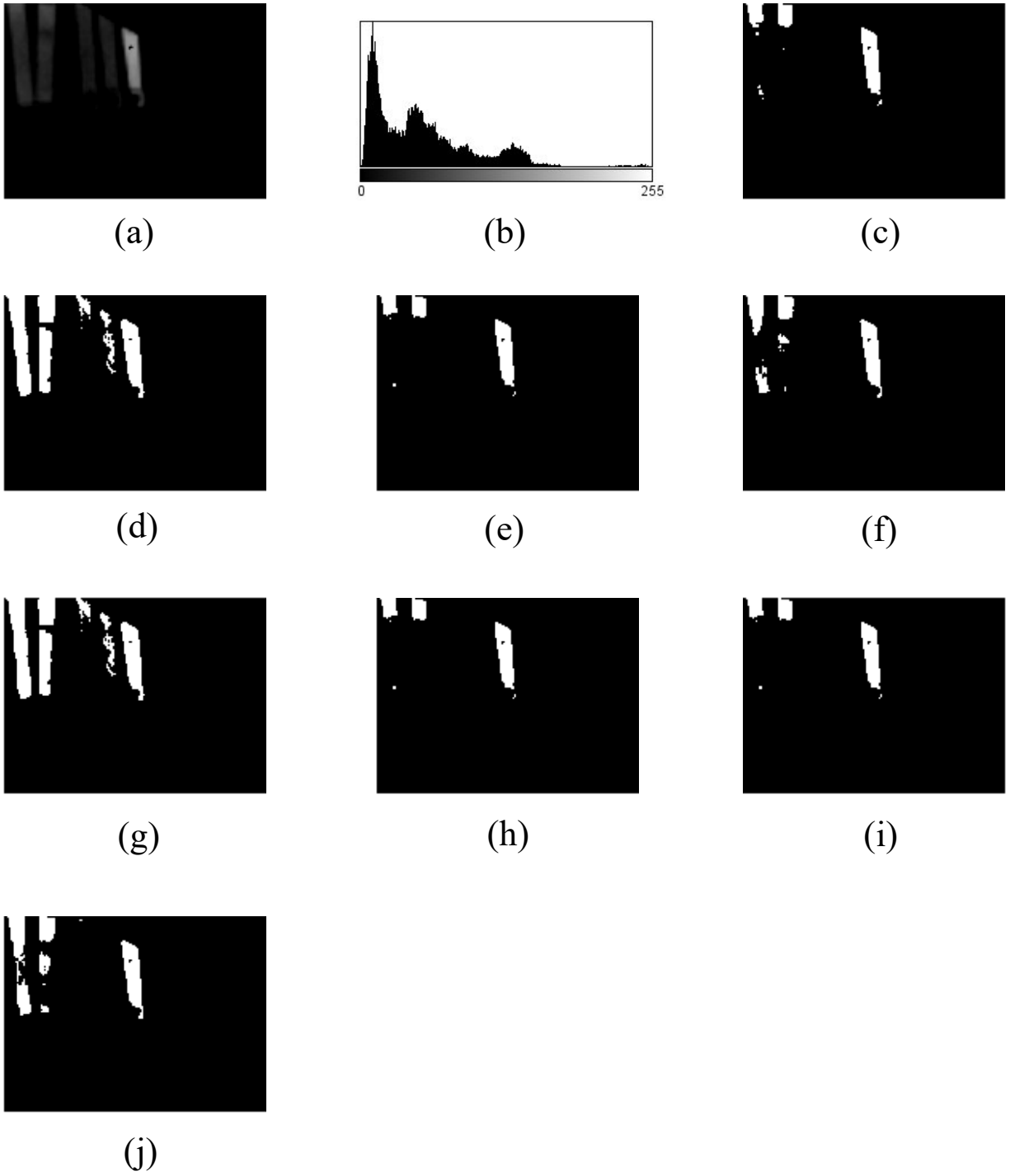

Figure 4.16*: Target hotspots extraction from Image-15 using Thresholding techniques (a) Enhanced Thermal Image (b) Histogram (c) Ground truth image (d) IsoData (e) MaxEntropy/Kapur (f) Moments*

4.2.16 Image-16Dataset

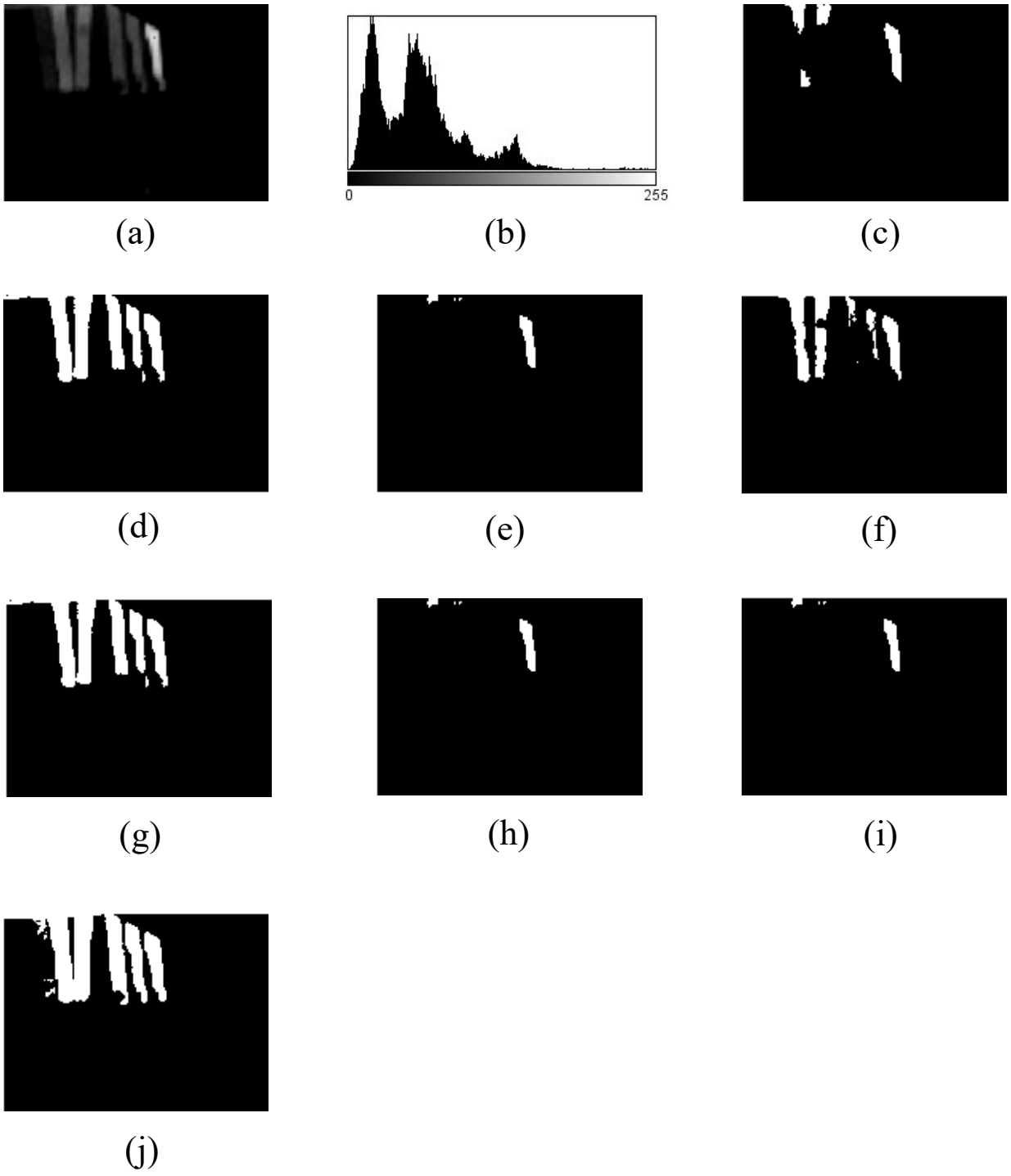

Figure 4.17*: Target hotspots extraction from Image-16 using Thresholding techniques (a) Enhanced Thermal Image (b) Histogram (c) Ground truth image (d) IsoData (e) MaxEntropy/Kapur (f) Moments*

4.2.17 Image-17 Dataset

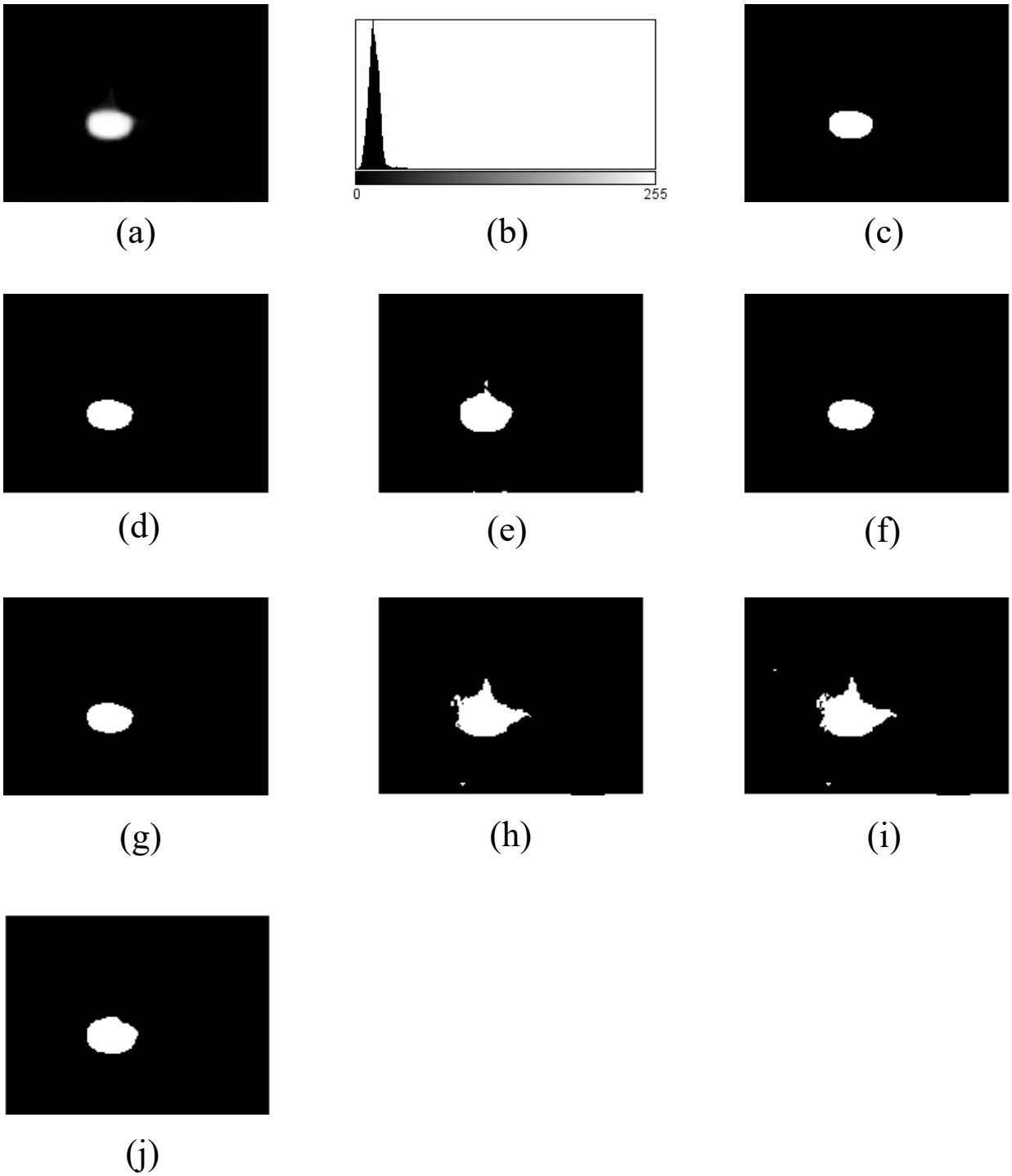

Figure 4.18*: Target hotspots extraction from Image-17 using Thresholding techniques (a) Enhanced Thermal Image (b) Histogram (c) Ground truth image (d) IsoData (e) MaxEntropy/Kapur (f) Moments*

4.2.18 Image-18 Dataset

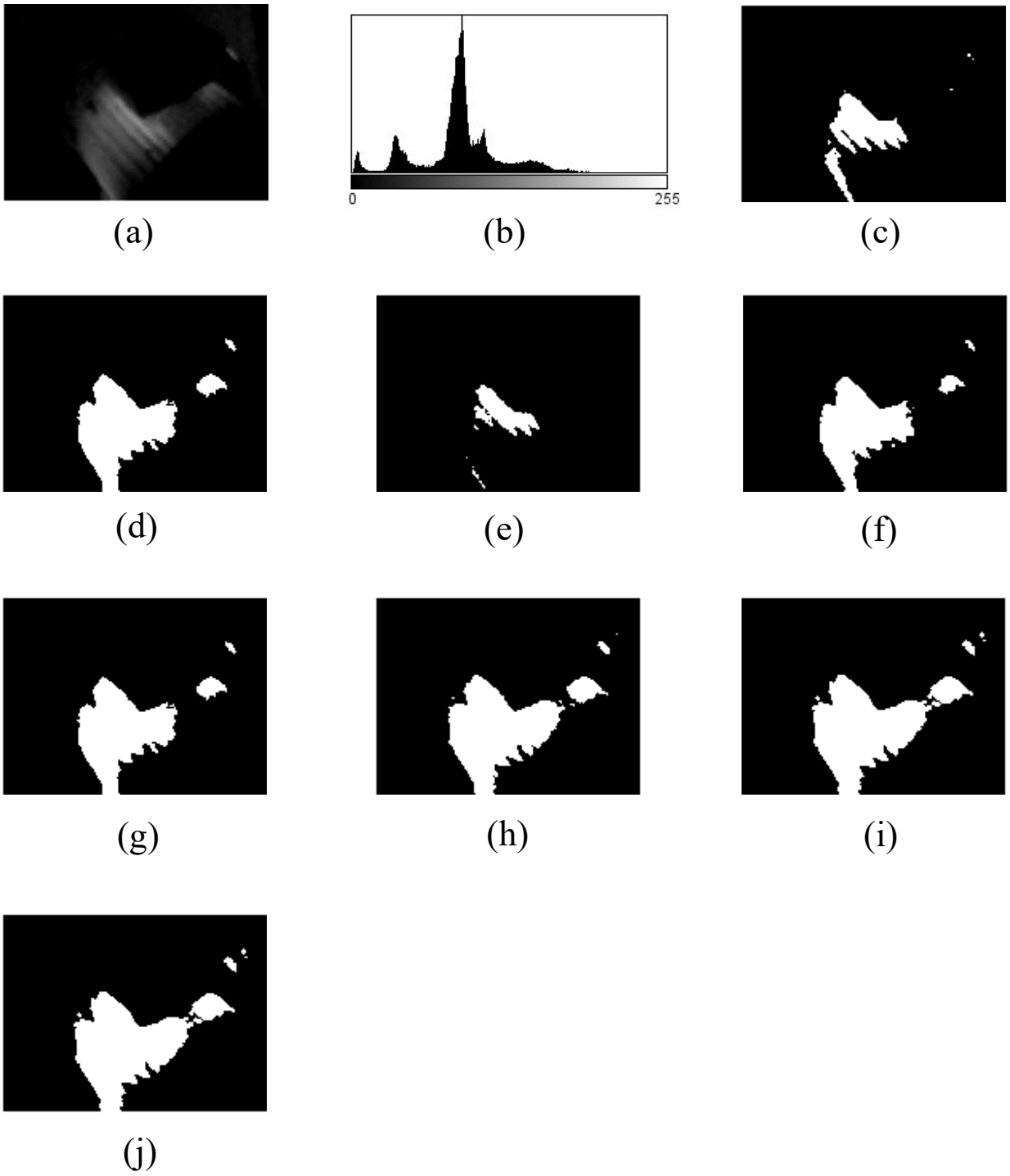

Figure 4.19*: Target hotspots extraction from Image-18 using Thresholding techniques (a) Enhanced Thermal Image (b) Histogram (c) Ground truth image (d) IsoData (e) MaxEntropy/Kapur (f) Moments*

4.2.19 Image-19 Dataset

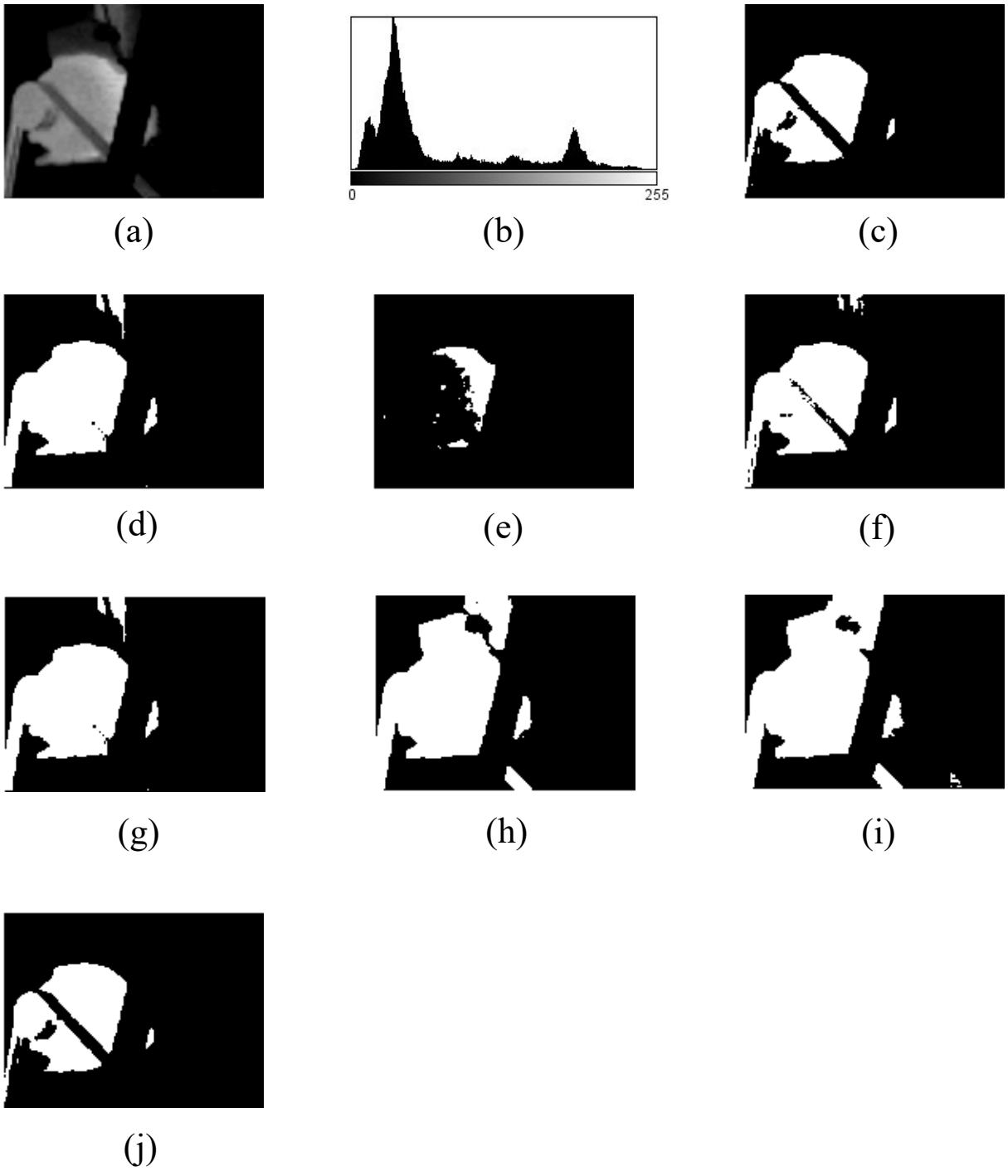

Figure 4.20*: Target hotspots extraction from Image-19 using Thresholding techniques (a) Enhanced Thermal Image (b) Histogram (c) Ground truth image (d) IsoData (e) MaxEntropy/Kapur (f) Moments*

4.2.20 Image-20 Dataset

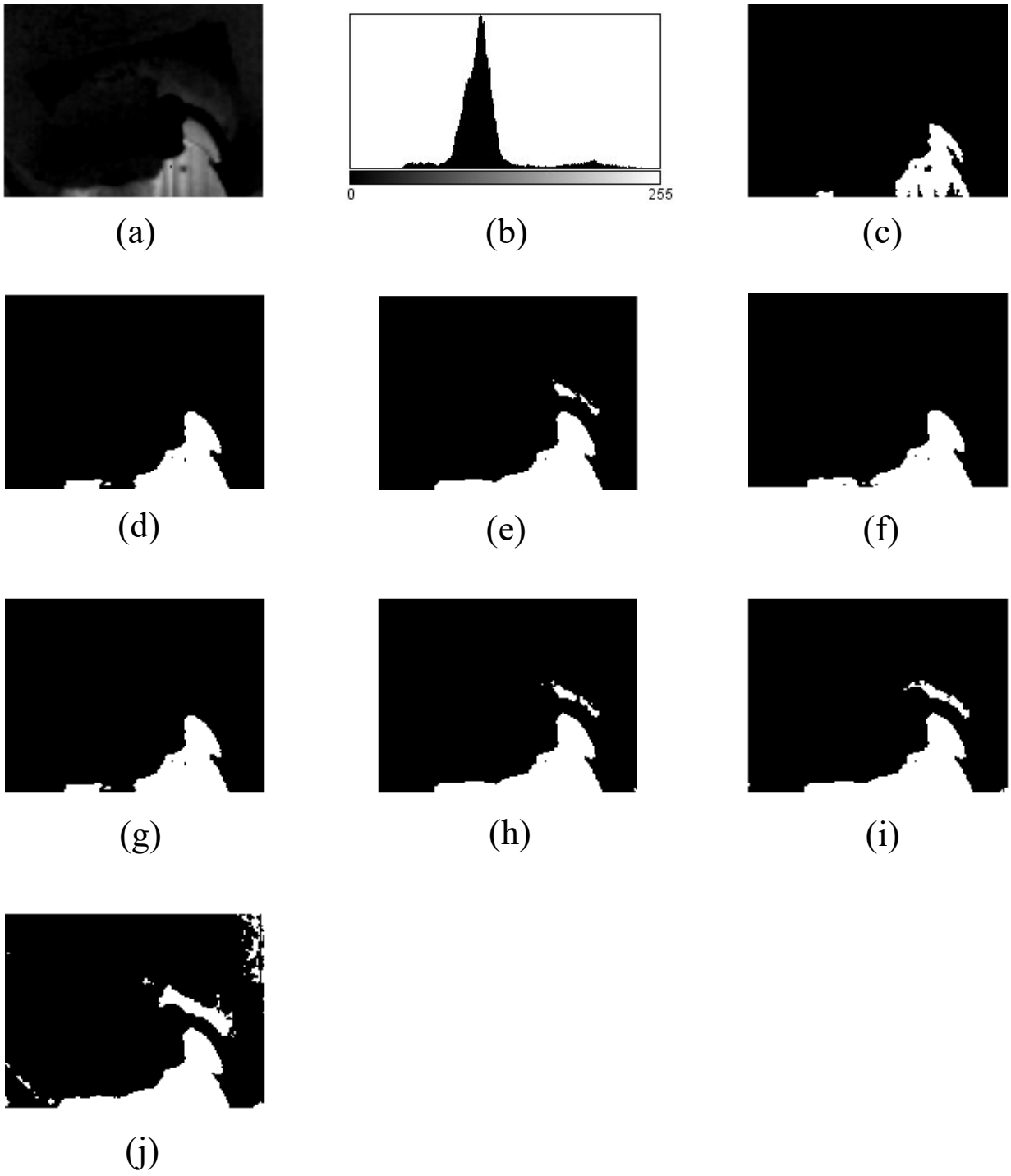

Figure 4.21*: Target hotspots extraction from Image-20 using Thresholding techniques (a) Enhanced Thermal Image (b) Histogram (c) Ground truth image (d) IsoData (e) MaxEntropy/Kapur (f) Moments*

4.2.21 Image-21 Dataset

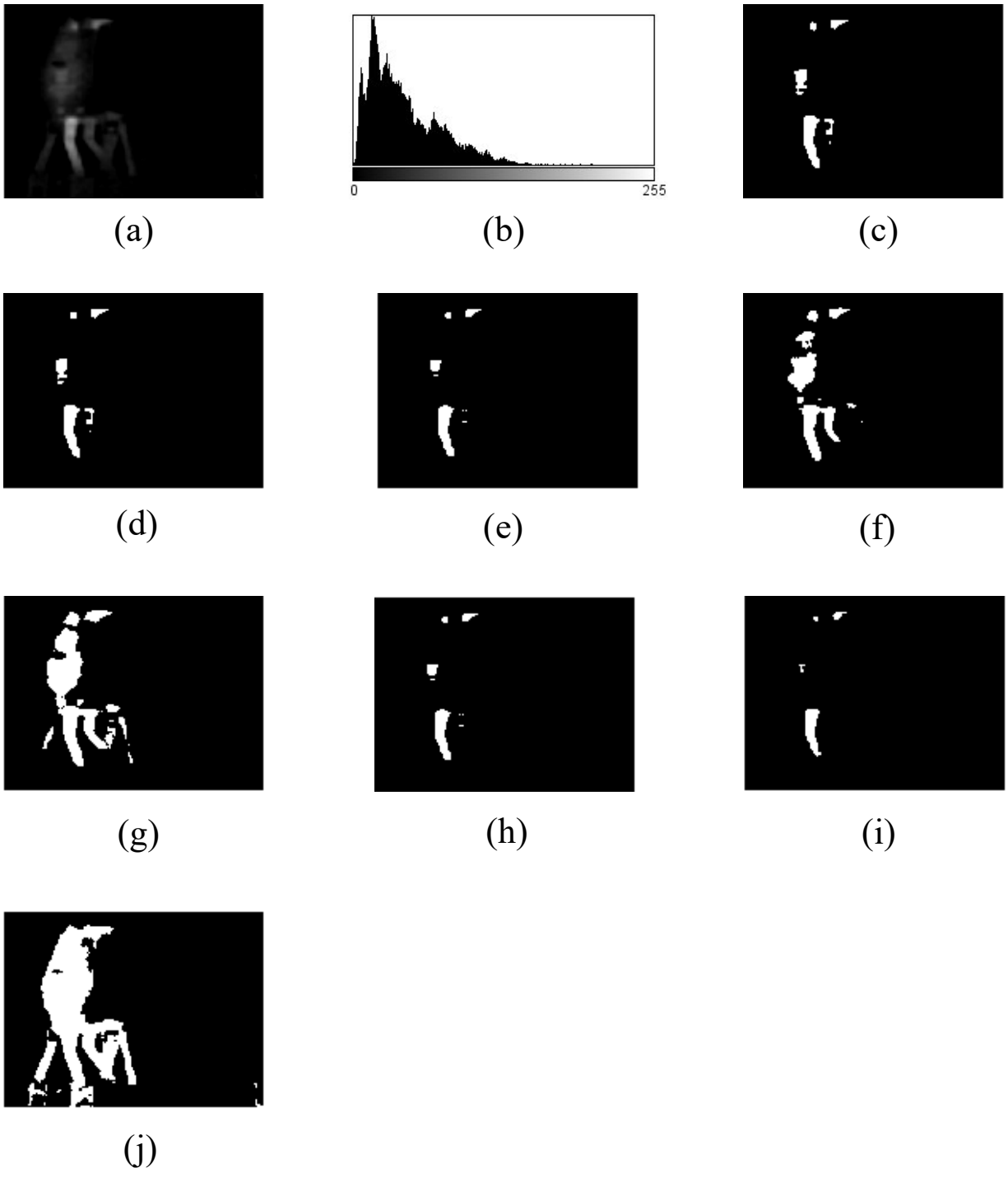

Figure 4.22*: Target hotspots extraction from Image-21 using Thresholding techniques (a) Enhanced Thermal Image (b) Histogram (c) Ground truth image (d) IsoData (e) MaxEntropy/Kapur (f) Moments*

4.2.22 Image-22 Dataset

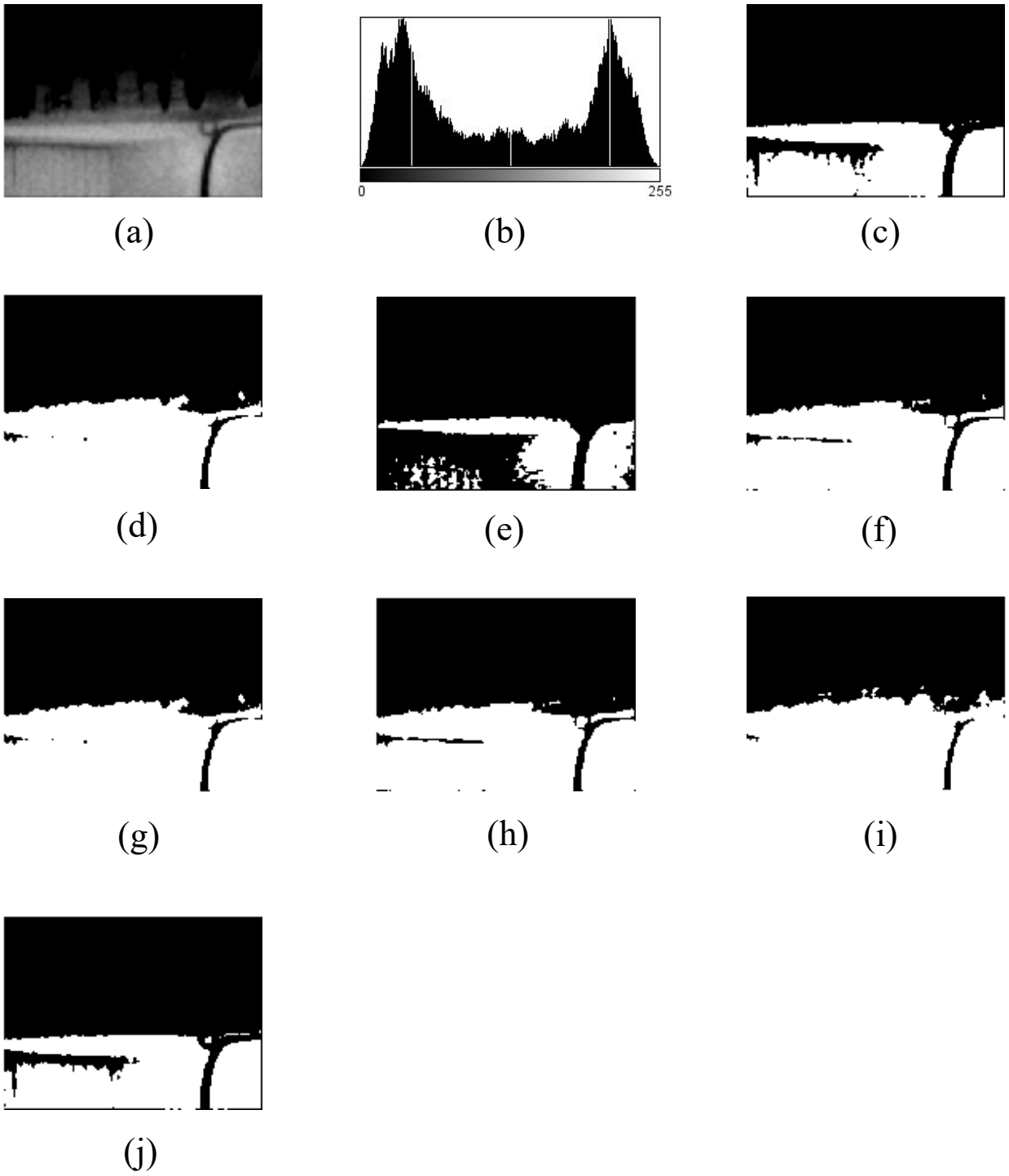

Figure 4.23*: Target hotspots extraction from Image-22 using Thresholding techniques (a) Enhanced Thermal Image (b) Histogram (c) Ground truth image (d) IsoData (e) MaxEntropy/Kapur (f) Moments*

4.2.23 Image-23 Dataset

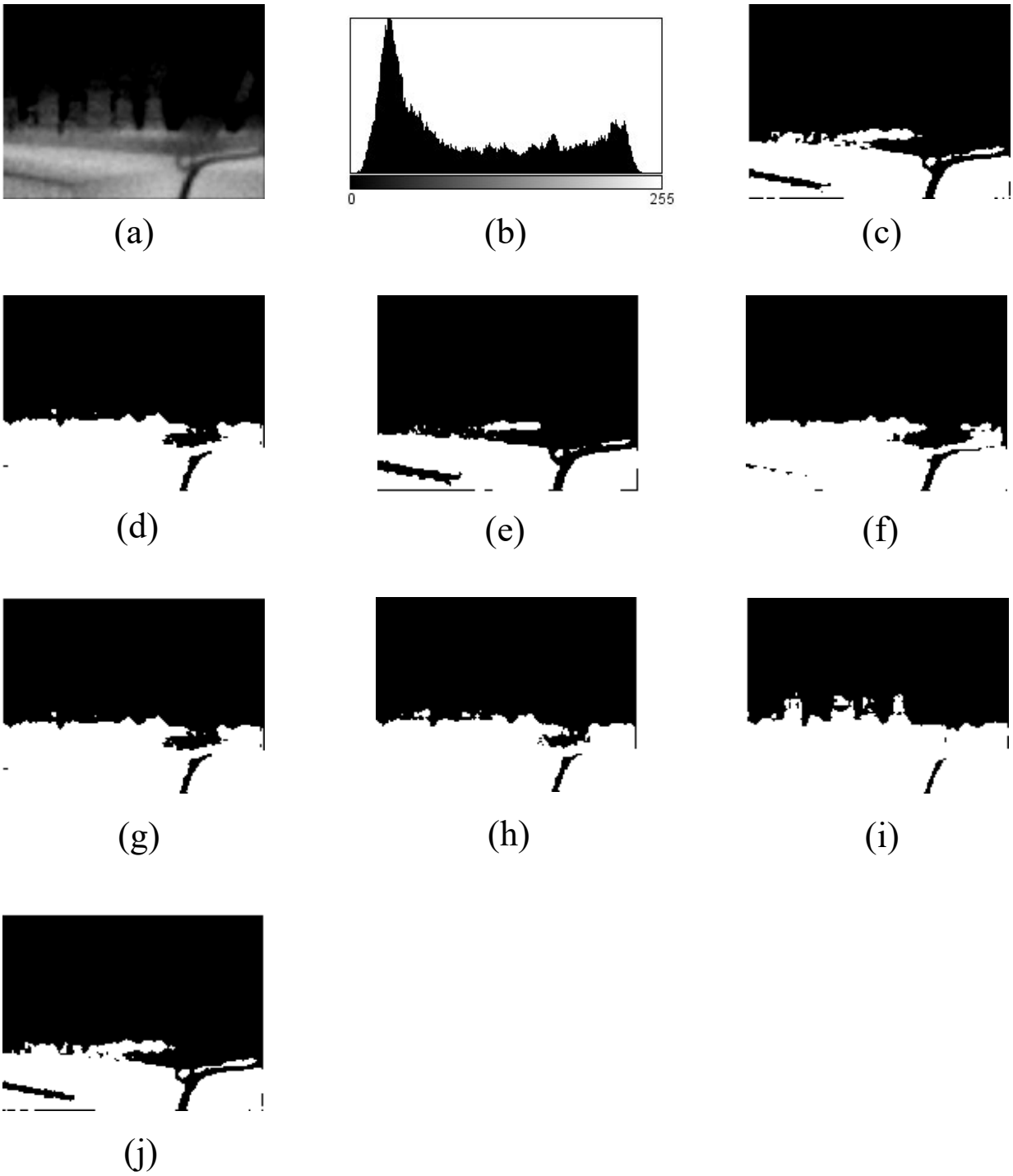

Figure 21*: Target hotspots extraction from Image-23 using Thresholding techniques (a) Enhanced Thermal Image (b) Histogram (c) Ground truth image (d) IsoData (e) MaxEntropy/Kapur (f) Moments*

4.2.24 Image-24 Dataset

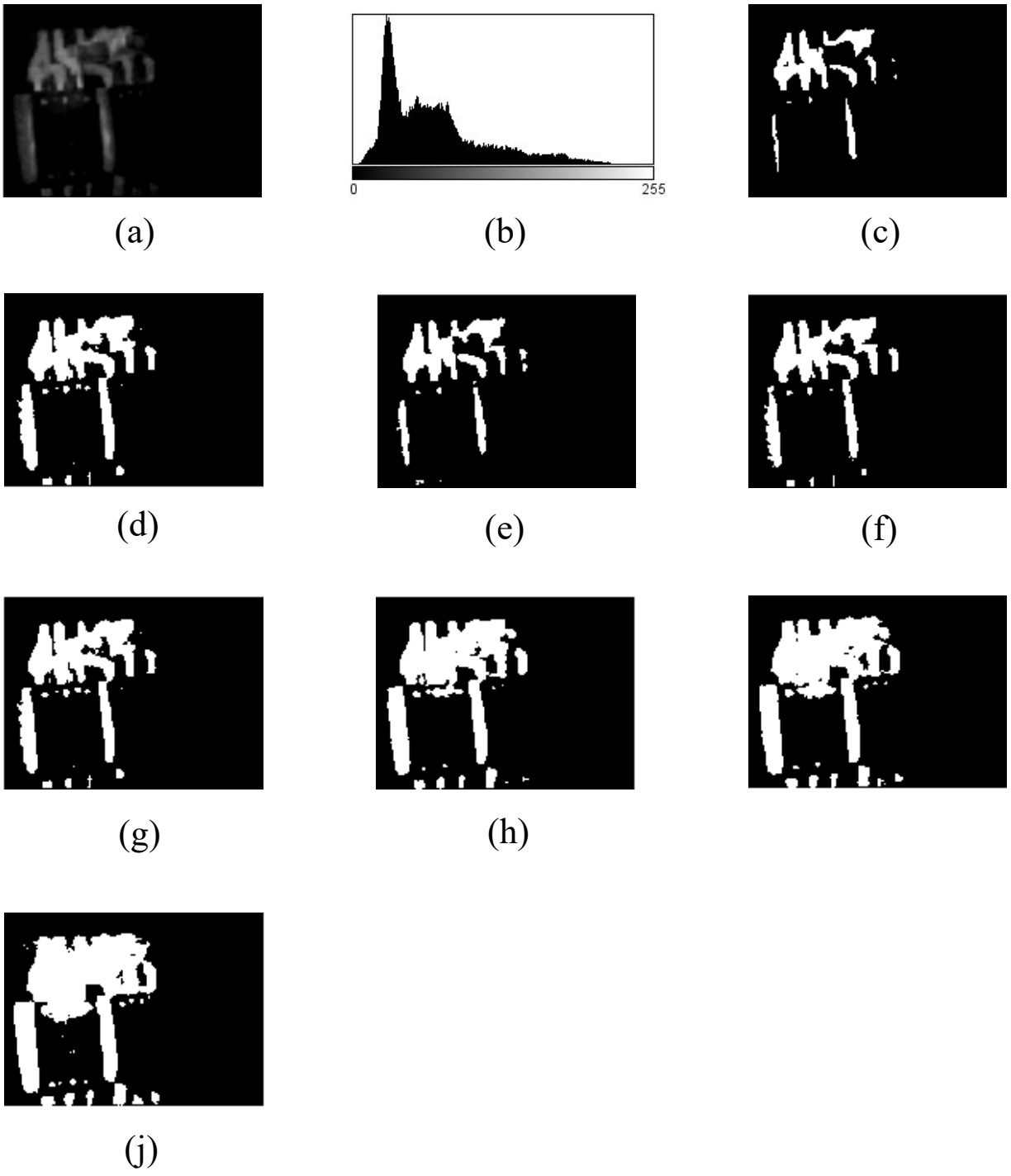

Figure 4.25*: Target hotspots extraction from Image-24 using Thresholding techniques (a) Enhanced Thermal Image (b) Histogram (c) Ground truth image (d) IsoData (e) MaxEntropy/Kapur (f) Moments*

4.3 Software and MATLAB Coding for Performance Evaluation

4.3.1 Software Usage

For the performance evaluation between ground truth and segmented image, firstly we needed to export the thermal image from Fluke Smart View Software as greyscale image. It is necessary to export the image as Greyscale because this type of image is only of 8 bits compare to the 24-bit RGB image. We don't need 24-bit type of data image for applying thresholding as we are only interested in black and white highlight area of the image. That's why for applying thresholding techniques properly, we exported all of the image as 8-bit greyscale image. Later, we used ImageJ Software to import the 8-bit images that were previously exported from the Fluke Smart View Software. After opening the images in ImageJ software, some enhancement was done to reduce the noise from the images. After that, manual thresholding was applied to all of the images to highlight the heat signatures ROI area properly. Thresholding was done completely manually for making the ground truth image as accurate as possible to compare with other thresholding techniques. Later, each enhanced image had gone through the IsoData, MaxEntropy/Kapur, MET, Otsu, Moments, RenyiEntropy, Yen thresholding techniques profile of the ImageJ Software. Thus, we got 7 different segmented images from 7 different thresholding techniques to compare the overall performance.

So, from a thermal image first we got a greyscale image then it was converted to a greyscale image. After that image was enhanced for noise reduction and we manually found segmented ground truth image by applying global thresholding manually. Later, we applied 7 different thresholding techniques for getting 7 different segmented images for comparing with the ground truth image to compare every thresholding techniques performance.

We used total 24 thermal image for this procedure. So, from 1 thermal image we got 8 different segmented images. Among them one is ground truth image and other seven image is from seven different thresholding techniques. So, all together we got 192 segmented images from 24 thermal image to perform the evaluation of performances among seven different thresholding techniques.

After that, all of the images were exported from ImageJ software as binary image to a folder for reading those binary images at MATLAB and applying performance evaluation code to get the final test results among ground truth and segmented images. All together custom MATLAB code was run for 168 times to get the final performance evaluation results. After every run of the MATLAB code respective data was exported to Excel Sheet for further summarization of the Data.

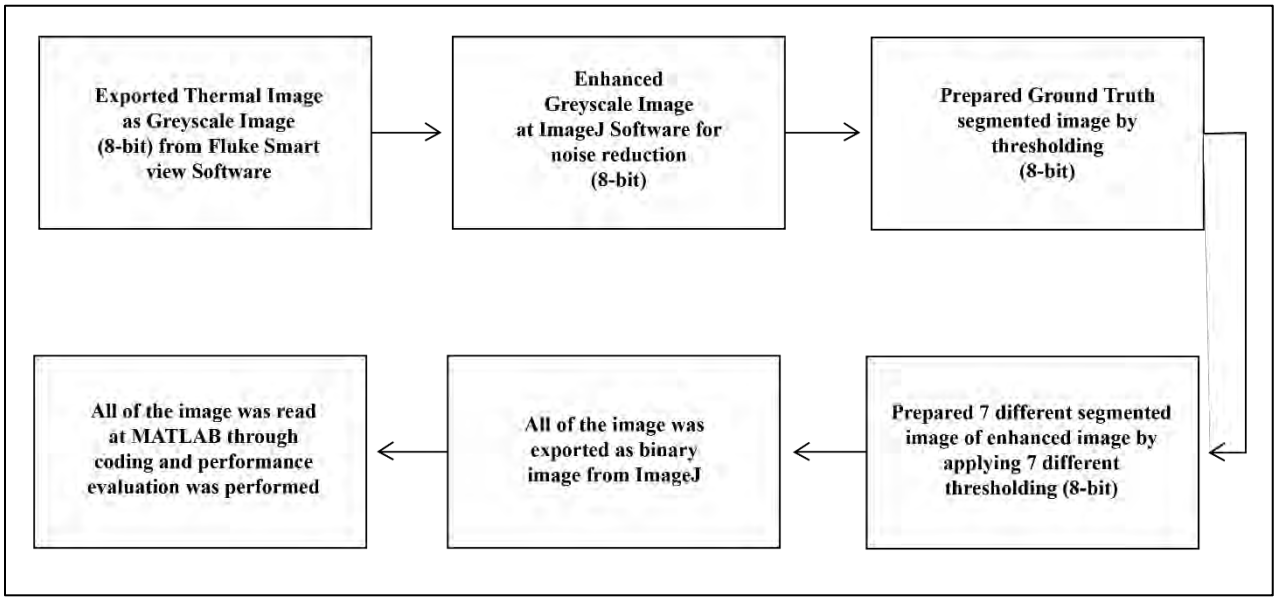

Figure 4.26*: Flowchart for performance evaluation of different thresholding techniques using software and coding.*

4.3.2 MATLAB Coding

As we all know MATLAB has powerful Image Processing Toolbox to analyze image that's why we opted for MATLAB to get the overlap results and accuracy of ground truth and segmented image to find out the FPR, TPR, Accuracy, Precision, MCC, Dice, Jaccard Index, Error (%) results. MATLAB code was designed to read the ground truth image and other segmented image to compare each other at a time [24-26].

MATLAB Code:

```
function [output] = PerformanceAnalysisNew(A, B)
  % Copyright 2019 by Dang N. H. Thanh. Email: thanh.dnh.cs@gmail.com
  % Visit my site: https://sites.google.com/view/crx/sdm
  % Need to install the image processing toolbox
  % ================================================================
  % A and B need to be binary images
  % A is the ground truth, B is the segmented result.
  % MCC - Matthews correlation coefficient
  % Note: Sensitivity = Recall
  % TP - true positive, FP - false positive,
  % TN - true negative, FN - false negative

  % If A, B are binary images, but uint8 (0, 255),
  % Need to convert to logical images.

  % Modified by Asaduzzaman Abir,
  % Final Version 6th April, 2020.

  if(isa(A,'logical'))
      X = A;
  else
      X = ~imbinarize(A);
  end
  if(isa(B,'logical'))
      Y = B;
  else
      Y = ~imbinarize(B);
  end

  % Error Calculation

  img1g_totpx = numel( A );
  img2g_totpx = numel( B );
  img1g_NB = length( A(A~=0) );
  img2g_NB = length( B(B~=0) );
```

```
   diffPx = abs( img1g_NB - img2g_NB );
   Error = (diffPx/img1g_totpx)*100;

   % Evaluate TP, TN, FP, FN

   sumindex = X + Y;
   TP = length(find(sumindex == 2));
   TN = length(find(sumindex == 0));
   substractindex = X - Y;
   FP = length(find(substractindex == -1));
   FN = length(find(substractindex == 1));

   P = TP + FN; % Total positive for the true class (= reference)
   N = FP + TN; % Total negative for the true class (= reference)

   FPR = FP/N; % False positive rate

   TPR = TP/P; % True positive rate

   Accuracy = (TP+TN)/(FN+FP+TP+TN);


   Precision = TP/(TP+FP);


   MCC = (TP*TN-FP*FN)/sqrt((TP+FP)*(TP+FN)*(TN+FP)*(TN+FN));


   % For MATLAB2017b+, can call: Dice = dice(A, B), but A, B

   % need to be converted to the logical form

   % For MATLAB2017b+, can call: Jaccard = jaccard(A, B), but

   % A, B need to be converted to the logical form


   Dice = 2*TP/(2*TP+FP+FN);


   Jaccard = Dice/(2-Dice);

   %Code to get output

   %PerformanceAnalysisNew(imread('1.png'), imread('2.png'))


   output = [FPR, TPR, Accuracy, Precision, MCC, Dice, Jaccard, Error];

end
```

4.3.3 Images of execution procedure through Software & Coding

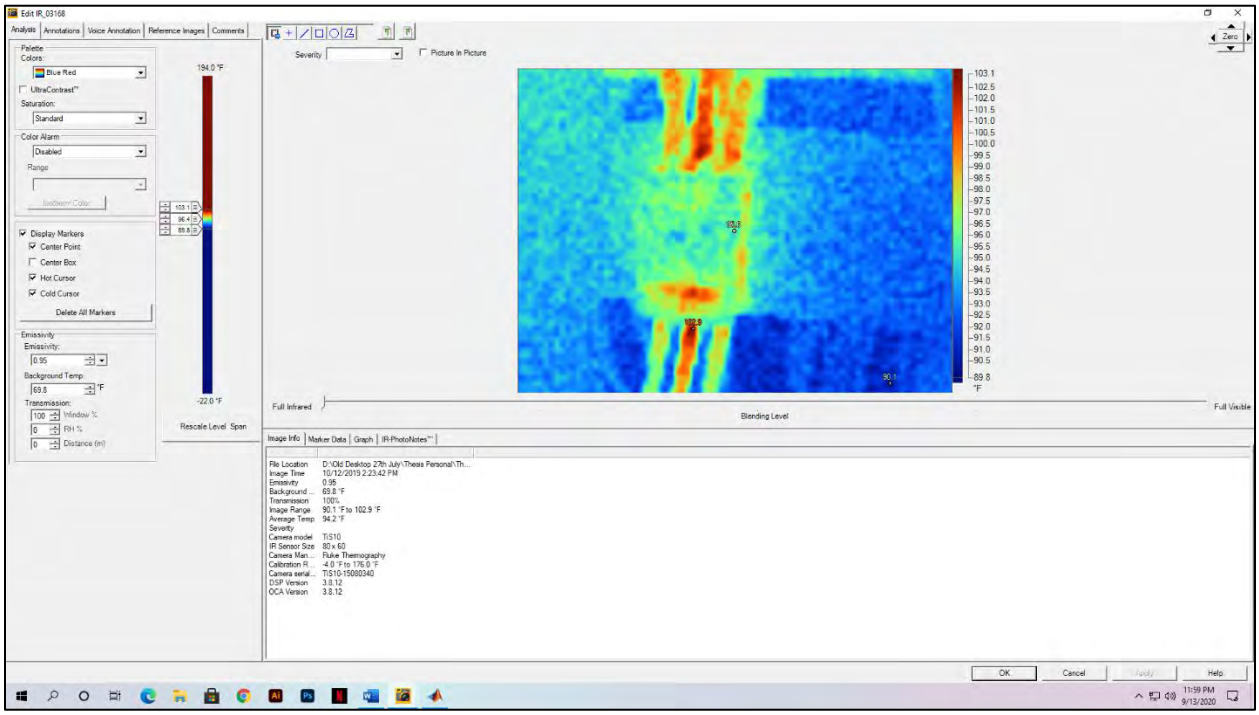

***Figure 4.27**: Viewing Thermal Image via Fluke Smart View Software*

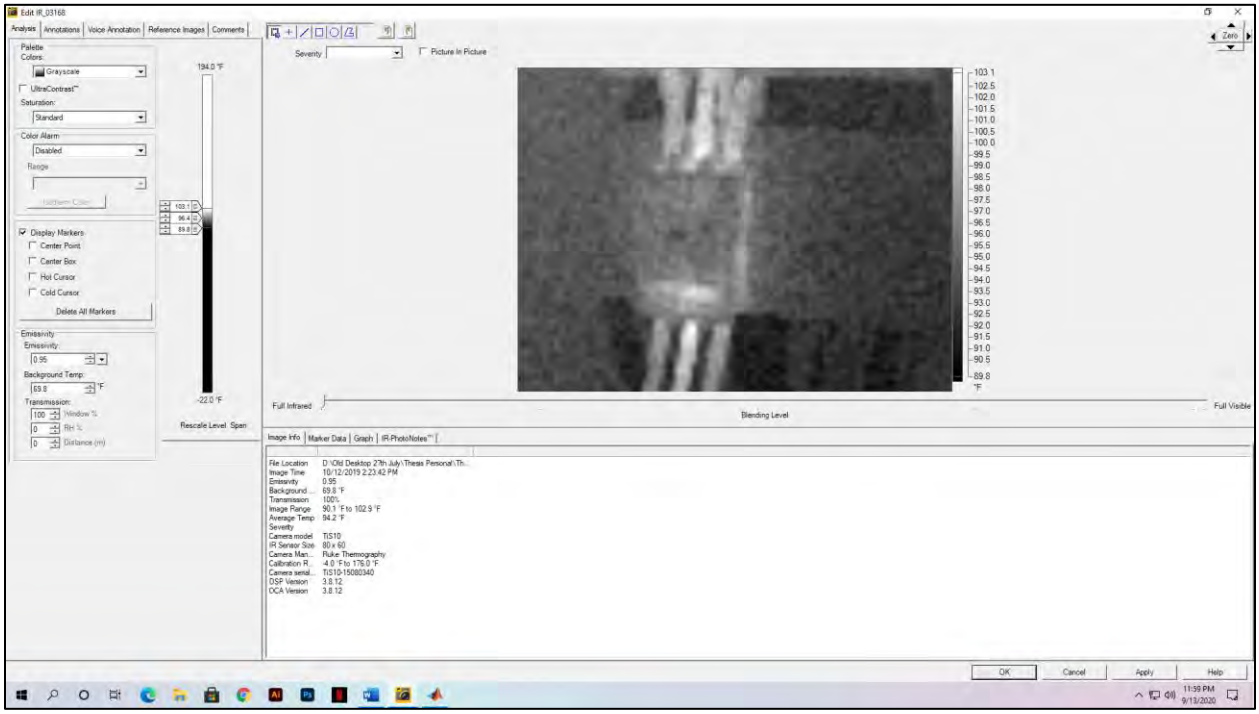

***Figure 4.28**: Converting Thermal Image via Fluke Smart View Software*

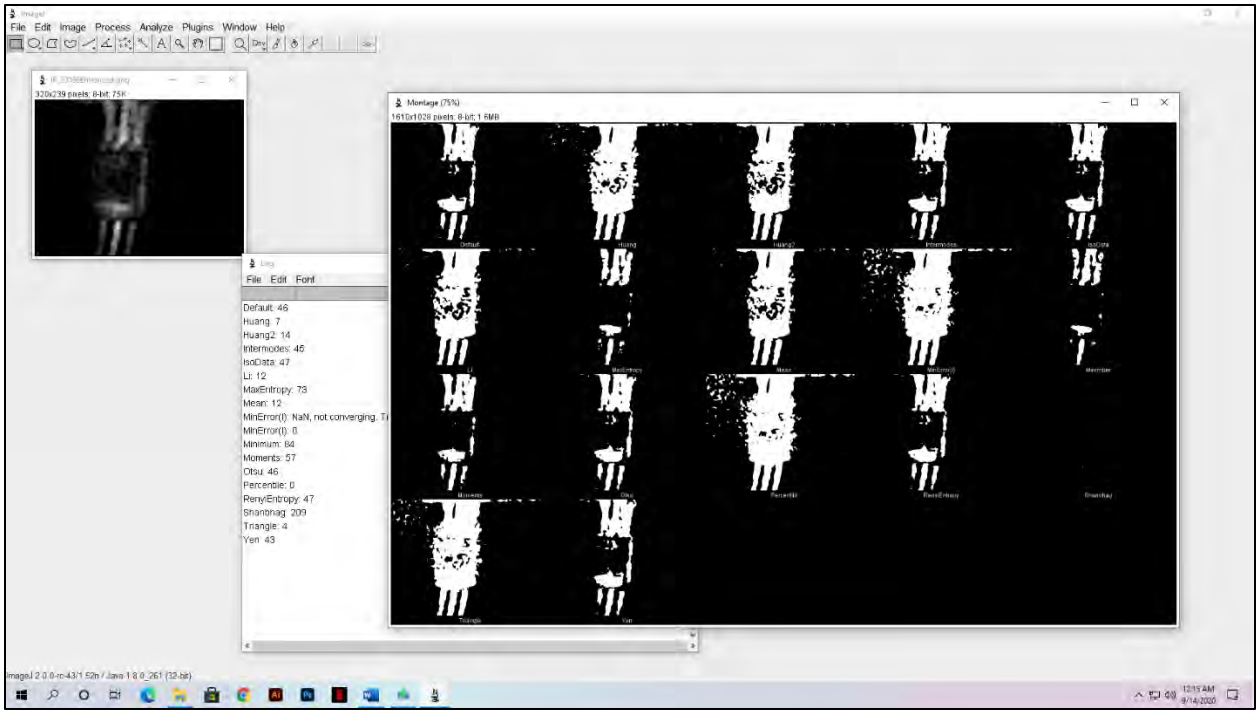

***Figure 4.29**: Performing thresholding via ImageJ Software*

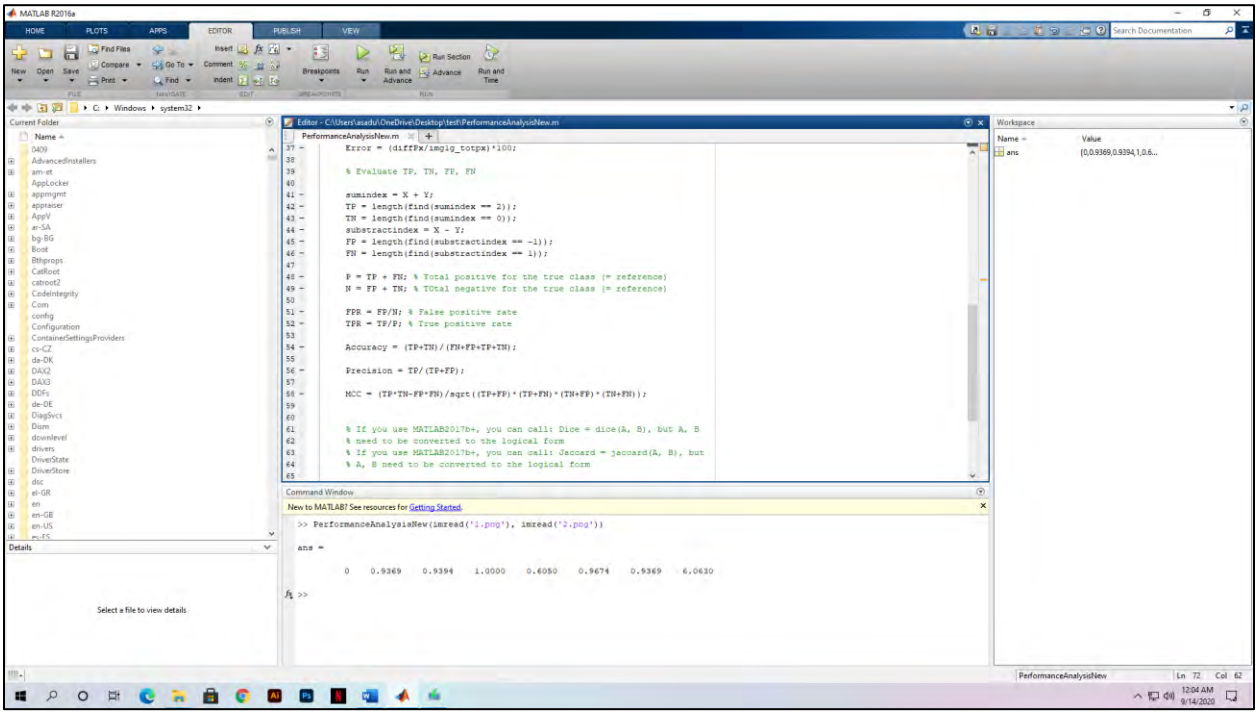

***Figure 4.30**: Running code at MATLAB for measuring different terms result for evaluation*

4.3.4 Performance data tables of different thresholding techniques

Table 4.1: *IsoData Thresholding Test Result*

Image No	FPR	TPR	Accuracy	Precision	MCC	Dice	Jaccard	Error (%)
1	0	0.94	0.93	1	0.60	0.96	0.94	6.06
2	0	0.83	0.84	1	0.4631	0.90	0.83	15.82
3	0	0.94	0.94	1	0.6359	0.97	0.94	5.42
4	0	0.97	0.97	1	0.8387	0.98	0.97	2.53
5	0	0.97	0.97	1	0.7116	0.98	0.97	2.93
6	0	0.89	0.94	1	0.8921	0.94	0.89	5.69
7	0	0.91	0.94	1	0.8819	0.95	0.91	5.83
8	0	0.45	0.68	1	0.5138	0.62	0.45	31.06
9	0	0.75	0.82	1	0.6938	0.85	0.75	17.19
10	0	0.91	0.91	1	0.4982	0.95	0.91	8.67
11	0	0.86	0.86	1	0.3465	0.92	0.87	13.06
12	0	0.93	0.93	1	0.6686	0.96	0.93	6.57
13	0	0.94	0.95	1	0.7059	0.97	0.95	4.79
14	0	0.97	0.97	1	0.669	0.98	0.97	2.48
15	0	0.95	0.95	1	0.6089	0.97	0.95	4.78
16	0	0.92	0.92	1	0.4825	0.96	0.93	7.16
17	0	0.99	0.99	1	0.9574	0.99	0.99	0.17
18	0	0.92	0.92	1	0.6404	0.96	0.92	7.00
19	0	0.93	0.94	1	0.8334	0.96	0.93	5.65
20	0	0.97	0.97	1	0.8356	0.98	0.97	2.29
21	0.0009	1	0.99	0.99	0.9766	0.99	0.99	0.09
22	0	0.84	0.89	1	0.79	0.91	0.84	10.83
23	0	0.89	0.91	1	0.8223	0.94	0.89	8.02
24	0	0.92	0.92	1	0.6616	0.96	0.92	7.06
Average =	0.0000375	0.90	0.92	0.99	0.6972	0.94	0.90	7.55

Table 4.2: *MaxEntropy/Kapur Thresholding Result*

Image No	FPR	TPR	Accuracy	Precision	MCC	Dice	Jaccard	Error
1	0	0.97	0.97	1	0.77	0.98	0.97	2.40
2	0.58	1	0.96	0.96	0.63	0.98	0.96	3.21
3	0.16	1	0.99	0.99	0.90	0.99	0.99	0.68
4	0.21	1	0.98	0.98	0.88	0.99	0.98	1.39
5	0	0.96	0.96	1	0.66	0.98	0.96	3.78
6	0.65	1	0.70	0.65	0.47	0.79	0.65	29.30
7	0.27	1	0.90	0.87	0.79	0.93	0.87	9.19
8	0.44	1	0.81	0.74	0.64	0.85	0.74	18.98
9	0.31	1	0.90	0.87	0.77	0.93	0.87	9.52
10	0.54	1	0.98	0.98	0.66	0.99	0.98	1.77
11	0	0.98	0.98	1	0.75	0.99	0.98	1.56
12	0	0.99	0.99	1	0.92	0.99	0.99	0.92
13	0	0.98	0.98	1	0.91	0.99	0.98	1.02
14	0	0.99	0.99	1	0.92	0.99	0.99	0.36
15	0.002	1	0.99	0.99	0.96	0.99	0.99	0.22
16	0.01	1	0.98	0.98	0.66	0.93	0.98	1.31
17	0	0.98	0.98	1	0.77	0.99	0.98	1.19
18	0.02	1	0.97	0.97	0.70	0.98	0.97	2.70
19	0.13	1	0.87	0.86	0.46	0.93	0.86	12.49
20	0	0.95	0.95	1	0.74	0.97	0.95	4.18
21	0.0052	1	0.99	0.99	0.86	0.99	0.99	0.51
22	0.16	1	0.86	0.83	0.68	0.91	0.83	13.46
23	0.03	1	0.97	0.96	0.93	0.98	0.96	2.36
24	0	0.97	0.97	1	0.84	0.98	0.97	2.30
Average =	0.15	0.99	0.95	0.95	0.76	0.96	0.94	5.20

Table 4.3: *Moments Thresholding Test Result*

Image No	FPR	TPR	Accuracy	Precision	MCC	Dice	Jaccard	Error
1	0	0.95	0.95	1	0.66	0.97	0.95	4.50
2	0	0.88	0.89	1	0.54	0.93	0.88	10.76
3	0	0.96	0.96	1	0.71	0.98	0.96	3.60
4	0	0.98	0.98	1	0.88	0.99	0.98	1.65
5	0	0.96	0.96	1	0.66	0.98	0.96	3.78
6	0	0.97	0.98	1	0.97	0.98	0.97	1.28
7	0	0.94	0.96	1	0.92	0.97	0.94	3.33
8	0	0.74	0.85	1	0.75	0.85	0.74	14.25
9	0	0.83	0.88	1	0.77	0.90	0.83	11.77
10	0	0.96	0.96	1	0.66	0.97	0.96	3.85
11	0	0.93	0.93	1	0.47	0.96	0.93	6.58
12	0	0.94	0.94	1	0.70	0.97	0.94	5.37
13	0	0.96	0.96	1	0.78	0.98	0.96	3.03
14	0	0.98	0.98	1	0.76	0.99	0.98	1.45
15	0	0.98	0.99	1	0.86	0.99	0.98	0.98
16	0	0.96	0.96	1	0.65	0.98	0.96	3.07
17	0	0.99	0.99	1	0.96	0.99	0.99	0.14
18	0	0.94	0.94	1	0.68	0.97	0.94	5.48
19	0	0.95	0.96	1	0.88	0.97	0.95	3.56
20	0	0.96	0.97	1	0.80	0.98	0.96	2.88
21	0	0.97	0.97	1	0.66	0.98	0.97	2.37
22	0	0.86	0.90	1	0.81	0.92	0.86	9.08
23	0	0.92	0.94	1	0.86	0.95	0.92	5.91
24	0	0.94	0.95	1	0.72	0.97	0.94	4.94
Average =	0	0.94	0.95	1	0.76	0.97	0.94	4.74

Table 4.4: *Otsu Thresholding Test Result*

Image No	FPR	TPR	Accuracy	Precision	MCC	Dice	Jaccard	Error
1	0	0.93	0.93	1	0.59	0.96	0.93	6.31
2	0	0.83	0.84	1	0.46	0.90	0.83	15.82
3	0	0.94	0.94	1	0.62	0.96	0.94	5.70
4	0	0.97	0.97	1	0.83	0.98	0.97	2.53
5	0	0.96	0.96	1	0.70	0.98	0.96	3.04
6	0	0.89	0.94	1	0.89	0.94	0.89	5.68
7	0	0.91	0.94	1	0.88	0.95	0.91	5.83
8	0	0.44	0.68	1	0.50	0.61	0.44	31.49
9	0	0.75	0.82	1	0.69	0.85	0.75	17.18
10	0	0.90	0.90	1	0.48	0.94	0.90	9.35
11	0	0.86	0.86	1	0.34	0.92	0.86	13.05
12	0	0.93	0.93	1	0.66	0.96	0.93	6.56
13	0	0.94	0.95	1	0.70	0.97	0.94	4.79
14	0	0.97	0.97	1	0.66	0.98	0.97	2.48
15	0	0.95	0.95	1	0.60	0.97	0.95	4.78
16	0	0.92	0.92	1	0.48	0.96	0.92	7.16
17	0	0.99	0.99	1	0.95	0.99	0.99	0.17
18	0	0.92	0.92	1	0.64	0.96	0.92	7.00
19	0	0.93	0.94	1	0.83	0.96	0.93	5.65
20	0	0.97	0.97	1	0.83	0.98	0.97	2.29
21	0	0.94	0.94	1	0.50	0.97	0.94	5.45
22	0	0.84	0.89	1	0.79	0.91	0.84	10.83
23	0	0.89	0.91	1	0.82	0.94	0.89	8.02
24	0	0.92	0.92	1	0.65	0.95	0.92	7.30
Average =	0	0.89	0.92	1	0.67	0.94	0.89	7.86

Table 21: *RenyiEntropy Thresholding Test Result*

Image No	FPR	TPR	Accuracy	Precision	MCC	Dice	Jaccard	Error
1	0	0.93	0.93	1	0.60	0.96	0.93	6.06
2	0	0.78	0.73	1	0.40	0.87	0.78	20.43
3	0	0.91	0.92	1	0.56	0.95	0.91	7.70
4	0.21	1	0.98	0.98	0.88	0.99	0.98	1.39
5	0	0.95	0.96	1	0.65	0.97	0.95	3.92
6	0.46	1	0.79	0.72	0.62	0.84	0.72	20.78
7	0	0.92	0.94	1	0.89	0.95	0.92	5.26
8	0.39	1	0.82	0.76	0.68	0.86	0.76	17.11
9	0.22	1	0.93	0.91	0.84	0.95	0.91	6.70
10	0.03	1	0.99	0.99	0.97	0.99	0.99	0.12
11	0	0.98	0.98	1	0.75	0.99	0.98	1.56
12	0	0.96	0.96	1	0.79	0.98	0.96	3.26
13	0	0.98	0.98	1	0.85	0.99	0.98	1.80
14	0	0.99	0.99	1	0.92	0.99	0.99	0.36
15	0.00	1	0.99	0.99	0.96	0.99	0.99	0.22
16	0.01	1	0.98	0.98	0.66	0.99	0.98	1.31
17	0	0.96	0.97	1	0.61	0.98	0.96	2.95
18	0	0.89	0.90	1	0.57	0.94	0.89	9.49
19	0	0.84	0.86	1	0.68	0.91	0.84	13.08
20	0	0.95	0.95	1	0.73	0.97	0.95	4.37
21	0.00	1	0.99	0.99	0.86	0.99	0.99	0.51
22	0	0.87	0.91	1	0.82	0.93	0.87	8.69
23	0	0.87	0.90	1	0.80	0.93	0.89	9.22
24	0	0.88	0.88	1	0.56	0.93	0.88	11.08
Average =	0.06	0.94	0.93	0.97	0.74	0.95	0.92	6.56

Table 4.6: *Yen Thresholding Test Result*

Image No	FPR	TPR	Accuracy	Precision	MCC	Dice	Jaccard	Error
1	0	0.92	0.93	1	0.57	0.96	0.92	6.89
2	0	0.75	0.76	1	0.37	0.85	0.75	23.5
3	0	0.90	0.91	1	0.53	0.95	0.90	8.93
4	0.21	1	0.98	0.98	0.88	0.99	0.98	1.39
5	0	0.95	0.95	1	0.64	0.97	0.95	4.08
6	0.42	1	0.81	0.74	0.65	0.85	0.74	19.00
7	0	0.83	0.89	1	0.79	0.90	0.83	10.99
8	0.44	1	0.81	0.74	0.64	0.85	0.74	18.98
9	0.22	1	0.93	0.91	0.84	0.95	0.912	6.70
10	0.03	1	0.99	0.99	0.97	0.99	0.99	0.12
11	0	0.98	0.98	1	0.75	0.99	0.98	1.56
12	0	0.96	0.96	1	0.78	0.98	0.96	3.50
13	0	0.97	0.97	1	0.84	0.98	0.97	2.01
14	0	0.99	0.99	1	0.92	0.99	0.99	0.36
15	0.00	1	0.99	0.99	0.96	0.99	0.99	0.22
16	0.01	1	0.98	0.98	0.66	0.99	0.98	1.31
17	0	0.96	0.96	1	0.60	0.98	0.96	3.18
18	0	0.89	0.89	1	0.55	0.94	0.89	10.32
19	0	0.82	0.85	1	0.65	0.90	0.82	14.97
20	0	0.94	0.95	1	0.72	0.97	0.94	4.77
21	0.00	1	0.99	0.99	0.73	0.99	0.99	0.91
22	0	0.80	0.86	1	0.75	0.89	0.80	13.21
23	0	0.82	0.86	1	0.73	0.90	0.82	13.05
24	0	0.85	0.86	1	0.52	0.92	0.85	13.46
Average =	0.06	0.93	0.92	0.97	0.71	0.95	0.91	7.65

Table 4.7: *MET Thresholding Test Result*

Image No	FPR	TPR	Accuracy	Precision	MCC	Dice	Jaccard	Error
1	0	0.82	0.83	1	0.39	0.90	0.82	16.75
2	0	0.77	0.78	1	0.39	0.87	0.77	21.69
3	0	0.87	0.88	1	0.47	0.93	0.87	11.92
4	0	0.61	0.63	1	0.30	0.76	0.61	36.14
5	0	0.67	0.68	1	0.24	0.80	0.67	31.58
6	0.19	1	0.91	0.86	0.83	0.92	0.86	8.83
7	0	0.96	0.97	1	0.95	0.98	0.96	2.26
8	0.76	1	0.67	0.63	0.98	0.77	0.63	32.74
9	0.70	1	0.78	0.76	0.47	0.86	0.76	21.34
10	0	0.75	0.76	1	0.30	0.85	0.75	23.87
11	0	0.72	0.73	1	0.22	0.84	0.72	26.99
12	0	0.93	0.93	1	0.66	0.96	0.93	6.56
13	0	0.75	0.77	1	0.37	0.86	0.75	22.74
14	0	0.90	0.90	1	0.41	0.95	0.90	9.16
15	0	0.99	0.99	1	0.92	0.99	0.99	0.36
16	0	0.89	0.90	1	0.42	0.94	0.89	9.77
17	0	0.99	0.99	1	0.82	0.99	0.99	0.86
18	0	0.89	0.89	1	0.55	0.94	0.89	10.32
19	0.00	1	0.99	0.99	0.98	0.99	0.99	0.39
20	0	0.91	0.91	1	0.61	0.95	0.91	8.03
21	0	0.86	0.86	1	0.34	0.92	0.86	13.02
22	0	0.98	0.98	1	0.97	0.99	0.98	1.21
23	0	0.99	0.99	1	0.98	0.99	0.99	0.72
24	0	0.82	0.83	1	0.48	0.90	0.82	16.29
Average =	0.06	0.88	0.86	0.96	0.59	0.91	0.85	13.90

Chapter 5

Results & Discussion

5.1 Combined Performance Evaluation Results

Table 5.1: *Average Test Result of Each Thresholding Techniques*

Technique	FPR	TPR	Accuracy	Precision	MCC	Dice	Jaccard	Error (%)
IsoData	0.0000375	0.90	0.92	0.99	0.6972	0.94	0.90	7.55
MaxEntropy/ Kapur	0.15	0.99	0.95	0.95	0.76	0.96	0.94	5.20
Moments	0	0.94	0.95	1	0.76	0.97	0.94	4.74
Otsu	0	0.89	0.92	1	0.67	0.94	0.89	7.86
RenyiEntropy	0.06	0.94	0.93	0.97	0.74	0.95	0.92	6.56
Yen	0.06	0.93	0.92	0.97	0.71	0.95	0.91	7.65
MET	0.06	0.88	0.86	0.96	0.59	0.91	0.85	13.90

5.2 Final Results

From Table 5.1, we can see the average performance test results of seven different thresholding techniques that we applied earlier on our collected thermal images. Each thresholding technique's final average test results consist of average from test results data of 24 individual images. By taking the average from Data Table 4.1 of the IsoData Thresholding Result, we get the final result for the IsoData thresholding technique at Data Table 5.1. In this similar way, the average final result for MaxEntropy/Kapur, Moments, Otsu, RenyiEntropy, Yen, MET thresholding technique was placed into Data Table 5.1 from the Chapter-4 Data Table 4.1-4.7 respectively. After placing all of the

index data value, we can see that Moments thresholding technique provides overall better performance evaluation test results compared to six other thresholding techniques. From the Moments thresholding technique, we got the lowest possible error rates that indicate better segmentation comparing with ground truth image. Moreover, other test values of Moments thresholding technique is also better compared to others. The error rate of the Moments thresholding technique is 4.7383% which is better than the Error rate of MaxEntropy/Kapur, which is 5.2044%. So, the Moments thresholding technique shows significant improvement in detecting hotspots automatically with much better accuracy. The average FPR, TPR, Accuracy, Precision, MCC, Dice, Jaccard Index, Error (%) were used for evaluating the overall performance.

Chapter 6

Conclusion

6.1 Summary

The primary motivation behind this research was to compare the different thresholding techniques to find out which technique is the best suitable and accurate for Hotspot detection of electrical equipment using IRT imaging techniques. To, perform this research we needed to collect the thermal image of different electrical equipment. So, after capturing a lot of thermal images, we choose 24 among them for final testing. Before applying thresholding techniques, a normal inspection of those images was performed using the Fluke Smart View Camera software to come to the conclusion that those images are suitable for performing the necessary performance evaluation through seven different thresholding techniques. So, after performing the necessary segmentation test and comparing it with the ground truth image we found test results for 24 images for each different thresholding category. After analyzing all of the results, it was found that Moments thresholding technique performs best in terms of FPR, TPR, Accuracy, Precision, MCC, Dice, Jaccard Index, Error (%) test values.

6.2 Future Recommendation

There are many thresholding techniques that can be implemented for automatic IRT inspection of the electrical equipment but the performance and accuracy of every thresholding technique are not the same. And all of them do not work well with the hotspot detection of electrical equipment. That's why for implementing more advanced automatic hotspot detection, it is essential to choose the best thresholding techniques with minimum error rate to get the best possible result and avoid false alarm from an automatic hotspot detection system. That's why we tried to compare well-known regularly used thresholding techniques for hotspot detection of our collected images to find out which thresholding technique performs best. And we do perform this test among 24 different

image samples to minimize error as much as possible that could occur if we perform this task between very few sample images. So, for automatic IRT inspection in the future, the Moments Thresholding algorithm can be used with confidence to get better inspection results and implementing a fully automated system for analyzing the Hotspot of electrical equipment.

Reference

[1] A. S. N. Huda, S. Taib, M. S. Jadin and D. Ishak, "A semi-automatic approach for thermographic inspection of electrical installations within buildings," *Energy Buildings*, vol. 55, pp. 585-591, 2012.

[2] R. A. Epperly, G. E. Heberlein and L. G. Eads, "A tool for reliability and safety: predict and prevent equipment failures with thermography," Record *of Conference Papers. IEEE Industry Applications Society 44th Annual Petroleum and Chemical Industry Conference*, Banff, Alberta, Canada, 1997, pp. 59-68, doi: 10.1109/PCICON.1997.648167.

[3] B. Li, X. Zhu, S. Zhao and W. Niu, "HV Power Equipment Diagnosis Based on Infrared Imaging Analyzing," *2006 International Conference on Power System Technology*, Chongqing, 2006, pp. 1-4, doi: 10.1109/ICPST.2006.321512.

[4] M. Jadin and S. Taib, "Recent progress in diagnosing the reliability of electrical equipment by using infrared thermography," *Infrared Physics & Technology*, 55(4), pp.236-245, 2009.

[5] Z. Delong and Z. Junbin, "Minimum Error Thresholding Based on Two Dimensional Histogram," *2009 WRI World Congress on Computer Science and Information Engineering*, Los Angeles, CA, 2009, pp. 169-175, doi: 10.1109/CSIE.2009.797.

[6] Q. Q. Wang, Z. Peng, L. Liu, "An Adaptive Method of Image Segmentation," *Transactions of Beijing Institute of Technology*, vol. 23, no. 4, pp. 521-524, Aug 2003.

[7] A. S. N. Huda, M. S. Jadin, S. Taib, "Extracting electrical hotspots from infrared images using modified Kapur thresholding technique," April 2013.

[8] T. Zouagui, H. Benoit-Cattin and C. Odet, “Image segmentation functional model,” *Pattern Recognition*, 37(9), pp.1785-1795, 2009.

[9] B. Sankur, “Survey over image thresholding techniques and quantitative performance evaluation,” *Journal of Electronic Imaging*, 13(1), p.146, 2012.

[10] P. Sahoo, S. Soltani and A. Wong, “A survey of thresholding techniques,” *Computer Vision, Graphics and Image Processing*, 41(2), pp.233-260, 1988.

[11] Hui-Fuang Ng, “Automatic thresholding for defect detection,” *Third International Conference on Image and Graphics (ICIG'04)*, Hong Kong, China, 2004, pp. 532-535, doi: 10.1109/ICIG.2004.43.

[12] A. Magid, S. R. Rotman and A. M. Weiss, “Comments on Picture thresholding using an iterative selection method,” in *IEEE Transactions on Systems, Man, and Cybernetics*, vol. 20, no. 5, pp. 1238-1239, Sept.-Oct. 1990, doi: 10.1109/21.59988.

[13] M. Thompson, R. O. Duda, and P. E. Hart, “Pattern Classification and Scene Analysis,” Leonardo, vol. 7, no. 4, p. 370, 1974.

[14] Flavior. Dias Velasco, “Thresholding using the ISODATA Clustering Algorithm,” *IEEE Transactions on Systems, Man, And Cybernetics*, vol. Smc-10, No. 11, November 1980.

[15] J. Kapur, P. Sahoo and A. Wong, “A new method for gray-level picture thresholding using the entropy of the histogram,” *Computer Vision, Graphics, and Image Processing*, 29(3), pp.273-285.

[16] H. Kiani, R. Safabakhsh and E. Khadangi, “Fast recursive segmentation algorithm based on Kapur's entropy,” 2009 *2nd International Conference on Computer, Control and Communication*, Karachi, 2009, pp. 1-6, doi: 10.1109/IC4.2009.4909269.

[17] N. Otsu, “A Threshold Selection Method from Gray-Level Histograms,” in *IEEE Transactions on Systems, Man, and Cybernetics*, vol. 9, no. 1, pp. 62-66, Jan. 1979, doi: 10.1109/TSMC.1979.4310076.

[18] S. Luo, Q. Zhang, F. Luo, Y. Wang and Z. Chen, “An improved moment-preserving auto threshold image segmentation algorithm,” *International Conference on Information Acquisition, 2004. Proceedings.*, Hefei, 2004, pp. 316-318, doi: 10.1109/ICIA.2004.1373378.

[19] Wen-Hsiang Tsai, “Moment-Preserving Thresholding: A New Approach”. Department of Information Science, National Chiao Tung University, Hsinchu, Taiwan 300 Republic of China. 377-393, 1985.

[20] P. Sahoo and G. Arora, “A thresholding method based on two-dimensional Renyi's entropy,” *Pattern Recognition*, 37(6), pp.1149-1161, 2004.

[21] A. Yimit, Y. Hagihara, T. Miyoshi, Y. Hagihara, Q. Yimit, “Fast Method for Two-dimensional Renyi’s Entropy-based Thresholding”. *International Journal on Computer Science and Engineering (IJCSE),* Vol. 4 No, ISSN: 0975-3397, February 2012.

[22] Jui-Cheng Yen, Fu-Juay Chang, and Shyang Chang, “A New Criterion for Automatic Multilevel Thresholding”, *IEEE Transactions on Image Processing*, vol. 4, No. 3, March 1995.

[23] J. Kittler, J. Illingworth, “Minimum error thresholding”, *Pattern Recognition*, vol. 19, no. 1, pp. 41-47, 1986.

[24] D. Thanh, D. Sergey, V. Prasath and N. Hai, “Blood Vessels Segmentation Method for Retinal Fundus Images Based on Adaptive Principal Curvature and Image Derivative Operators,” *ISPRS - International Archives of the Photogrammetry, Remote Sensing and Spatial Information Sciences*, XLII-2/W12, pp.211-218, 2019.

[25] D. Thanh, U. Erkan, V. Prasath, V. Kumar and N. Hien, “A Skin Lesion Segmentation Method for Dermoscopic Images Based on Adaptive Thresholding with Normalization of Color Models,” *2019 6th International Conference on Electrical and Electronics Engineering (ICEEE)*, 2019.

[26] D. Thanh, V. Prasath, L. Hieu and N. Hien, “Melanoma Skin Cancer Detection Method Based on Adaptive Principal Curvature, Colour Normalisation and Feature Extraction with the ABCD Rule,” *Journal of Digital Imaging*, 33(3), pp.574-585, 2019.